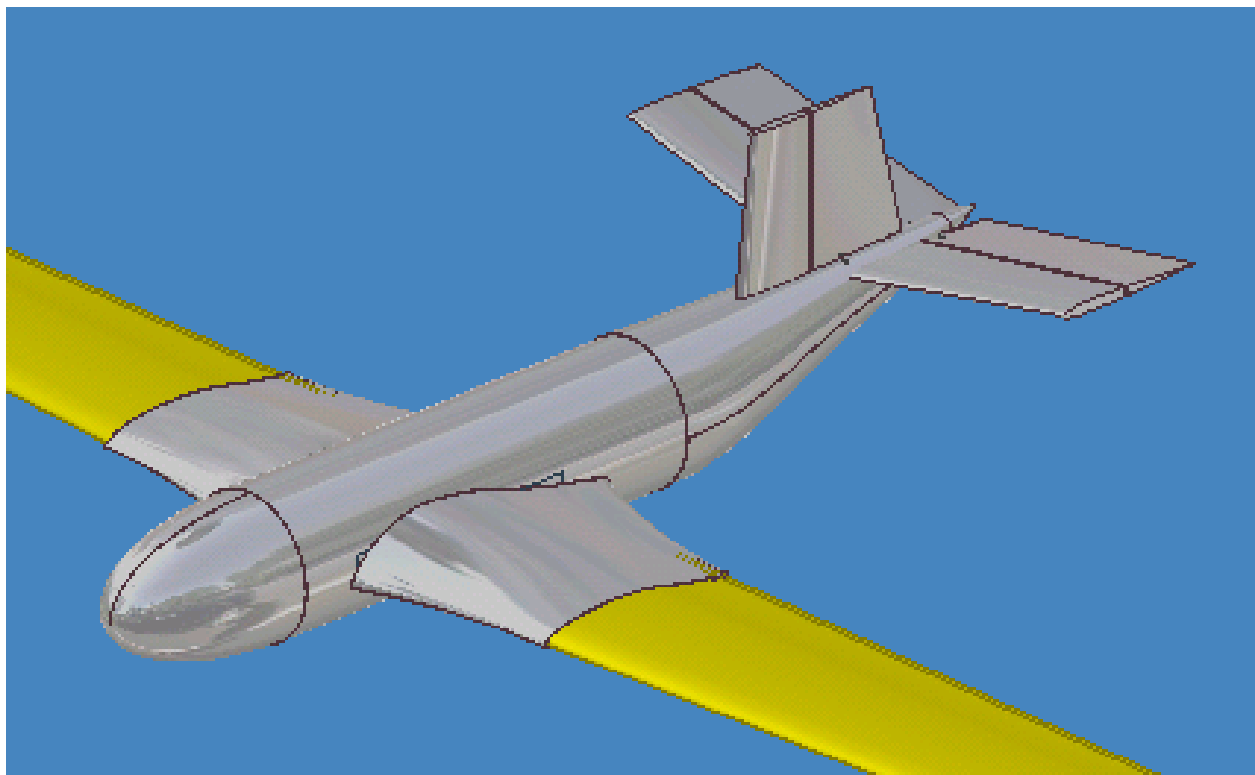


Advanced Logistics Delivery System Glider Design Team



Final Design Report
May 5, 2005



Advanced Logistics Delivery System

Team Members

Chris Imhof

Brian Mohns

Laura Morgan

David Rogers

Adam Russell

Andy Tuggle

Sean Tully

Lesley Walcourt

Charles Walston

Patrick Williams

Faculty Advisor

William H. Mason

Acknowledgment

We would like to acknowledge the Carderock Innovation Center and the Center for Innovations in Ship Design for providing us with this design project and feedback on it. We would also like to acknowledge and thank Geoff Hope for his assistance in the lifting assumption as opposed to the projectile assumption discussed in Chapter 5 of this report.

Advanced Logistics Delivery System

Executive Summary

This report provides the design specifications for an Advanced Logistics Delivery System. The Advanced Logistics Delivery System (ALDS) will be used to transport supplies to troops in hostile territories as an alternative to previously implemented techniques such as convoy lines and airdrops, which endanger soldiers and military personnel. The ALDS is a glider that is launched from a ship located at a safe distance off the shore of hostile territories. The glider's compact launch vehicle will be accelerated down a track that runs through the bottom of the ship, propelled by an electromagnetic motor system. This glider is then launched at an initial speed of 500 knots and an initial acceleration of 30g's. The glider will travel in its compact state until it reaches the apex of its flight. At that point inflatable wings stored inside the glider launch vehicle will deploy and carry the glider to its 50 mile range destination. The design premise for this glider comes from the Carderock Innovation Center and the Center for Innovations in Ship Design.

This report describes the design process for developing this glider from the initial design concepts to a final design. An analysis of the glider's aerodynamics, structures, inflatable wings, stability and control, weights and center of gravity, avionics system, sizing, and the cost of each glider is included in this report.

Table of Contents

Title Page.....	i
Team Roaster.....	ii
Executive Summary.....	iii
Table of Contents.....	iv
List of Figures.....	vi
List of Tables.....	viii
List of Symbols.....	ix
Chapter 1: Introduction and Request for Proposal.....	1
1.1 Introduction.....	1
1.2 Request for Proposal.....	1
Chapter 2: Initial Design Concepts.....	2
2.1 Inflatable Wing.....	2
2.2 Single Hinged Wing.....	4
2.3 Dual Hinged Wing.....	5
2.4 Telescoping Wings.....	6
2.5 Extension Spar Wing.....	7
2.6 Variations on Concepts.....	7
Chapter 3: Analysis of Initial Design Concepts.....	8
3.1 Design Comparison Matrix.....	8
3.2 Glider Design Selection.....	9
3.3 Final Glider Design.....	10
Chapter 4: Final Glider Configuration.....	10
4.1 Introduction.....	10
4.2 Original Glider Configuration.....	10
4.3 Final Glider Configuration.....	13
Chapter 5: Aerodynamics of the Launch and Climb.....	21
5.1 Introduction.....	21
5.2 Projectile Motion.....	21
5.3 Constant Flight Angle.....	23
5.4 Performance Analysis.....	25
5.5 Drag Buildup.....	28
Chapter 6: Aerodynamics of the Glide.....	29
6.1 Introduction.....	29
6.2 Initial Geometric and Performance Calculations.....	29
6.3 Airfoil Boundary Layer Analysis.....	32
6.4 ALDS Gliding Drag Analysis.....	35
6.5 Performance Analysis.....	36
Chapter 7: Glider Structural Design.....	38
7.1 Introduction.....	38
7.2 Materials.....	39
7.3 Structural Analysis of the Fuselage.....	40
7.4 Structural Analysis of the Wings.....	48
Chapter 8: Inflatable Wing Structures.....	50
8.1 Criteria for an Acceptable Wing.....	50
8.2 Original Concepts.....	52
8.3 Final Concept.....	53

Advanced Logistics Delivery System

8.3 Force, Moment and Pressure Calculations.....	54
8.4 Material Selection.....	56
Chapter 9: Wing Deployment.....	58
9.1 Introduction.....	58
9.2 Primary Inflation.....	58
9.3 Reserve Inflation.....	64
9.4 Future Thoughts.....	66
Chapter 10: Weights and Center of Gravity.....	67
10.1 Weights.....	67
10.2 Center of Gravity.....	71
Chapter 11: Analysis of Glider Stability and Control.....	72
11.1 Introduction.....	72
11.2 Constraints.....	72
11.3 Requirements.....	72
11.4 Launch Loads.....	73
11.5 Wing Deployment.....	73
11.6 Control System.....	74
11.7 Tail Configuration.....	75
11.8 Conventional Design Process.....	78
11.9 Computer Aided Design.....	80
11.10 Stability Derivatives.....	80
11.11 Longitudinal Stability.....	81
11.12 Pitch Control and Elevator Performance.....	83
11.13 Yaw Stability and Rudder Performance.....	86
11.14 Roll Stability and Control.....	87
11.15 Servo Motors.....	88
Chapter 12: Glider Avionics.....	91
12.1 Piccolo Plus: An Introduction.....	91
12.2 Components of the Piccolo Plus.....	93
12.3 Ground Station.....	94
12.4 Components of Avionics System.....	94
12.5 Avionics Integration to Glider Aircraft.....	96
12.6 Piccolo Pricing.....	97
Chapter 13: Sizing and Relationship to Ship Configuration.....	97
13.1 Introduction.....	97
13.2 Glider Storage.....	97
13.2.1 Volume Calculations.....	98
13.2.2 Glider Arrangement.....	98
13.3 Glider Storage Conclusions.....	99
Chapter 14: Cost Analysis.....	100
14.1 Individual Glider Costs.....	100
14.2 Costs per Pound Payload Deliverable.....	100
14.3 Cost Conclusions.....	102
Chapter 15: Conclusions and Future Work.....	103
References.....	104
Appendix A: Equations for Calculations.....	106
Appendix B: Boundary Layer Analysis Output.....	107

List of Figures

- 2.1 Inflatable Wing Glider
- 2.2 Single Hinged Glider
- 2.3 Dual Hinged Glider
- 2.4 Telescoping Wing Glider
- 2.5 Extension Spar Wing with Soft Skin
- 3.1 Glider Decision Tree
- 4.1 Original Glider Launch Vehicle
- 4.2 Top View of Internal Glider Configuration
- 4.3 Original Launch Vehicle Design
- 4.4 Final Glider Design
- 4.5 Payload Box Stacking
- 4.6 Original Glider Side Profile
- 4.7 Final Glider Side Profile
- 4.8 Final Glider Internal Arrangement
- 4.9 Original Glider Sodium Azide Tank Close-up
- 4.10 Rear View of Internal Arrangement of Motors and Avionics Package
- 4.11 Side View of Internal Structures
- 4.12 Dimensioned Top View
- 4.13 Dimensioned Top and Frontal View with Wings Deployed
- 5.1 Projectile Trajectories at Various Launch Angles
- 5.2 Free Body Diagram of ALDS During Launch
- 5.3 Variation of Apogee Height with Launch Angle
- 5.4 Variations in Apogee Height with Span
- 5.5 Variations in Apogee Height with Chord
- 5.6 Variations in Apogee Height with Temperature
- 6.1 Glider Comparison Chart
- 6.2 Taper Ratio versus Efficiency Factor
- 6.3 Exaggerated View of Wing Deflation
- 7.1 Diagram of Loading on Glider
- 7.2 Stringer Displacement along the Frame Edge
- 7.3 Stringer Cross Section
- 7.4 Optimized Stringer Cross Section
- 7.5 Stringer and Skin Panel Numbering Convention
- 7.6 Diagram of Payload Supports
- 7.7 Major Loads on Payload Supports
- 7.8 Frame and Payload Support Optimized Dimensions
- 7.9 Major Loads on Glider Wing
- 8.1 Five Spar Cross Section Concept
- 8.2 Original Fully Inflated Wing Concept
- 8.3 Combination of Original Concepts on Wortmann 170 Airfoil
- 8.4 Cross Section of University of Kentucky's "Big Blue"
- 8.5a Pressure Coefficient Along Chord
- 8.5b Normalized Lift Along Chord
- 8.6 Section Moment and Spar Diameter along Chord

Advanced Logistics Delivery System

- 8.7 Individual Required Wrinkling Pressure along Chord
- 9.1 Required Reactant Amounts for Varying Wing Pressure
- 9.2 Inflation Times per Wing
- 9.3 Reserve Inflation Controller Diagram
- 9.4 Reserve Pressure Controller Activity Compared with Pressure Loss
- 10.1 Fuselage Stringer Highlighted for Examining
- 10.2 Glider Weight Distribution
- 10.3 Glider Weight Distribution without Payload and Fuel
- 11.1 Locations of Center of Gravity and Pressure
- 11.2 Center of Pressure Shift Before and After Wing Deployment
- 11.3 Tails being considered for Glider
- 11.4 Final Tail Configuration
- 11.5 Tail Geometry
- 11.6 Typical Fuselage Lengths versus Overall Weight
- 11.7 Surface Area versus Moment Arm Length
- 11.8 Input and Output Properties for Programs used in Design Process
- 11.9 Summary of Primary Stability Derivatives
- 11.10 Coefficient of Pitch Moment versus Lift Coefficient
- 11.11 Coefficient of Pitch Moment versus Lift Coefficient for CG Range
- 11.12 C_m/C_L Slopes for Various Elevator Deflections at Desired CG
- 11.13 C_m/C_L Slopes for Various Elevator Deflections at Forward CG
- 11.14 C_m/C_L Slopes for Various Elevator Deflections at Aft CG
- 11.15 Coefficient of Yaw Moment vs. Yaw Angle
- 11.16 Coefficient of Yaw Moment vs. Rudder Deflection
- 11.17 Roll Rate vs. Rudder Deflection
- 11.18 Design Layout for Motor Connections
- 11.19 Approximate Torque Requirements
- 11.20 Approximate Torque Requirements
- 12.1 Piccolo Plus Avionics Package
- 12.2 Piccolo Plus Block Diagram
- 12.3 Autopilot Commands Page
- 12.4 Map Page
- B1 Wortmann FX 67-K-170 Contours
- B2 Wortmann FX 67-K-150 Contours
- B3 Skin Friction-Wortmann FX 67-K-170 Root Airfoil at One Percent Deflation
- B4 Skin Friction Graph - Wortmann FX 67-K-170 Rigid Root Foil
- B5 Wortmann FX-67-K-170 Rigid Airfoil Output
- B6 Wortmann FX-67-K-170 One Percent Deflated Airfoil Output
- B7 Section Lift to Drag Comparison for Root Airfoil
- B8 Tripped Flow Comparison Graph For Deflated Root Airfoil
- B9 Wortmann FX 67-K-150 Tip Airfoil at One Percent Deflation
- B10 Skin Friction Graph - Wortmann FX 67-K-150 Tip Foil
- B11 Wortmann FX 67-K-150 Rigid Tip Foil Output
- B12 Wortmann FX-67-K-150 One Percent Deflated Airfoil Output
- B13 Section Lift to Drag Comparison for Tip Airfoil
- B14 Output of Friction Analysis

List of Tables

- 3.1 Design Comparison Matrix
- 5.1 ALDS Zero Lift Drag Buildup During Launch
- 6.1 Initial Calculations for the ALDS Glider with a Range of 50 Miles
- 6.2 Analyzed Airfoil Profiles
- 6.3 Comparison of Rigid Wing and a One Percent Deflated Wing
- 6.4 Expected Lift to Drag Ratio for the ALDS Glider
- 6.5 Overall Performance Calculations
- 6.6 Overall Performance At Minimum Weight of 1400 lbs.
- 7.1 Carbon Fiber Material Properties
- 7.2 Composite Skin Material Properties
- 7.3 Table of Stringer Stresses
- 7.4 Table of Shear Stresses in Skin
- 10.1 Weights Grouping
- 10.2 Weight Breakdown and Totals
- 10.3 Distance and Moments
- 12.1 Key Characteristics of the Piccolo Plus
- 12.2 Piccolo Pricing
- 14.1 Cost Summary per Glider
- 14.2 Cost Comparison between Delivery Methods
- A1 Aerodynamics Equations Table

List of Symbols and Abbreviations

ALDS – Advance Logistics Delivery System

AR – Aspect Ratio

b – Wing Span

c – Chord

C_L – Lift Coefficient

C_D – Drag Coefficient

C_{D0} – Zero Lift Drag Coefficient

C_f – Friction Coefficient

CG – Center of Gravity

D – Drag

e – Oswald's Efficiency Factor

E – Young's Modulus

F – Force

FF – Friction Force

g – Gravitational Constant

L – Lift

m – Mass

M – Moment

P – Pressure

psi – Pounds per Square Inch

R – Gas Constant

s – Position

S – Planar Surface Area

S_{wet} – Wetted Surface Area

t – Time

t – Thickness

T – Temperature

v – Velocity

W – Weight

α – Launch Angle

ρ – Density

Chapter 1: Introduction and Request for Proposal

1.1 Introduction

The Virginia Tech glider team's objective is to provide a low cost, disposable glider to carry supplies to troops in hostile territories. The request for proposal for the glider known as the advanced logistics delivery system (ALDS), comes from the Carderock Innovation Center and the Center for Innovations in Ship Design. The main project drivers that the glider must achieve to be considered successful are the range requirement, the payload requirement, and the sizing requirement in addition to the low cost of the glider. These requirements will be discussed in more detail in the next section.

The glider design fits into a larger project being by the Carderock Center. Carderock wants to be able to launch a glider from a ship in waters a safe distance off of the coast of hostile zones. The gliders will deliver supplies to troops in these areas. The glider design presented in this report is a solution that could be used for this situation. Many of the constraints on the glider occur because the glider is being launched off of a ship and safe distance away from land. The glider needs to be both durable to withstand launch accelerations and disposable at the same time.

The glider will undergo three stages of flight on its course from the ship to hostile territory. The first phase is the launch phase, in which the launch vehicle will travel along the track in the ship propelled by an electromagnetic motor. The vehicle is then launched from the ship and enters the climb portion of the flight in which the glider starts at its launch initial velocity and climbs to the apex of the flight. Before stall occurs at apex of the trajectory the glider's wings are deployed. The glider completes the third segment of its flight by gliding back down to the ground to the troops below.

1.2 Request for Proposal

The request for proposal (RFP) comes from the Carderock Innovation Center and the Center of Innovations in Ship Design. The requirements in the request for proposal come from the economical

Advanced Logistics Delivery System

and mission requirements of the navy and from the limitations that the ship places on the glider. The requirements of the RFP are as follows:

- The glider must have the room and structural stability to carry 1000 pounds of payload.
- The glider without the payload must weigh around 500 pounds.
- The glider must be able to withstand a launch acceleration of 30g's and a launch speed of 500 knots.
- The glider must be inexpensive and disposable.
- The glider must maintain a cruise speed of 60 knots.
- The glider launch pod dimensions must fit in a tunnel with a 10 ft diameter.
- The glider must have a range of 50 miles.

When the design process began the glider was required to be 15 ft in length. That requirement later changed and is a key difference between the initial design concepts and the final concept.

Chapter 2: Initial Design Concepts

The first step taken in the design process was to come up with several different design concepts for the glider. Five different designs were considered and they are discussed in this section.

2.1 Inflatable Wing

The inflatable wing glider is pictured in figure 2.1. The glider has a flying wing shaped body and a V-tail for stability. The inflatable wings on the glider will use a gas to increase the pressure in the wing once the glider reaches apex.

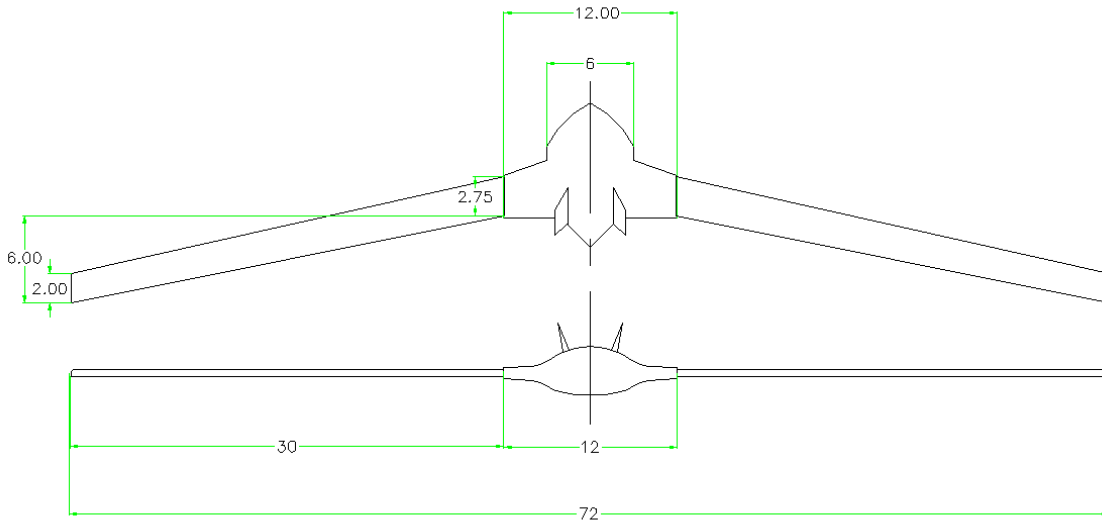


Figure 2.1 Inflatable Wing Glider

The inflatable wing glider has a relatively compact launch shape which will make it easy to fit the launch vehicle into the launch tube. The glider will also be stable during launch due to the flying wing shape of the launch vehicle and its roll control. The flying wing shape will also provide structural stability during the launch phase in which the vehicle under goes the most extreme accelerations. The inflatable wing glider is also relatively simple because there are few moving mechanical parts. The lack of moving parts reduces the opportunity for unexpected failures. The V-tail on the launch body provides stability during the flight.

The major drawback of the inflatable glider is that the inflatable wings will need to be 25 to 30 ft span on each side which will require a large amount of pressure to maintain structural stability and because of this large amount of pressure there will be structural complications at the junction of the pod and wing. Another drawback of the inflatable wing is that the inflation device for the wings will need to be placed near the wing tips of the launch pod to reduce the total inflated length and there may not be sufficient room available.

Advanced Logistics Delivery System

2.2 Single Hinged Wing

The single hinged wing glider is pictured below in figure 2.2. The single hinged wing has the streamlined body shape that is popular in gliders such as the Nimbus 2, see table 6.1. The wing of the single hinged glider will be rotated out at apex using either a spring or a hydraulic mechanism.

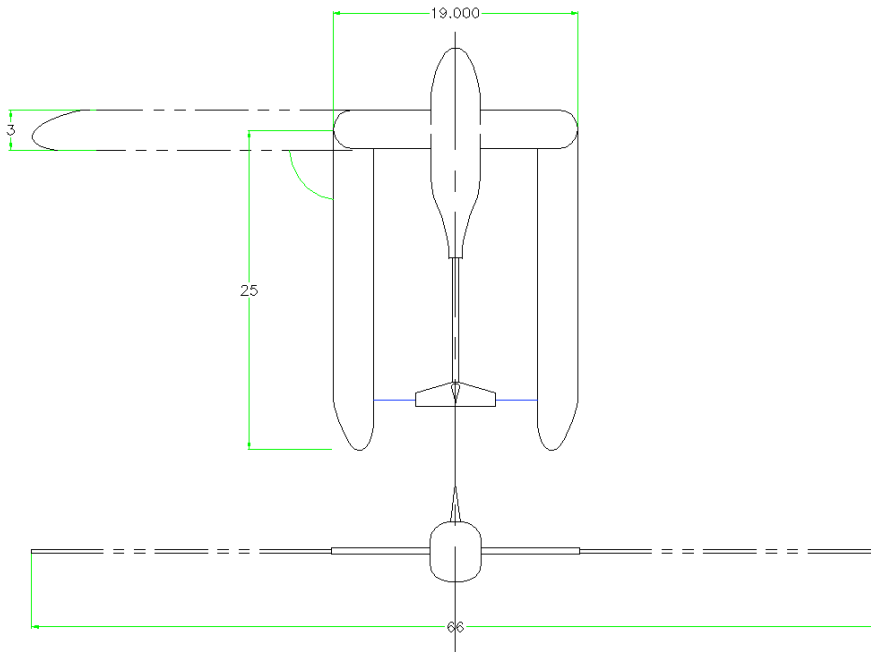


Figure 2.2 Single Hinged Glider

The advantages of using the single hinged wing are that the folded wings will provide stability during launch, the majority of the wing will experience no aerodynamic interruptions during the glide phase of the trip, the solid wings will also be less subject to failure during the glide phase than the inflatable wings, and the tail provides stability in both the launch and glide phases. The aircraft shape of the body also provides a simple way to load the fuselage through the nose cone.

The main disadvantages of using the single hinged wing is that for the launch vehicle to fit into the launch tunnel span-wise the glider will have to be longer than it can be and still fit through the turn in the tunnel. Another disadvantage is that structural oscillations may occur in the long wing extensions during the high accelerations of launch, which could lead to structural failure or an unstable

Advanced Logistics Delivery System

climb after launch. Also, during wing deployment large moments may occur because of the large rotating arm that could send the aircraft into an unstable alignment. A final disadvantage is the long tail which may be subject to structural failure during launch.

2.3 Dual Hinged Wing

The dual hinged wing has a similar wing design to the single hinged wing except that there are two hinges that rotate to get the wing to full span. The dual hinged wing fuselage is a simple aerodynamic shape that allows the tips of the wings to be attached to the fuselage. The wings will be extended out at apex in a similar manner to the single hinged wing using either a spring or a hydraulic mechanism. The dual hinged wing glider is pictured in figure 2.3.

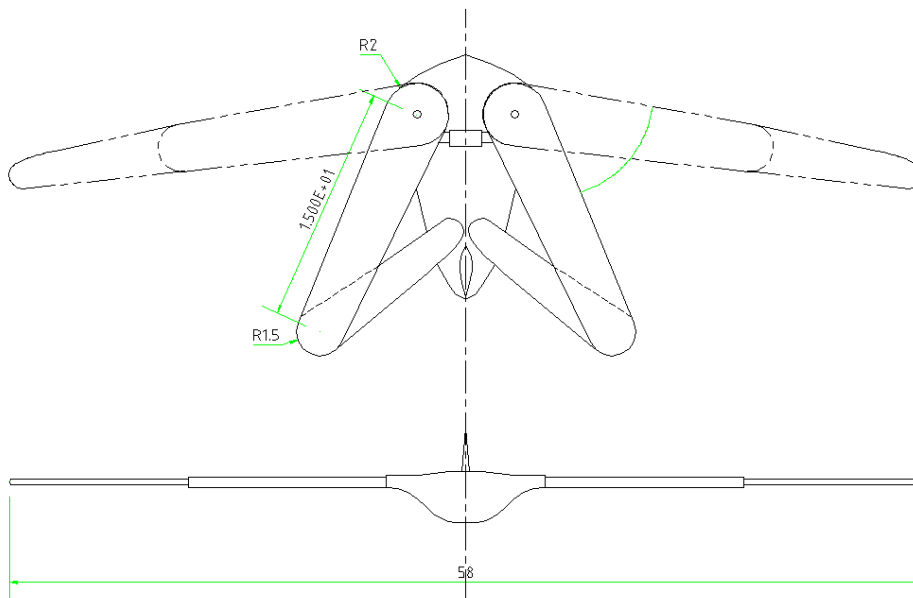


Figure 2.3 Dual Hinged Glider

Some qualities of the dual hinged glider that make it desirable are the dual hinged glider has solid wings that are more resistant to structural failure than the inflatable wing glider. The folded wings of the glider also create more stability during the launch phase of the flight. The vertical stabilizer in place of a tail will provide stability in both the launch and glide phases of the trip.

Advanced Logistics Delivery System

The dual hinged design however is more mechanically complex than the previous two design concepts allowing more room for unexpected errors in the wing deployment. Another problem with the dual hinged glider is that the hinges would have to withstand large loads during all stages of the glider's flight. The wings again run the risk of oscillating during launch which could lead to structural instability.

2.4 Telescoping Wings

The telescoping wing glider has a simple aerodynamic fuselage shape with wings that first rotate out around a hinge attached to the fuselage and then slide the second part of the wing span from the first section of the wing. The telescoping wing glider is shown in figure 2.4.

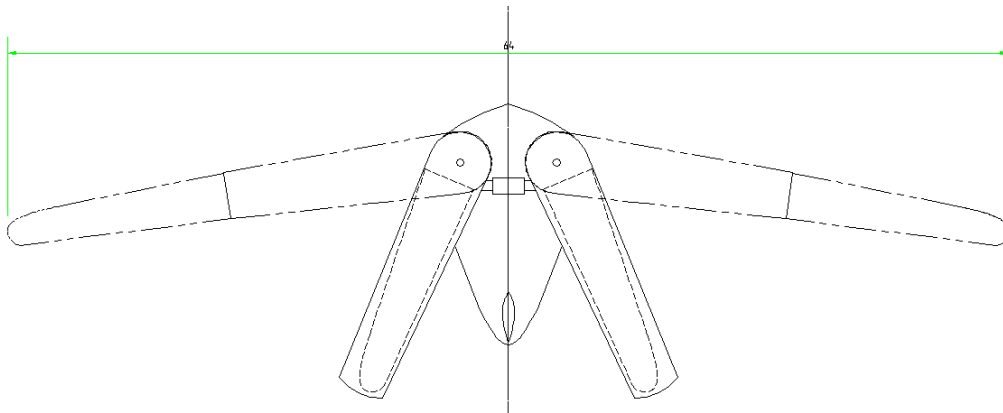


Figure 2.4 Telescoping Wing Glider

The telescoping wing glider reduces the need for a second hinge in the dual hinged glider, which will result in improved aerodynamic qualities of the wings. The hinged wings however still provide stability during launch and the climb portion of the flight.

The telescoping wing however would make it difficult to have a spar that spans the entire wing and would force the load to be carried by the wing skin at the point where the two wing parts join. It would also be difficult to place struts in the first half of the wing because there would be little room left for them due to the second part of the wing being placed inside it for the launch. There is again the

Advanced Logistics Delivery System

possibility of failure with the wing deployment system because of the complexity of moving parts that could be damaged at anytime, particularly during launch under such extreme loads.

2.5 Extension Spar Wing

The extension spar wing is composed of rigid spars that are covered by a soft wing skin. The spars fold up into the fuselage for launch and are deployed using a spring mechanism at apex. The extension spar is shown in figure 2.5. The extension spar wing would be used with a fuselage body shape similar to that of the inflatable wing where the extension wing could be compressed down into the sides of the fuselage.

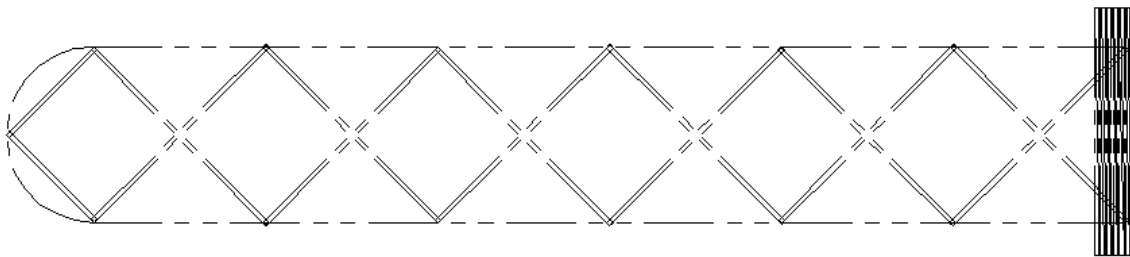


Figure 2.5 Extension Spar Wing with Soft Skin

The extension spar provides a light weight compact wing solution to the expanding wing problem. The extension spar would be inexpensive compared to other options and leave the most room for cargo because the compressed spars would not take up much of the fuselage room. The disadvantages of using the extension spar are that it may be difficult to have the wing taper because of the material would have to expand to fit over the folded spars and also the extended wing would be flat and therefore have poor aerodynamic characteristics during the glide phase of the flight.

2.6 Variations on Concepts

All of the five concepts described above have their merits and disadvantages. Combining the different aspects of each of the gliders to try and extract the best of different designs resulted in changing the fuselage shape of two of the gliders. The aircraft shaped body of the Nimbus 2 was

Advanced Logistics Delivery System

determined to be more aerodynamic than the flying wing and the simple aerodynamic shape. Therefore alternate versions of the inflatable wing glider and the dual hinged glider were done with the aircraft shaped body.

Chapter 3: Analysis of Initial Design Concepts

3.1 Design Comparison Matrix

The top ranking design criteria for the success of the glider as evaluated by the glider team are simplicity, cost, weight, launch vehicle size, launch stability, fast wing deployment, deployed wing structure stability, deployed wing aerodynamics, and control during the glide. Each of the design concepts was evaluated by whether or not it would sufficiently satisfy each of these design criteria. A matrix of how many of the criteria each glider satisfies is in table 3.1.

Table 3.1 Design Comparison Matrix

Design Criteria	Inflatable Wing	Dual Hinged	Single Hinged	Telescoping Wings	Extension Spar
Simplicity	Yes	No	Yes	No	Yes
Cost	No	No	No	No	Yes
Weight	Yes	No	No	No	Yes
Launch Size	Yes	No	No	No	Yes
Launch Stability	Yes	Yes	Yes	Yes	Yes
Fast Deployment	Yes	No	No	No	Yes
Wing Structure Stability	No	Yes	No	Yes	No
Wing Aerodynamics	Yes	No	No	Yes	No
Glide Control	Yes	Yes	Yes	Yes	No

The comparison matrix clearly shows that the inflatable wing glider and the extension spar glider are the strongest glider design candidates based on the design criteria list. The criteria in the table are sorted by general criteria, criteria for launch, criteria for wing deployment, and criteria for the glide

Advanced Logistics Delivery System

phase. The inflatable wing glider appears to be a strong candidate in all areas of the criteria whereas the extension spar glider is only a strong candidate up until the wings are deployed. After that point it does not satisfy any of the design criteria. The dual hinged wing glider and the telescoping wing glider also appear to be decent candidates over the actual flight of the glider but they do not satisfy the overall criteria.

3.2 Glider Design Selection

The design criteria matrix reduced the number of possible glider design from five to two designs. The two remaining designs are the inflatable wing glider with the aircraft body shape and the telescoping wing glider with the simple aerodynamic shape. The inability of the extension spar glider to perform efficiently in the glide phase of the flight because of the lack of an aerodynamic shape in the flat wings kept it from being one of the top two choices because the glide region of the flight is the longest portion and will determine exactly how much range the glider can achieve. In figure 3.1 the decision tree showing how the glider team arrived at their final glider design is shown.

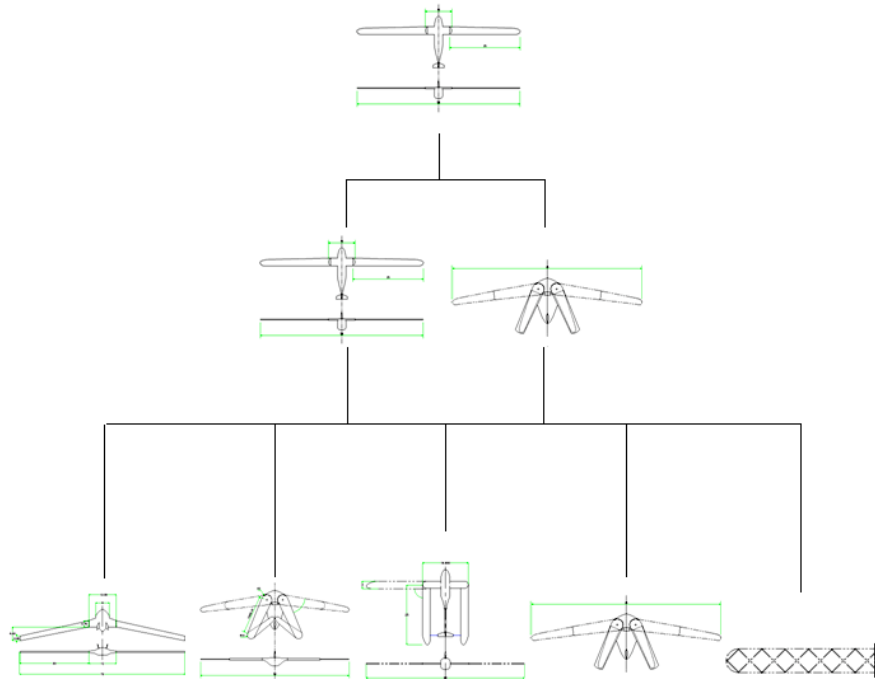


Figure 3.1 Glider Design Decision Tree

3.3 Final Glider Design

As the decision tree above shows, the final glider design chosen from the initial 5 designs concepts is the inflatable wing design with the aircraft shaped fuselage. The inflatable wing glider was chosen for its mechanical simplicity, its potential for being low cost, its low weight, and its potential for superior aerodynamic performance during wing deployment and the glide. The final configuration for the inflatable wing glider is discussed in the next chapter.

Chapter 4: Final Glider Configuration

4.1 Introduction

The glider configuration discussed in this section is a general overview of the glider design. Most of the reasons for why the glider configuration appears this have not yet been discussed, but will be discussed throughout the remainder of the report. The glider configuration assumes a chemical reaction of the same type as the one used in car airbags will be used for the inflatable wing deployment. The actual discussion of how the “airbag” process works is covered in Chapter 9.

4.2 Original Glider Configuration

The inflatable wing glider design was chosen as the design concept that would best accomplish the main object of the project without violating any of the RFP requirements. Instead of using the simple aerodynamic shape of the flying wing for the glider fuselage the more streamlined shape of the Nimbus 2, see table 6.1, was chosen for the fuselage. The original glider design is pictured below in figure 4.1.

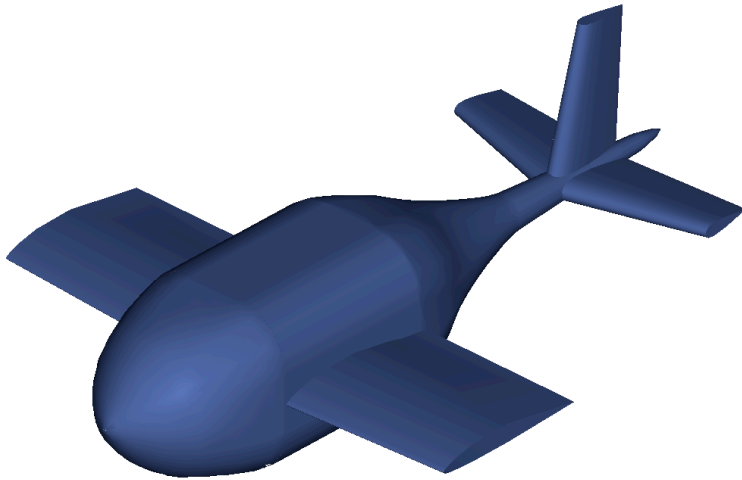


Figure 4.1 Original Glider Launch Vehicle

For the inflatable wing glider configuration, the fuselage is separated into three sections. The nosecone will provide space for the airbag fuel, assuming that a fuel holding tank can be made to the desired dimensions. The center section of the fuselage will be used mainly to enclose the payload and direct the airbag fuel to the spars. The rear section of the fuselage will be used to hold the avionics assembly, including the power supply and antennas. Figure 4.2 shows the internal configuration for the glider from the top.

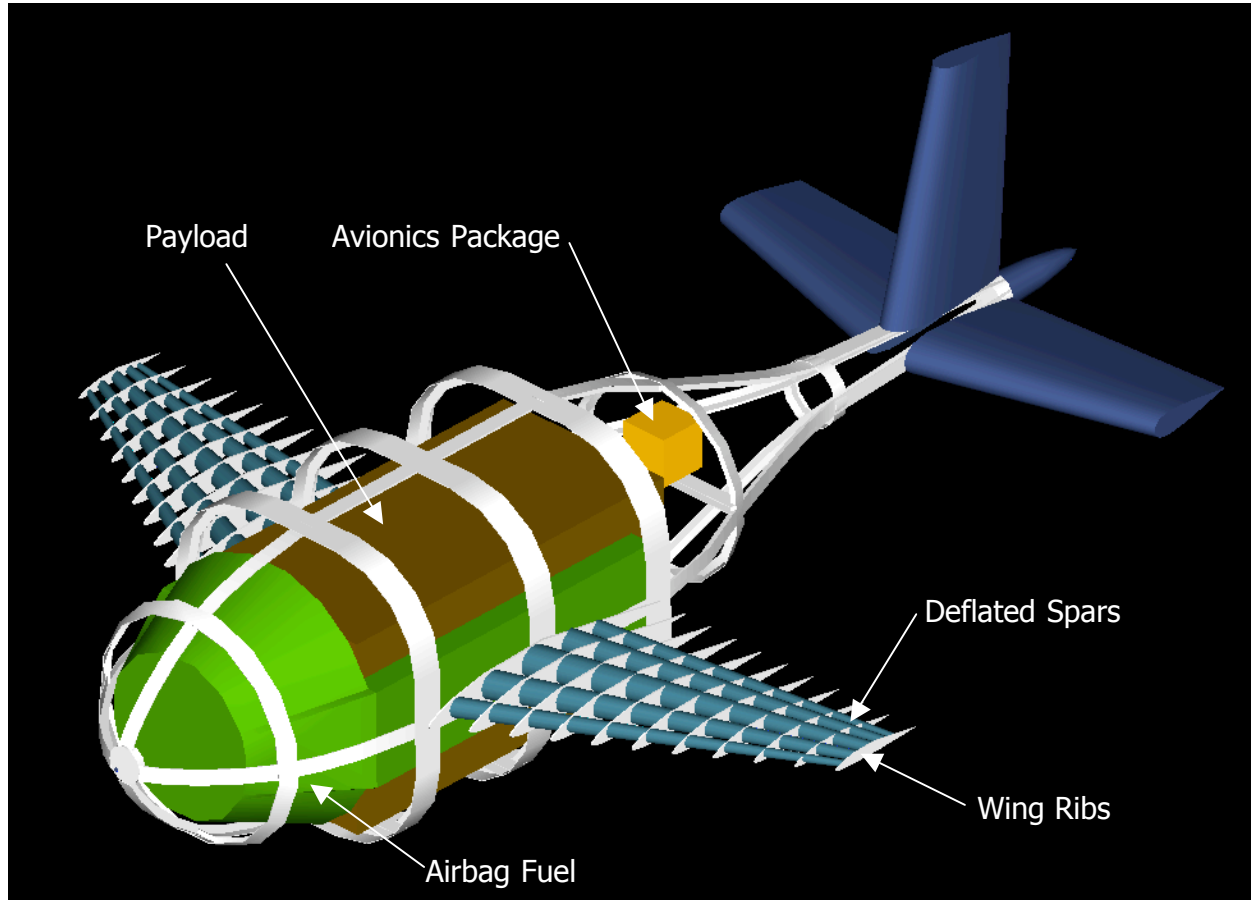


Figure 4.2 Top View of Internal Configuration

The airbag fuel tank consists of a larger, truncated, cone shaped unit that will hold the majority of the fuel, and two smaller rectangular arms that extend around the sides of the payload. These two arms will also hold fuel, and have extending cylinders that connect to the inflatable spars through holes in the fuselage skin. The fuel, when reacted, will be directed into the inflatable spars and extend the wings for the glide phase.

The payload is a 2x2x4 ft. box that sits in the center portion of the fuselage on cross beams connected to the fuselage ribs. The dimensions of this payload package were determined by considering the following criteria. First, it is required to hold a 1,000 lb payload and assuming the load has an average density of water, these dimensions will meet this weight requirement. Second, the payload box has to be of valid size to hold various supplies for ground troops. Making a package

Advanced Logistics Delivery System

1X1X16 ft. would help in streamlining the fuselage, but restrict bulkier materials that may need to be transported. Finally, a rectangular shape was chosen rather than a cylindrical so that the payload boxes could be stacked and stored easily on the ship. This shape will maximize the amount of payload stored per unit volume of holding space on the ship.

The rear section of the fuselage, although the longest component of the three, does not provide much room for storage because of its streamlined shape. Therefore it houses the avionics package, power supply, and antennae, which sit behind the fuselage on a cross beam connected to a fuselage rib.

A general assembly procedure for the fuselage and the components that it houses will proceed as follows. The avionics package will first be mounted in the rear section of the fuselage. The center section of the fuselage will then be attached to the rear, and the payload will be placed into the center section and secured in place. The airbag fuel tank will then be secured around the payload with the “arms” of the airbag fuel going on the right and left sides of the payload. The nosecone will then be attached to the center component of the fuselage, completing the assembly.

4.3 Final Glider Configuration

The design described above was refined to result in a more aerodynamic final glider design. A major change in the RFP, that the glider could be longer than 15 ft, made many of these changes possible. One of the first changes that can be seen in the glider configuration is the shape and size of the fuselage. For the initial concept, shown in figure 4.3, the fuselage had a bulky front section that tapered off rapidly to the tail. The sides of the fuselage were flat, and curves wrapped around the corners of the payload box; which had dimensions 2 X 2 X 4 feet giving a total volume of 16 cubic feet. The chord wise length of the fuselage was 15 feet, and had a cross sectional width of 3 ft. The final glider design is shown in figure 4.4.

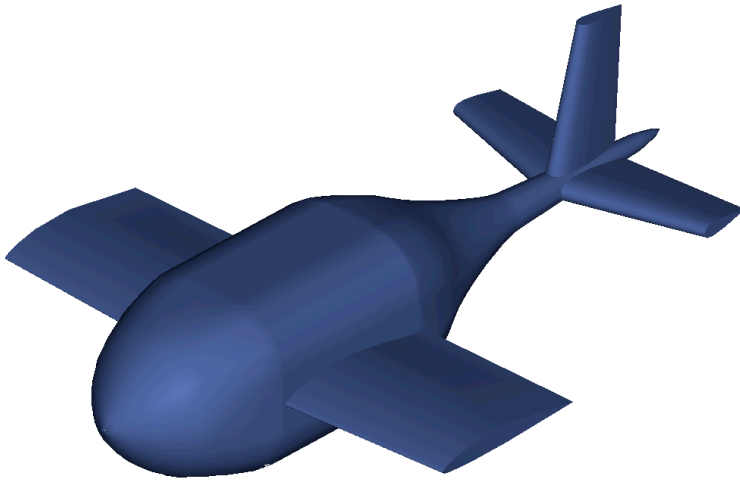


Figure 4.3 Original Launch Vehicle Design

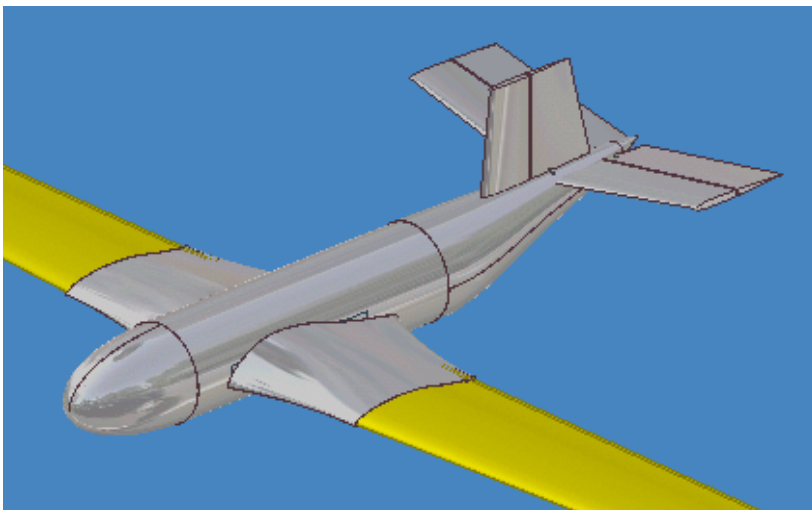


Figure 4.4 Final Glider Design

One of the changes made to the glider was the cross sectional shape of the fuselage. It is now circular with a diameter of 2.5 feet. One of the motivating factors for this change was the decision to change the size and shape of the payload. The payload used for the final design has dimensions 1.5 X 1.5 X 9 feet giving a total volume of 20.25 cubic feet. The change in the payload box was made for three reasons. The first being that a greater volume of material can be transported, increasing from 16 to 20.25 cubic feet. This volume of 20.25 ft allows for bulkier cargo that is less dense than water and

Advanced Logistics Delivery System

still maintains the 1000 lb payload. The payload is exactly equal to 1000 lbs when 40% dry cargo is used and 60% wet cargo is used, based on the average dry and wet cargo densities of 21 lb/ft^3 and 62.4 lb/ft^3 respectively. The second reason is due to the shipping procedures of naval material. Supplies are currently shipped using 3 X 3 X 3 ft. pallets; the revised shape of the payload box will allow for 3 individual 1.5 X 1.5 X 3 ft. rectangular boxes from each pallet to be loaded into the fuselage, as shown in figure 4.5.

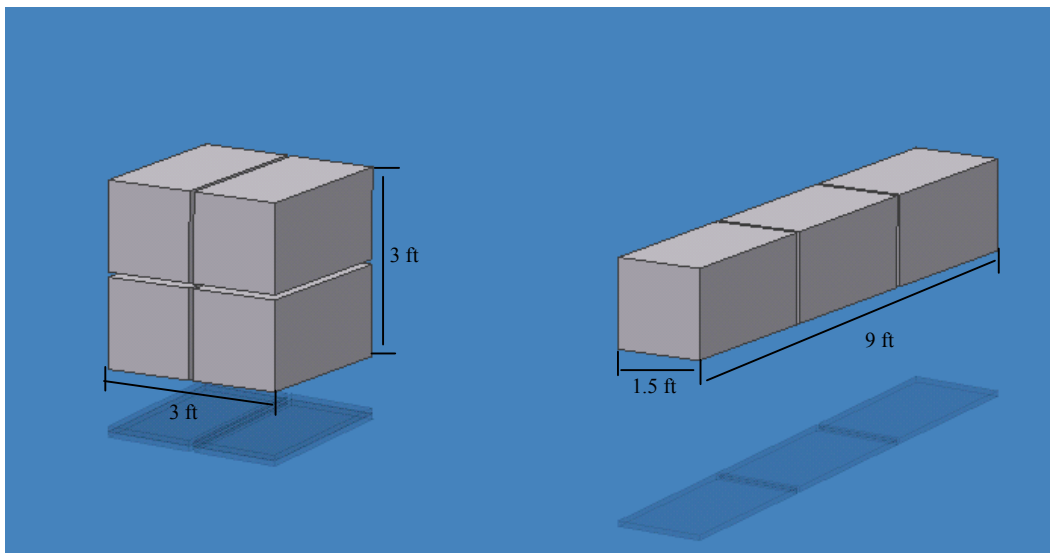


Figure 4.5 Payload Box Stacking

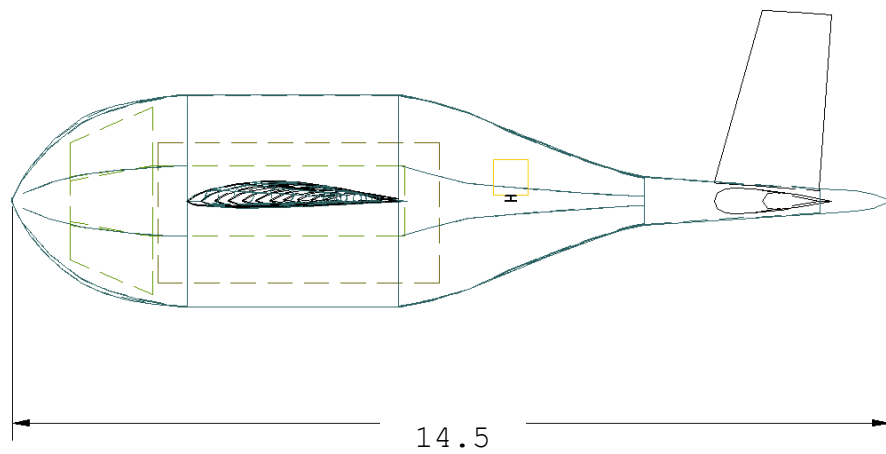
The third reason for changing the payload dimensions is so that the fuselage can be constructed in a more streamlined shape. The initial glider concept had abrupt curves that would have caused high drag due to flow separation. The revised fuselage has a more gradual aft section that will reduce this problem.

The overall length of the glider has also been changed from 14.5 to 18.5 feet. This was done so that the new payload box could be contained within the fuselage, and also allowed the tail to be moved further back, creating greater control moments when control surfaces are deflected. It should also be noted that the tail has been elevated in the final concept. This was done to reduce the amount of

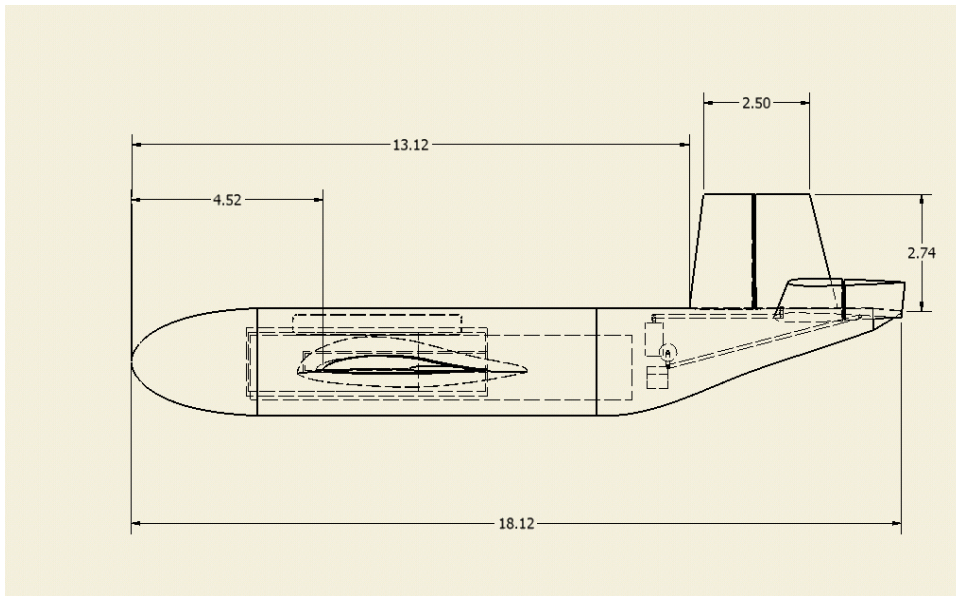
Advanced Logistics Delivery System

separated flow that will come in contact with the tail, which creates the potential for control problems.

Figures 4.6 and 4.7 show the original and final glider design concepts from a side profile. These figures show the change in length and the elevated tail section.



4.6 Original Glider Side Profile



4.7 Final Glider Side Profile

Advanced Logistics Delivery System

Further design was also done on the solid structure wings that attach to the fuselage and hold the inflatable wing material. In the initial concept, solid wing sections were shown, but structural concepts were ambiguous. The final design concept has a banjo frame design that will provide structural support and allows the necessary volume needed to hold the deflated wing material. This design will also aid in the streamlining of the fuselage by decreasing the sharp angles at the connection points of the fuselage and solid wing structures.

The sodium azide storage tank, which holds the fuel for the wing inflation, has also been modified after calculations showed that less than half of the expected volume was needed. The front conical section in front of the payload box is no longer necessary; the sodium azide that will be used to inflate the wings can be contained in the “arms” alone. This provides a reduction in weight, and will allow access to the payload box through the nose of the aircraft following landing. Figure 4.8 shows the final sodium azide storage in grey as well as the other internal structures of the glider. Figure 4.9 shows the original sodium azide storage in green.

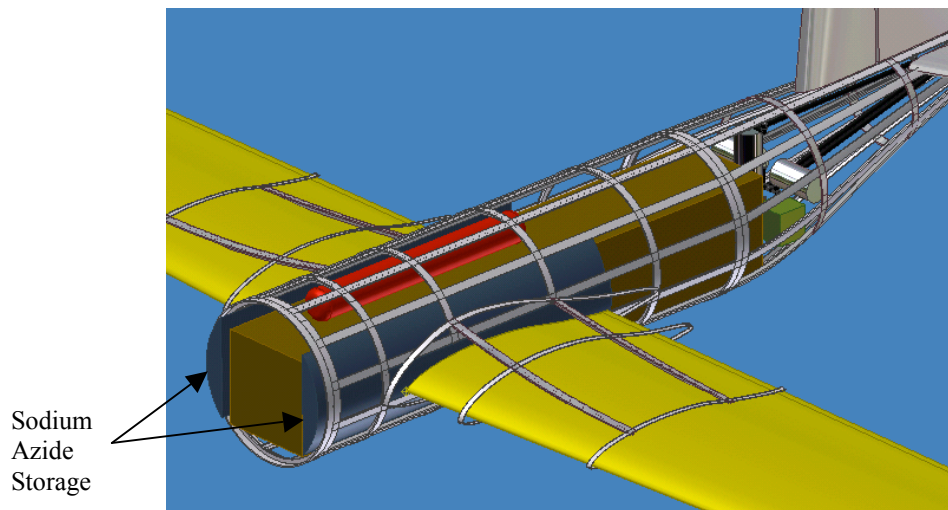


Figure 4.8 Final Glider Internal Arrangement, no Sodium Azide in Nose Cone

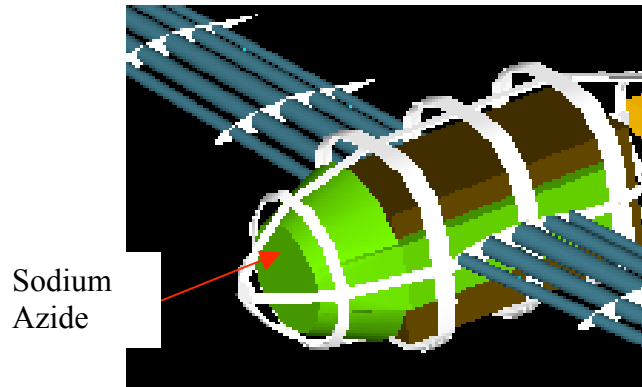


Figure 4.9 Original Glider Sodium Azide Tank Close-up.

A nitrogen tank was added above the top of the payload to control inflation during the glide phase, it is the red cylinder on top of the payload box in figure 4.8. This tank will allow for corrections to wing pressure to be made after the original inflation and is described in Chapter 9. The cylindrical cross section of the fuselage and position of the payload box allows clearance for this additional part.

Lastly, servo motors were added to the rear section of the fuselage, and are used to deflect the control surfaces on the tail of the glider. These motors, along with the avionics package and supplementary battery pack are bracketed to the frames and stringers of the fuselage, behind the payload. Control linkages extend back from these motors to the horizontal stabilizers and the rudder. The motors and avionics packages are shown in figure 4.10 and 4.11. Also in figure 4.11 the nitrogen tank placement on top of the payload box can be seen.

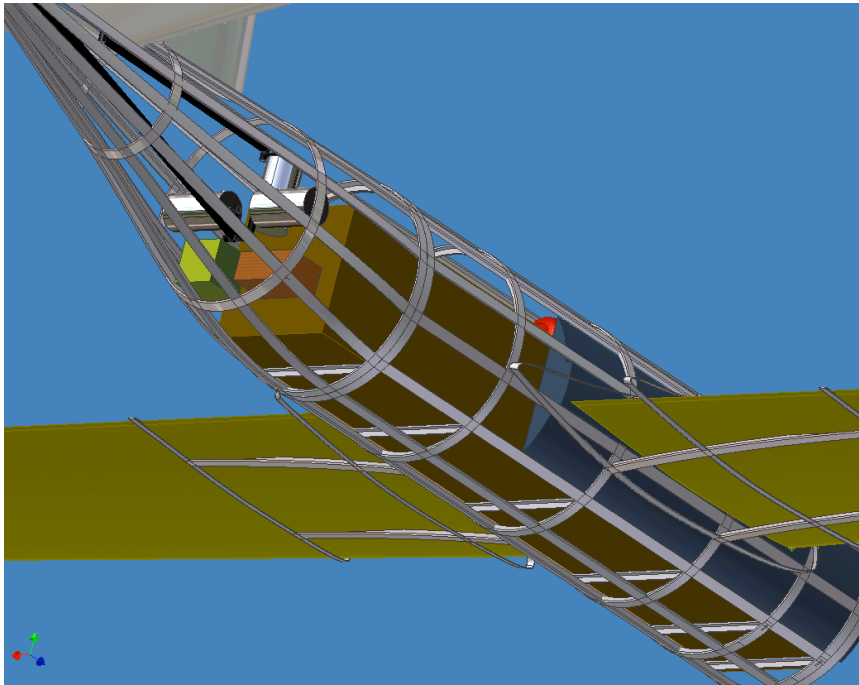


Figure 4.10 Rear View of Internal Arrangement of Motors and Avionics Package

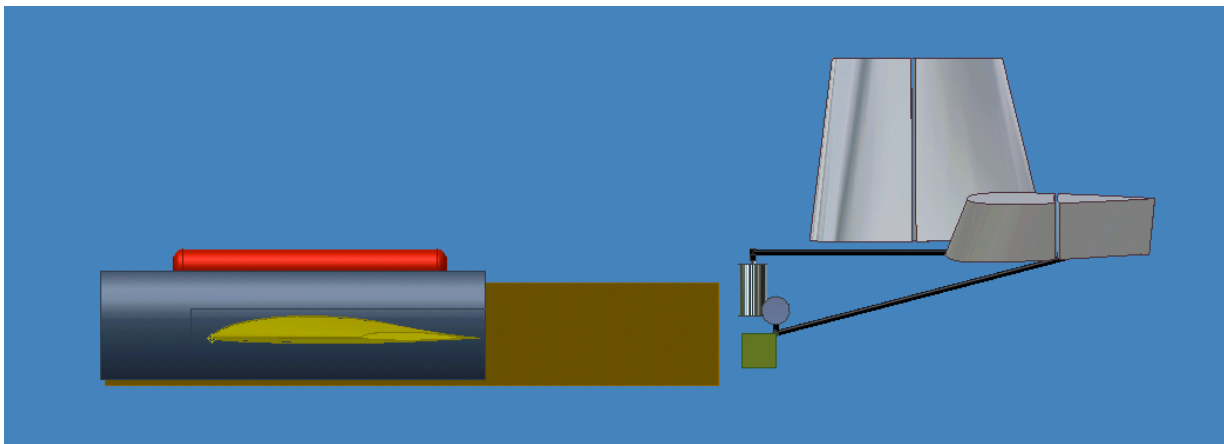
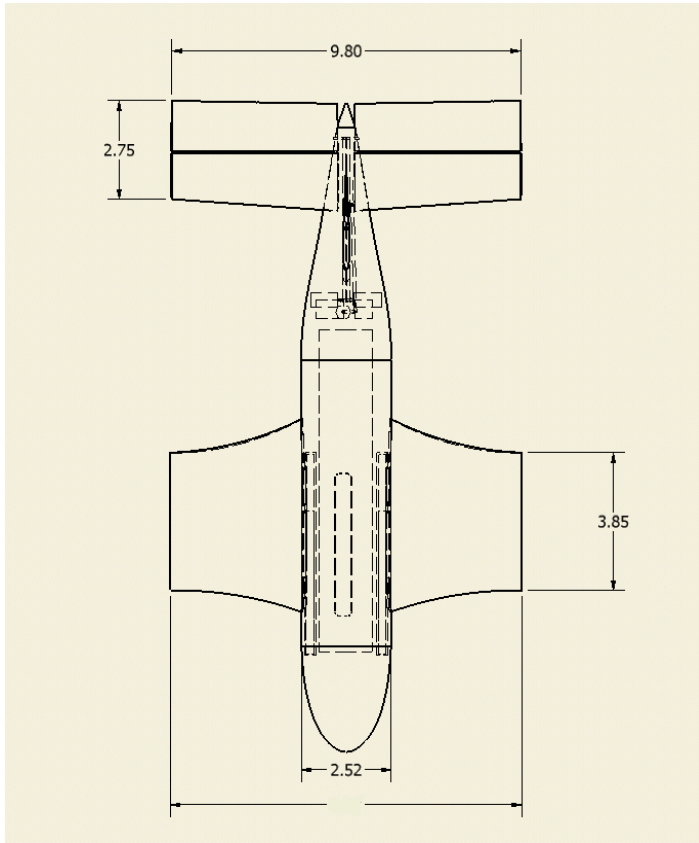


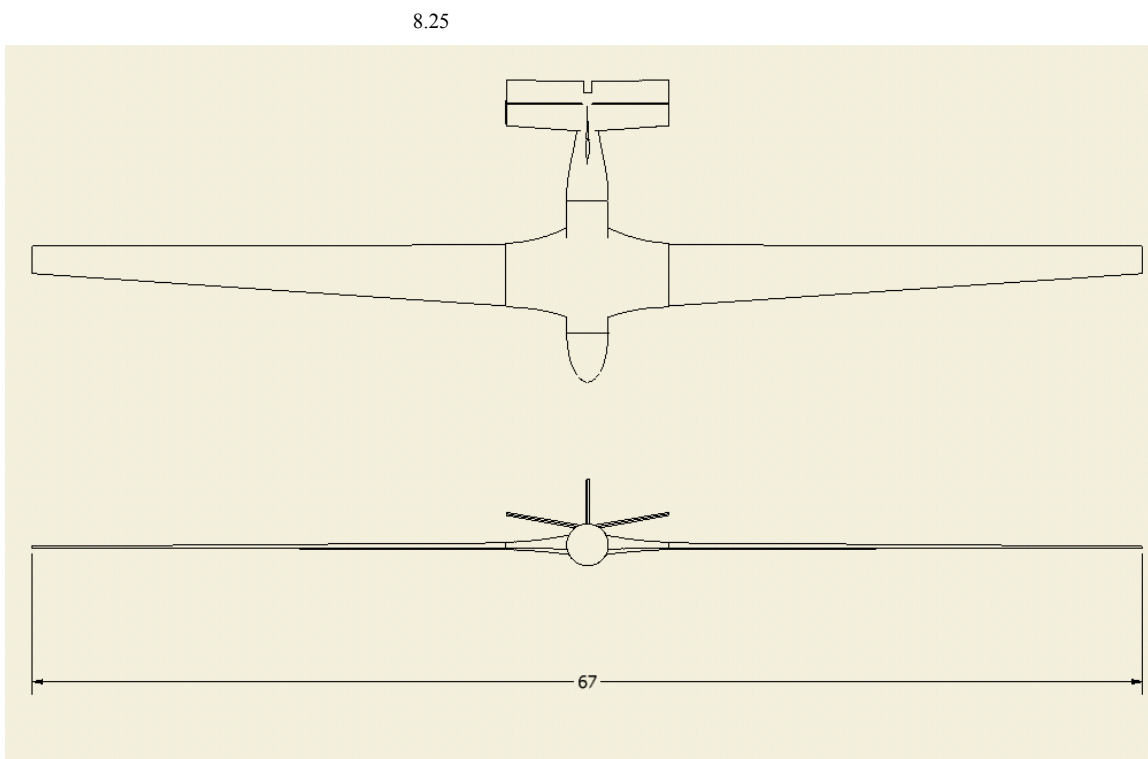
Figure 4.11: Side View of Internal Structures

The finalized dimensions of the launch vehicle are shown in figure 4.12. The expanded wing span dimension is shown in figure 4.13 as well as a frontal view of the glider.

Advanced Logistics Delivery System



4.12: Dimensioned Top View



4.13: Dimensioned Top and Frontal View with Wings Deployed

Chapter 5: Aerodynamics of the Launch and Climb

5.1 Introduction

There are two key factors in determining the range of a glider: the lift to drag ratio (L/D) and the altitude at which the wings are deployed. Currently, the best gliders and sailplanes can achieve a maximum L/D of around 40. This is not expected to be a reasonable approximation for what the ALDS will be able to achieve because it incorporates an inflatable wing, which will hinder the aerodynamics of the vehicle. For this reason an L/D ratio of 33 is used as an estimate for this section of the report. With the 50 mile range requirement and an L/D around 33, the glider needs to reach an altitude of 8000ft. This section will focus on achieving this height and even surpassing it if possible, since an increased apogee height would allow for a lower L/D which would in turn lower the costs of each vehicle. Two different approaches were studied to determine if and how the glider is to achieve this height. The first was to approximate the motion of the aircraft as a projectile, ignoring all aerodynamic effects, and the second was to consider controlling the launch vehicle such that it could generate lift and maintain a constant climb angle, which was suggested by Geoff Hope of Naval Surface Warfare Center, Carderock Division.

5.2 Projectile Motion

With the projectile motion model, it is assumed that the only force acting on the body is gravity. This is a considerable approximation since the glider will be launched at a speed of 500 knots and has aerodynamic controls allowing it to stay aligned with the flow, but was considered to be a good starting point. The standard kinematics equations (Eqns. 5.1 and 5.2) can be used to determine the flight path of the body.

Advanced Logistics Delivery System

$$s = s_o + \frac{ds_o}{dt}t + \frac{1}{2} \frac{d^2s}{dt^2}t^2$$

(Eqns 5.1 and 5.2)

$$\frac{ds}{dt} = \frac{ds_o}{dt} + \frac{d^2s}{dt^2}t$$

In these equations, s is the position of the body in the horizontal and vertical directions and t is time. The derivation of these equations is not included, but can be obtained in any standard physics textbook. The results of these equations are plotted in Figure 5.1 for a range of launch angles, α , and an initial velocity of 500 knots.

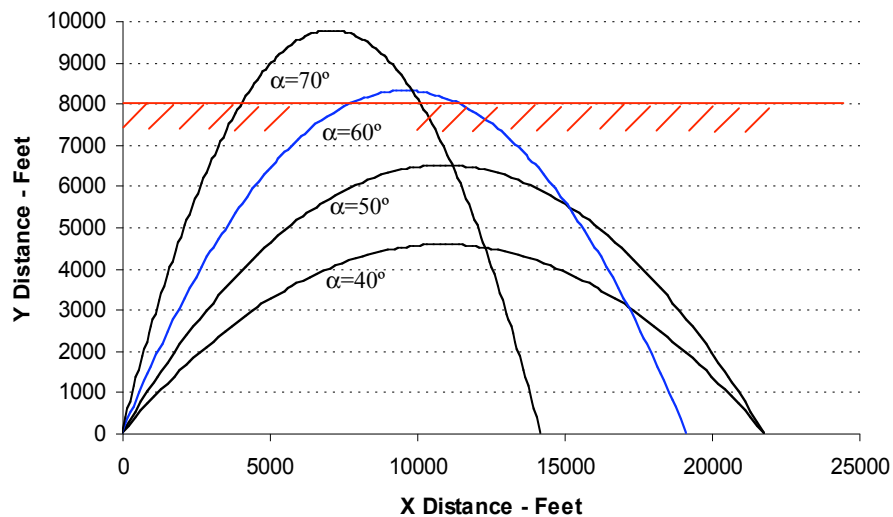


Figure 5.1: Projectile Trajectories at Various Launch Angles

This figure shows that under the projectile motion assumptions a launch angle of approximately 60° would be necessary to reach 8000ft. When this was discussed with the ship design group it was determined that a launch angle this large is not feasible and would result in increased load factors being imposed on both the glider and launch system. For this reason other methods of achieving the 8000ft mark were pursued.

Advanced Logistics Delivery System

5.3 Constant Flight Angle

In this situation, the glider is launched from the ship at a given angle and it is assumed to maintain a straight flight path using its aerodynamic controls. To maintain this flight path the launch vehicle must continually increase its angle of attack to compensate for the lost velocity. This process is continued up until a few seconds before the vehicle stalls, at which time the nose is pitched down and the wings are deployed. A free body diagram of the forces acting on the vehicle during this phase is presented in Figure 5.2.

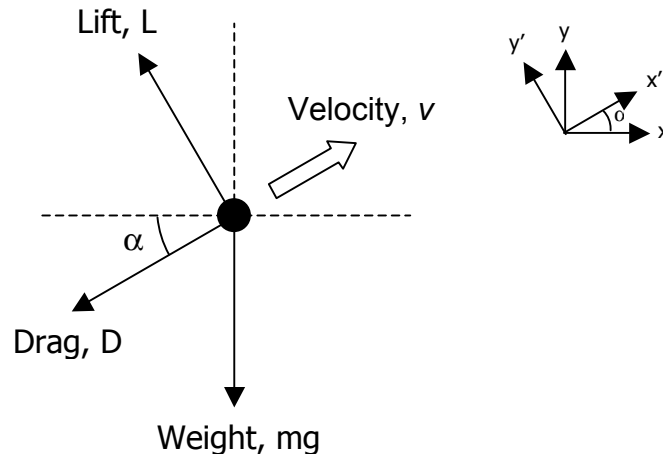


Figure 5.2: Free Body Diagram of ALDS during launch

Resolving the forces parallel, x' , and perpendicular, y' , to the direction of flight result in the following equations:

$$F_{x'} : -D - mg \sin \alpha = m \frac{d^2 x'}{dt^2} \quad (\text{Eqns 5.3 and 5.4})$$

$$F_{y'} : L - mg \cos \alpha = 0$$

To determine the magnitudes of the lift and drag forces, equations 5.5 and 5.6 were used. These include both the induced and parasite components of drag.

Advanced Logistics Delivery System

$$L = \frac{1}{2} \rho V^2 S C_L$$

$$D = \frac{1}{2} \rho V^2 S C_D = \frac{1}{2} \rho V^2 S \left(C_{D_0} + \frac{C_L^2}{\pi AR \epsilon} \right) \quad (\text{Eqns 5.5 and 5.6}) \quad (\text{Bertin, 2002})$$

In these equations, ρ is the density of the air, ϵ is Oswald's efficiency factor, S is the planar surface area, and AR is the aspect ratio of the wing. Substituting equations 5.5 and 5.6 into equations 5.3 and 5.4 yields the following equations of motion:

$$\frac{d^2 x'}{dt^2} = - \frac{mg^2 \cos^2 \alpha}{\frac{1}{2} \rho \left(\frac{dx'}{dt} \right)^2 S \pi AR \epsilon} - g \sin \alpha - \frac{\rho \left(\frac{dx'}{dt} \right) S C_{D_0}}{2m} \quad (\text{Eqns 5.7 and 5.8})$$

$$\frac{dy'}{dt} = 0$$

This system of second order differential equations could not be solved analytically, so the *ode45* function in MATLAB was used to solve them numerically. Figure 5.3 is a plot of the resulting apogee height that occurs at a $C_{L,max}$ of 1.0 over varying launch angles. As indicated on the graph, to reach the necessary 8000ft altitude a launch angle between 30° and 40° is required. Proceeding to a launch angle greater than this would allow the glider to reach higher altitudes, but the rate at which this increase occurs with respect to changes in launch angle decreases rapidly. And as mention previously, increases in launch angle result in significantly larger loads being applied to both the glider and launch system. So a launch angle of 30° was chosen with the idea that the extra couple of feet could be made up with optimization.

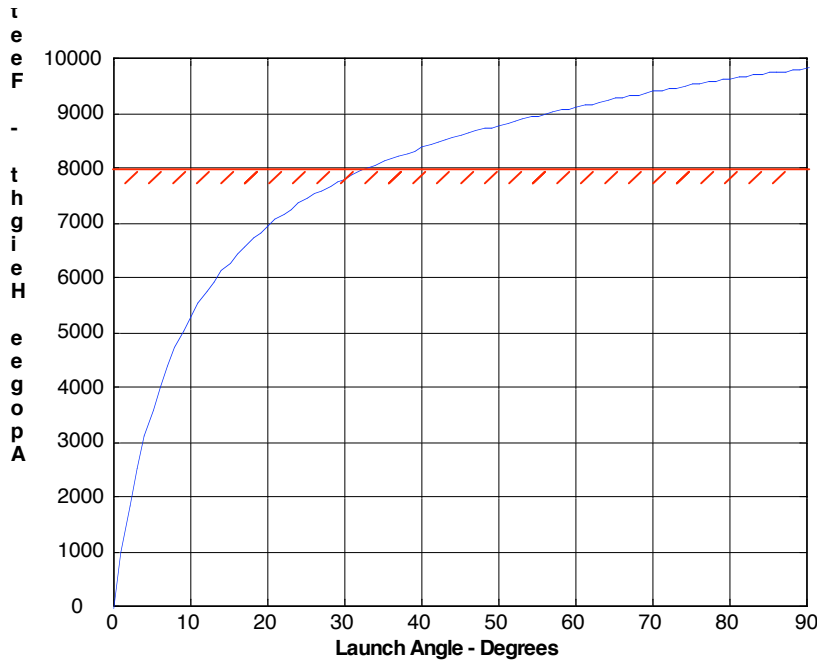


Figure 5.3: Variation of Apogee Height with Launch Angle

5.4 Performance Analysis

The original configuration of the launch vehicle had a wing span of 9.5ft, a chord length of 3.5ft, and a wetted surface area of 270ft². These dimensions were estimates used to compare and contrast many of the earlier concepts, but have not been optimized to provide the maximum height possible. To find these optimal values, sensitivity analyses were run using equations 5.7 and 5.8. To make these equations as representative as possible, Oswald’s efficiency factor was varied using the following equation:

$$\epsilon = \epsilon_0 \left(1 - \left(\frac{d}{b} \right)^2 \right) \quad \text{(Equation 5.9) (Raymer, 1999)}$$

where b is the wing span, d is the diameter of the fuselage, and ϵ_0 is the estimated value for the efficiency factor with the wings inflated. This variation in efficiency is necessary because during the launch phase the wing span is of a similar size compared to the diameter of the fuselage. If this were

not the case, as with most airplanes, then a change in wing span would have a greatly reduced effect on the efficiency factor. The results of this study can be seen in the following graphs:

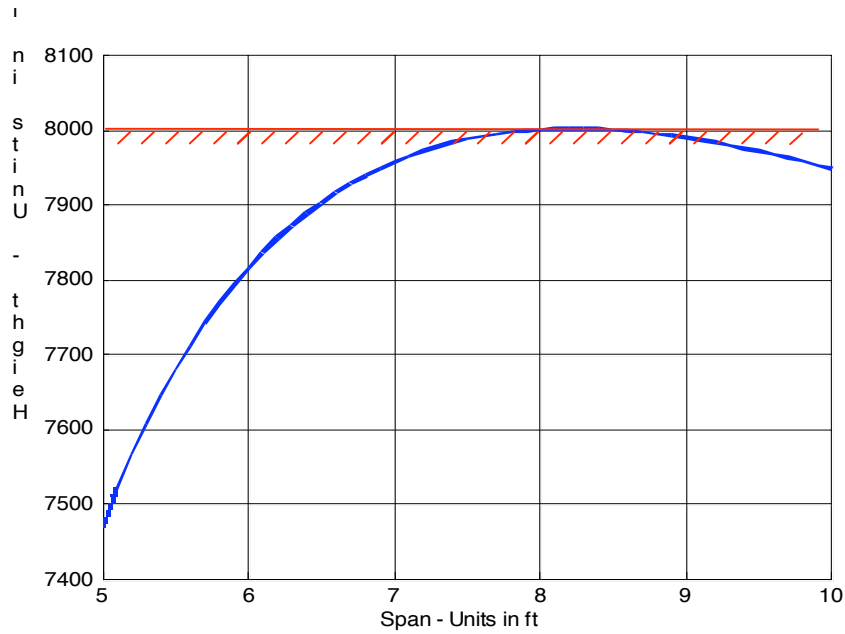


Figure 5.4: Variations in Apogee Height with Span

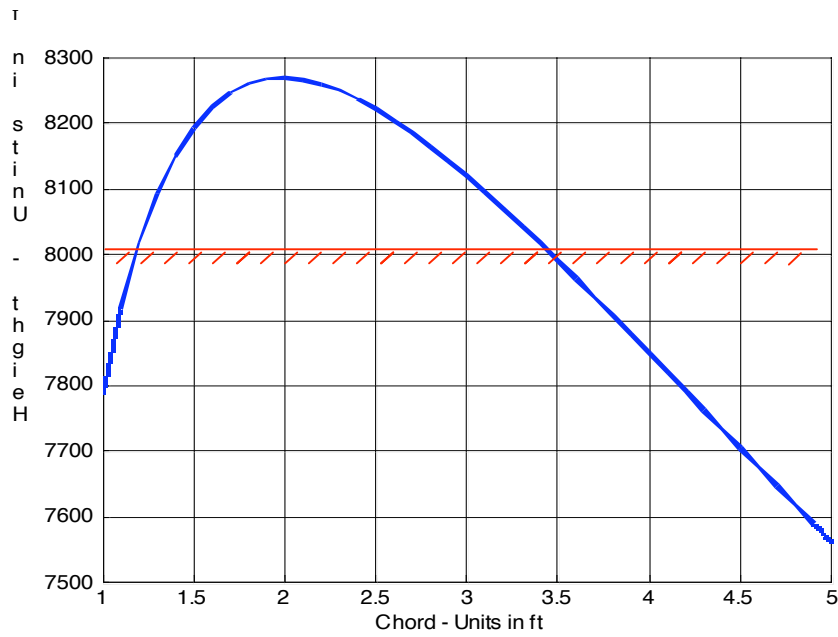


Figure 5.5: Variations in Apogee Height with Chord

Advanced Logistics Delivery System

Figure 5.4 shows that the initial wing span of 9.5ft should be decreased to 8.25ft to allow for an increase of approximately 50ft in altitude. This goes against intuition which would indicate that a decrease in span would result in a decrease in available lift and therefore a decrease in altitude, especially since C_{D0} is assumed to be constant. But upon further review of the equations of motion (Eqns 5.7 and 5.8), this relationship can be understood by considering the changes in acceleration due to this decrease in wing span. Figure 5.5, the sensitivity analysis for changes in chord length, also indicates that the chord length needs to be decreased to achieve higher altitudes. Just a 1ft decrease in length would allow the glider to gain an extra 200ft of altitude before the inflatable wings would be deployed. Unfortunately, decreasing the chord length would have an adverse effect on both the amount of structure in the wing and the flight characteristics during glide. These factors would decrease the overall range of the glider, so the chord length is left at 3.5ft.

An additional sensitivity analysis was also made for changes in sea level temperature to determine the range of weather conditions in which the glider would be able to operate. The results of this analysis are shown in Figure 5.6 and show that the launch vehicle will be able to achieve the 8000ft benchmark in dry weather conditions above 525°R (65.3°F).

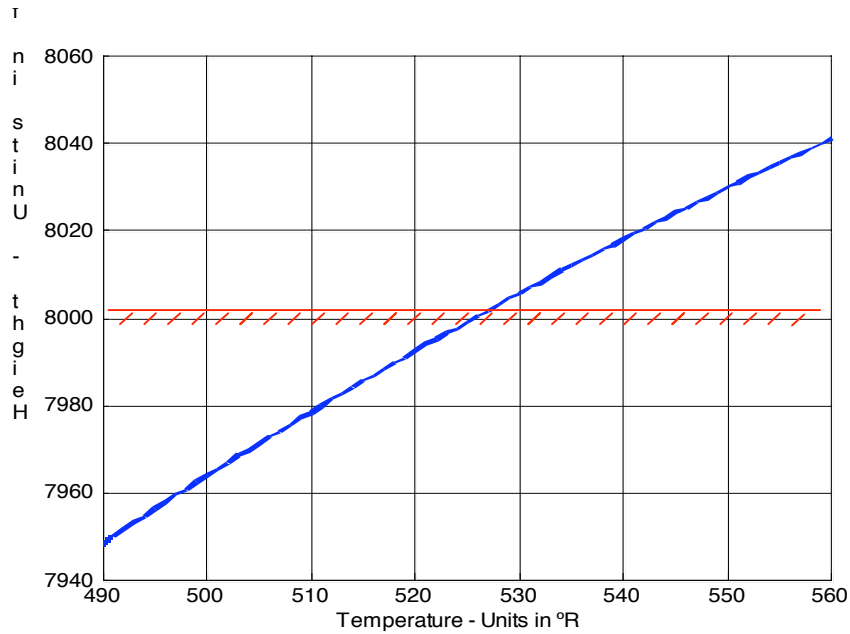


Figure 5.6: Variations in Apogee Height with Temperature

5.5 Drag Buildup

All drag calculations were done using the FRICTION program (Mason 2005). This program requires the input of a reference surface area, altitude, Mach number, characteristic length, the location of transition, and the fineness ratio for each component. With this information the program produces the following table and calculates the zero lift drag coefficient.

Table 5.1: ALDS Zero Lift Drag Buildup During Launch (Mach = 0.76)

	Characteristic Length (ft)	Re	C _f	FF	S _{wet} (ft ²)	C _{D0}
Fuselage	18.13	8.83E+07	0.00202	1.0952	117.00	0.0057
Wings	4.62	2.25E+07	0.00247	1.3587	68.89	0.0051
Horizontal Tail	2.88	1.40E+07	0.00266	1.4400	57.50	0.0048
Vertical Tail	2.75	1.34E+07	0.00268	1.4400	25.00	0.0021
C_{D0} Total						0.0177

The input for this data was taken from the optimized dimensions determined in the following section and show that the zero lift drag coefficient, C_{D0}, is estimated to be around 0.0177, a full 23 counts lower than the initial estimate of 0.02.

Chapter 6: Aerodynamics of the Glide

6.1 Introduction

The primary goal once the wings are deployed at the apex of the flight is finding ways to reduce the drag as much as possible, and therefore maximizing the lift to drag ratio and increasing the range of the glider. Some of the means considered for reducing drag were wing sizing, the reduction of skin friction over the glider, and analysis of high lift airfoils. All analyses were done based on the launch apogee calculations described in the previous section, where the ALDS glider is required to have at least a maximum lift to drag ratio of 33 to glide for 50 miles from an apogee height of 7750 feet.

6.2 Initial Geometric and Performance Calculations

A comparison of previously built gliders that have weights around 1500 pounds was conducted to get a perspective on how the glider should be sized. Four gliders that have similar specifications to each other and to requirements of the ship launched glider are listed in Figure 6.1. A general approximation based on the aspect ratios of the gliders in table was made for ALDS and was estimated to be some where in the area of 25 to 30.

Advanced Logistics Delivery System

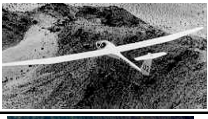
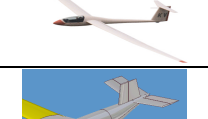
Glider Name	Weight (lbs.)	Wingspan (ft.)	Wing Area (sqft.)	Mean Chord Length (ft.)	Aspect Ratio	L/D Max	Airfoil (Root/Tip)	Picture
604 Glasflugel	1230	72.17	175	2.42	29.8	49	Wortmann FX 67-K-170/FX 67-K-150	
Caproni A-21	1420	66.9	174.3	2.61	25.65	43	Wortmann FX 67-K-170/FX 60-126	
Sportina Aviacija LAK 12 Lietuva	1433	67	157.5	2.35	28.5	50	Wortmann FX 67-K-170	
Nimbus 2	1433	66.6	154.9	2.33	28.6	49	Wortmann FX 67-K-170/FX 67-K-150	
Advanced Logistics Delivery System Glider	1500	67	174.2	2.60	25.77	33	Wortmann FX 67-K-170/FX 67-K-150	

Figure 6.1 Glider Comparison Chart

Once the range of aspect ratios was determined, the taper ratio and efficiency factor were calculated using Simple Lifting Line Theory (Mason, 2005) and assuming that there is no wing twist. A graph of the overall wing efficiency versus the taper ratio is shown in Figure 6.2. The graph was made using inputs of the angle of attack in reference to the zero lift angle of attack, the aspect ratio, the taper ratio, and the angle of incidence for the root and tip foil. Finding the efficiency only depends on the taper ratio, aspect ratio, and incidence angles, so nominal values of the angle of attack were used for plotting the graph in Figure 6.2.

Advanced Logistics Delivery System

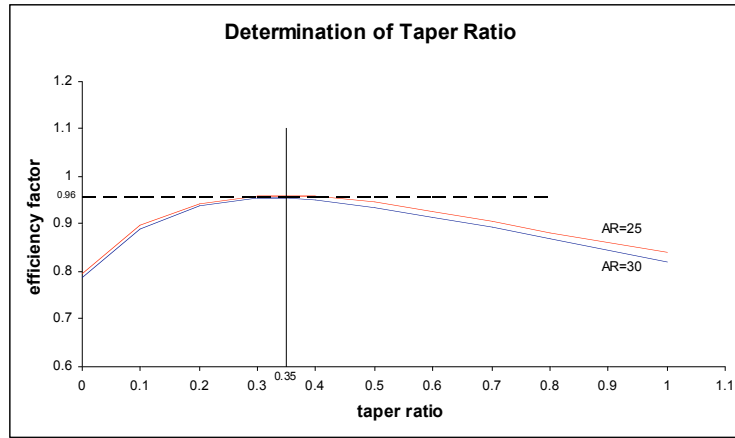


Figure 6.2 Taper Ratio versus Efficiency Factor

After repeated runs for various taper ratios, aspect ratios of 25 and 30, and incidence angles of zero degrees, a range of maximum efficiency was determined to be between 0.9601 and 0.954 at a taper ratio of 0.35. To get the highest efficiency possible, a mean chord of 2.6 and span of 67 feet were used, which corresponds to an aspect ratio of 25.77 with an efficiency of 0.96. With the taper ratio of 0.35, the root chord and the tip chord were determined to be 3.852 feet and 1.348 feet respectively. From the geometry determined above, the initial performance calculations for the ALDS glider were calculated using the equations in Table A1 in Appendix A that were compiled from Bertin, 2002 and Marchman 2001 and are presented below in Table 6.1.

Table 6.1: Initial Calculations for the ALDS Glider with a Range of 50 Miles

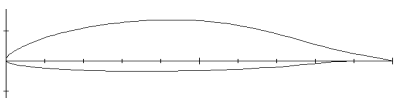
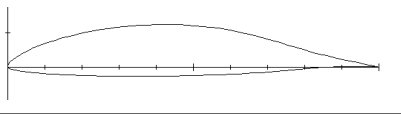
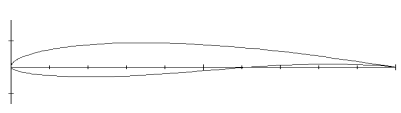
Advanced Logistics Delivery System Glider Design Requirements			
Weight (lbs.)	1500	C_{Lmax}	1.1775
Range (ft.)	264000	V_{max} (ft/s)	88.106
L/D_{max}	33	Mach Number	0.0811
Minimum Altitude (ft.)	7750	C_{D0}	0.01784
Aspect Ratio	25.77	C_{Di}	0.01786
Span (ft.)	67	C_D	0.0357
Root/Tip Chord (ft.)	3.852/1.348	Glide Angle (deg.)	-1.74
Wing Area (sq. ft.)	174.2	Minimum Sink (ft/s)	-2.68
Efficiency Factor	0.96	Root Reynolds Number	1780000
Taper Ratio	0.35	Tip Reynolds Number	623000

6.3 Airfoil Boundary Layer Analysis

Skin friction and pressure drag coefficients are the two components of the zero-lift drag coefficient that can be easily calculated for the wings, fuselage, and tail. The wings account for roughly fifty percent of the overall zero lift drag coefficient, which makes the wing airfoils the primary concern, specifically in the case of the ALDS glider, because the majority of its span is comprised of inflated material. Judging by the previously calculated zero lift drag coefficient of 0.01784, the estimated zero lift drag coefficient of the wing is 0.00892.

For the ALDS glider, the only way to obtain high lift is from the geometry of the airfoil. For the airfoil analysis, the airfoils from the gliders in Figure 6.1 were used. Every glider in the chart used the Wortmann FX 67-K-170 as its root airfoil, which is a good indication of its performance. As for the tip airfoil, the gliders used the Wortmann FX 60-126, the Wortmann FX 67-K-150, and the Wortmann 67-K-170. The root and tip airfoils that are displayed in Table 6.2 were analyzed at their respective Reynolds numbers of 1.78×10^6 and 6.23×10^5 .

Table 6.2: Analyzed Airfoil Profiles

Airfoil	Thickness (%c)	Leading Edge Radius (%c)	Camber (%c)	Trailing Edge Angle (deg)	Profile
Wortmann FX 67-K-170	0.1701	0.0087	0.0507	16.79	
Wortmann FX 67-K-150	0.1498	0.0081	0.0483	9.861	
Wortmann FX 60-126	0.1259	0.0095	0.0356	6.52	

All the boundary layer analyses were done using XFOIL 6.9 (Drela, 2005). The input requirements for the program are the Reynolds Number, the Mach number, the airfoil contours, and the angle of attack. The program can output a variety useful data and can analyze the airfoil over ranges of

Advanced Logistics Delivery System

angle of attack or lift coefficients. The primary output analyzed was the point of transition on the airfoil, the angle of attack that maximum lift to drag ratio occurs, and the value of the zero lift drag coefficient at the maximum lift to drag ratio of the airfoil. After boundary layer analysis of the root and tip foils, the Wortmann FX 67-K-170 was determined to be adequate for the root airfoil and the Wortmann FX 67-K-150 was used for the tip airfoil.

While in flight, the airfoil is going to see a possible decrease in internal pressure as the ALDS glider decreases in altitude. When the wings are inflated at an altitude of around 8000 feet, the external pressure will be 10.92 psi and when the glider lands the pressure is going to be around 14.70 psi. The airfoil will be inflated to a pressure of 1000 psi (justification for this number is found in chapter 8) to keep rigid against the lifting forces that are expected in the glide phase, so deflation due to the altitude decrease will be minimal.

Major losses in lift could occur if the inflatable airfoils were to transition to turbulent flow due to a non-rigid wing. In order to simulate deflation of the airfoil, the contours of the airfoil were modified using a simple sine wave modification that is illustrated in Figure 6.3. The figure shows an exaggerated view of how the airfoil was expected to lose pressure. The sine

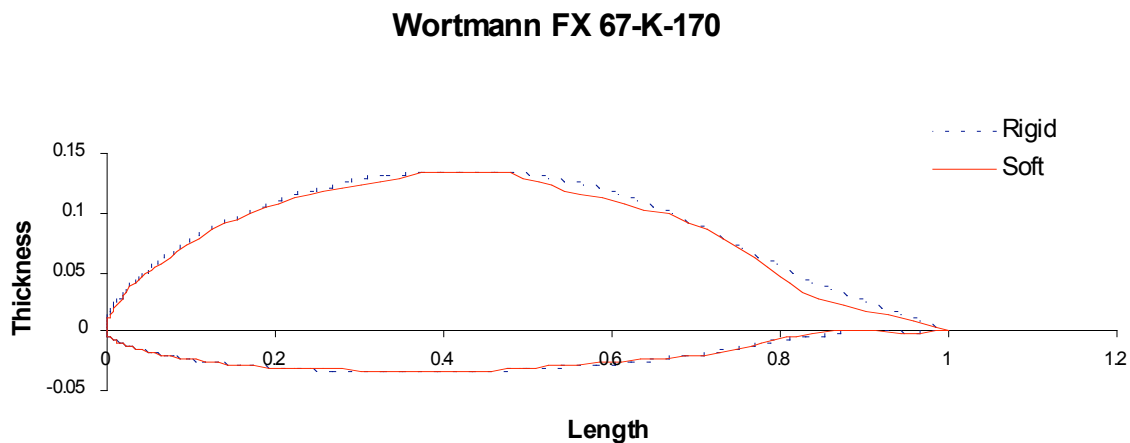


Figure 6.3: Exaggerated View of Wing Deflation

Advanced Logistics Delivery System

wave approximation was made so that there was smooth transition between contour points so boundary layer analysis could be conducted. The wing will be fitted with a pressure valve that will increase the airfoil pressure from a spare onboard tank if pressure drops by 10 psi, which translates to a one percent change in the airfoil contour position. The original and modified contours are presented in Figure B1 and Figure B2 in Appendix B. A comparison of the zero-lift drag coefficients and section lift coefficients for both airfoils are shown in graphs in Figure B7 and Figure B13 in Appendix B and the maximums are compared in Table 6.3. The graphs show how the Wortmann FX 67-K-170 has a much greater loss in lift after deflation than the Wortmann FX 67-K-150. Even with a one percent loss of pressure inside the wing, the zero lift drag on the wing was below the maximum allowable drag coefficient of 0.00892.

Table 6.3 Comparison of Rigid Wing and a One Percent Deflated Wing

Airfoil	Type	CD0wing	% Change	Cl	% Change
Wortmann FX 67-K-170	Rigid	0.00629	21.62	1.0651	0.16
	Deflated	0.00765		1.0634	
Wortmann FX 67-K-150	Rigid	0.00852	-6.34	1.0367	9.59
	Deflated	0.00798		0.9373	

When the airfoils were deflated one percent, a laminar bubble formed along the upper surface of the airfoil. Graphs of the skin friction coefficient along the root and tip airfoil shown in Figure B3 and Figure B9 in Appendix B show that a laminar bubble forms at about 0.466 chord for the root airfoil and a small laminar bubble forms at about 0.5 chord on the tip airfoil. In an effort to further reduce the drag when the airfoil is partially deflated, the flow was tripped at 0.466 chord and transition was forced. A comparison of the lift and drag coefficients between the airfoil with the laminar bubble and the airfoil when the flow was tripped is presented in Figure B8 in Appendix B. The graph showed that tripping the flow before the formation of the laminar bubble had a relatively small effect on the overall values of lift and drag of the airfoil.

Advanced Logistics Delivery System

Tripping the flow also gave a view of what would happen if the airfoil lost enough pressure to trip the flow in front of the normal transition point. The airfoil requires the highest internal pressure at its leading edge, which is described in the section on internal wing structure. When a loss of pressure does occur, the leading edge surface will be the first area to see the effects. The graph in Figure B8 in Appendix B depicts how a loss of lift and an increase in drag occurs as the trip point moves further up chord of the airfoil.

6.4 ALDS Gliding Drag Analysis

Along with the drag generated from the wings of the glider, there is drag attributed to the fuselage, the horizontal tail, and the vertical tail. Analysis of the skin friction and pressure drag created by the fuselage, horizontal tail, and vertical tail were conducted using Friction (Mason, 2005). Combining the drag output from the Friction program and the zero lift drag coefficient of the wing provided by XFOIL will produce the overall drag of the glider in gliding flight.

To run the Friction program, certain aspects of the fuselage and tail needed to be calculated. For each component, the wetted area, reference length, and thickness ratio need to be calculated and whether the body is a planar body (the tail surfaces) or a body of revolution (the fuselage) and whether the flow is turbulent or laminar needs to be determined. Based on comparisons of tail airfoils for conventional gliders, the horizontal and vertical stabilizers are going to use the Wortmann FX 71-150/30 airfoil section. The flow was assumed turbulent over all surfaces to get the maximum drag on the aircraft. The inputs and outputs for the Friction program can be found in Figure B14, Appendix B. From the Friction program, the drag coefficient expected on the fuselage, horizontal tail, and vertical tail is 0.00461.

To find the lift coefficient of the glider, the Lifting Line Theory program was used (Mason, 2005). Inputs into the system included the angle of attack with respect to the zero lift angle of attack,

Advanced Logistics Delivery System

the taper ratio, the aspect ratio, and the angle of twist on the wings. The zero lift angle of attack for the rigid airfoil was -4.671 degrees and -5.107 degrees for the partially deflated airfoil. Each of the airfoils will achieve a maximum lift to drag ratio at an angle of attack of 5 degrees. Using the taper ratio of 0.35, an aspect ratio of 25.77, and zero twist angle, the lift coefficient from the Lifting Line program was 0.9781 for the rigid wing and 1.0222 for the one percent deflated wing. The Lifting Line Theory program also provided the induced drag of the glider, which was 0.01231 for the rigid airfoil and 0.01344 for the one percent deflated airfoil.

To account for any unforeseen drag in the ALDS glider such as a possible track attachment on the fuselage, the intersection point between the fuselage and wings, and the small crease that forms between the stub wings and the inflatable wing material, the zero lift drag was increased by twenty percent and the induced drag was increased by ten percent. Table 6.4 shows the overall lift and drag of the ALDS glider system as calculated from boundary layer analysis on the wing and the Lifting Line Theory and Friction programs (Mason, 2005).

Table 6.4: Expected Lift to Drag Ratio for the ALDS Glider

Finite Airfoil Type	CL	Cdi	CD	L/D
Rigid	0.97813	0.01354	0.02796	34.984
One Percent Deflation	1.02219	0.01479	0.02970	34.418

6.5 Performance Analysis

The performance of the overall glider is going to change based on the coefficients of lift and drag calculated in Section 6.4. With the higher lift to drag ratio, the range requirement of 50 miles will be easily met. The increased weight from the previously expect 1500 lbs benefits the overall performance of the glider by producing a larger velocity. Calculations of the performance for the rigid wing and the one percent deflated wing are depicted in Table 6.4 below. Based on the numbers in the table below, the glider should have no problems reaching its target range of 50 miles. In the table

Advanced Logistics Delivery System

below, there are two performance calculation columns for both the rigid and partially deflated airfoils. The first column has the zero-lift drag coefficient and lift coefficient at the maximum lift to drag ratio calculated using the equations from Table A2 in Appendix A and the lift to drag ratio calculated in Section 6.4, and the second column has the zero-lift drag coefficient calculated from the boundary layer and Friction analysis and the lift coefficient from Lifting Line Theory (Mason, 2005).

Table 6.5: Overall Performance Calculations

Performance of ALDS Glider with One Percent Deflated Wing					
Constants		Calculations			
		Based on L/Dmax		From Drag Analysis	
Altitude(ft)	7750				
Density(slugs/ft ³)	0.001884	Cd0	0.0164	Cd0	0.0149
Viscosity(lb s/ft ²)	3.58318E-07	Clmax	1.1290	Clmax	1.0222
Weight(lbs)	1759	Vmax(ft/s)	97.44	Vmax(ft/s)	99.79
Eff. Factor, e	0.96	Glide Ang(deg)	1.6642	Glide Ang(rad)	0.0290
L/D Max	34.42	W/S (lbs/ft ²)	10.10	W/S (lbs/ft ²)	10.10
Mean Wing Chord(ft)	2.6	Min Sink(ft/s)	2.83	Min Sink(ft/s)	2.90
Wing Span(ft)	67	Range(miles)	50.5	Range(miles)	50.5
Wing Area(ft ²)	174.2	Reynolds(root)	1.973E+06	Reynolds(root)	2.021E+06
Aspect Ratio	25.77	Mach	0.0897	Mach	0.0919
Performance of ALDS Glider With Rigid Wing					
Constants		Calculations			
		Based on L/Dmax		From Drag Analysis	
Altitude(ft)	7750				
Density(slugs/ft ³)	0.001884	Cd0	0.0159	Cd0	0.0144
Viscosity(lb s/ft ²)	3.58318E-07	Clmax	1.1108	Clmax	0.9781
Weight(lbs)	1759	Vmax(ft/s)	98.24	Vmax(ft/s)	100.63
Eff. Factor, e	0.96	Glide Ang(deg)	1.6373	Glide Ang(rad)	0.0286
L/D Max	34.98	W/S (lbs/ft ²)	10.10	W/S (lbs/ft ²)	10.10
Mean Wing Chord(ft)	2.6	Min Sink(ft/s)	2.81	Min Sink(ft/s)	2.88
Wing Span(ft)	67	Range(miles)	51.3	Range(miles)	51.3
Wing Area(ft ²)	174.2	Reynolds(root)	1.990E+06	Reynolds(root)	2.038E+06
Aspect Ratio	25.77	Mach	0.0904	Mach	0.0926

Performance analysis was also done for the minimum allowable weight on the glider of 1400 pounds. The minimum weight of 1400 pounds is the minimum weight that will allow the glider to reach the minimum altitude for a fifty-mile glide. The performance calculations assume that the lift to drag ratio stays constant with weight change, therefore the glider would still have the same range, but the time to the destination would be much longer due to a much slower glide velocity and lower sink rate. The performance equations table in Figure A2 in Appendix A indicates that a change in weight

Advanced Logistics Delivery System

will have an effect only on the velocity at L/D max, the sink rate, and the Reynolds number. Table 6.5 shows how a lighter weight would change the performance of the glider. Based on these numbers, the glider should fly at full payload or carry ballast to keep the weight at a maximum.

Table 6.6 Overall Performance At Minimum Weight of 1400 lbs

Constants		Calculations			
Altitude(ft)	7750	Based on L/Dmax		From Drag Analysis	
Density(slugs/ft ³)	0.001884	Cd0	0.0164	Cd0	0.0149
Viscosity(lb s/ft ²)	3.58318E-07	Clmax	1.1290	Clmax	1.0222
Weight(lbs)	1400	Vmax(ft/s)	86.93	Vmax(ft/s)	89.03
Eff. Factor, e	0.96	Glide Ang(deg)	1.6642	Glide Ang(rad)	0.0290
L/D Max	34.42	W/S (lbs/ft²)	8.04	W/S (lbs/ft²)	8.04
Mean Wing Chord(ft)	2.6	Min Sink(ft/s)	2.52	Min Sink(ft/s)	2.59
Wing Span(ft)	67	Range(miles)	50.5	Range(miles)	50.5
Wing Area(ft ²)	174.2	Reynolds(root)	1.761E+06	Reynolds(root)	1.803E+06
Aspect Ratio	25.77	Mach	0.0800	Mach	0.0820
Performance of ALDS Glider With Rigid Wing					
Constants		Calculations			
Altitude(ft)	7750	Based on L/Dmax		From Drag Analysis	
Density(slugs/ft ³)	0.001884	Cd0	0.0159	Cd0	0.0144
Viscosity(lb s/ft ²)	3.58318E-07	Clmax	1.1108	Clmax	0.9781
Weight(lbs)	1400	Vmax(ft/s)	87.64	Vmax(ft/s)	89.78
Eff. Factor, e	0.96	Glide Ang(deg)	1.6373	Glide Ang(rad)	0.0286
L/D Max	34.98	W/S (lbs/ft²)	8.04	W/S (lbs/ft²)	8.04
Mean Wing Chord(ft)	2.6	Min Sink(ft/s)	2.50	Min Sink(ft/s)	2.57
Wing Span(ft)	67	Range(miles)	51.3	Range(miles)	51.3
Wing Area(ft ²)	174.2	Reynolds(root)	1.775E+06	Reynolds(root)	1.818E+06
Aspect Ratio	25.77	Mach	0.0807	Mach	0.0826

Chapter 7: Glider Structural Design

7.1 Introduction

For this project, a majority of the structural emphasis is placed on the fuselage and the wings. Given the nature of the launch and glide phases of the aircrafts flight, these two components must be designed under two separate constraints. The fuselage, which will carry the 1000 pound payload, will be subjected to its greatest loads during the launch phase. During this phase it will encounter force due to its acceleration down the launch track, and it will also encounter a centripetal force as it travels through the curved portion of the track. Thus, the frames, stringers and payload supports must be

Advanced Logistics Delivery System

designed to handle both of these loads. The stub wings however will not be producing lift during the launch phase and therefore the high load factor at launch will not affect them nearly as much as the forces and moments during the gliding portion of flight. For the fuselage as well as the wing structural design, the forces and moments produced by the payload and lift will be calculated and appropriate stringers, frames, spars, and skin will be designed.

7.2 Materials

Before the sizing for the structural components could begin it was necessary to choose appropriate materials. For simplicity few materials will be used, one for the beam-like structural components (ie, spars, ribs, stringers, and frame) and one for the skin. All of these materials should be very light weight and have excellent strength. Through much research, it has been concluded that our glider should be made entirely out of composites. Composites, although expensive, are renowned for their remarkable strength and light weight. For the beam-like structural components, graphitized SIGRABOND type 1501 G carbon fiber-reinforced carbon was selected as one of the materials. This material is known for having excellent tensile stress and very light weight. The material properties of this type Carbon Fiber can be seen in the table below. It should be noted, however, that shear strength is different for varying composite structures, and will not be exactly the same for all carbon fibers. There is, however, an estimated shear strength for carbon fibers which is used in the following calculations.

Table 7.1 Carbon Fiber Material Properties (Carbon 2004 and Tsai 1992)

Tensile Strength (ksi)	49.3 – 58
Modulus of Elasticity (10 ⁶ psi)	10.15 – 12.33
Shear Strength (ksi)	9.86
Bulk Density (lbm/in ³)	0.05238 – 0.05599

The skin material, much like the beam materials should have high strength and be lightweight. The main function of the skin is to handle the shear loads on the fuselage, as well as resist flat-plate

Advanced Logistics Delivery System

compressive buckling in the wings. Generally, modern aircraft have composites for their skin. One manufacturer of composite skin material is E-A-R Specialty Composites. Their ISODAMP C-3002 damping composite skin is a good choice for our skin design, and a table of its material properties can be seen below.

Table 7.2 Composite Skin Material Properties (E-R-A 2002)

Tensile strength (psi)	11893
Tear strength (lb/in)	1504
Thickness (in)	Weight (lb/ft ²)
0.125	0.07
0.250	0.14
0.500	0.28

7.3 Structural Analysis of the Fuselage

The glider’s fuselage will consist of a thin skin carrying the shear loads. The skin encompasses the stringers and frame, which carry the longitudinal loads and support the payload. The loads that the fuselage will handle are that of the acceleration, and centripetal loads. A diagram of these loads and their magnitudes can be seen in the figure 7.1 below.

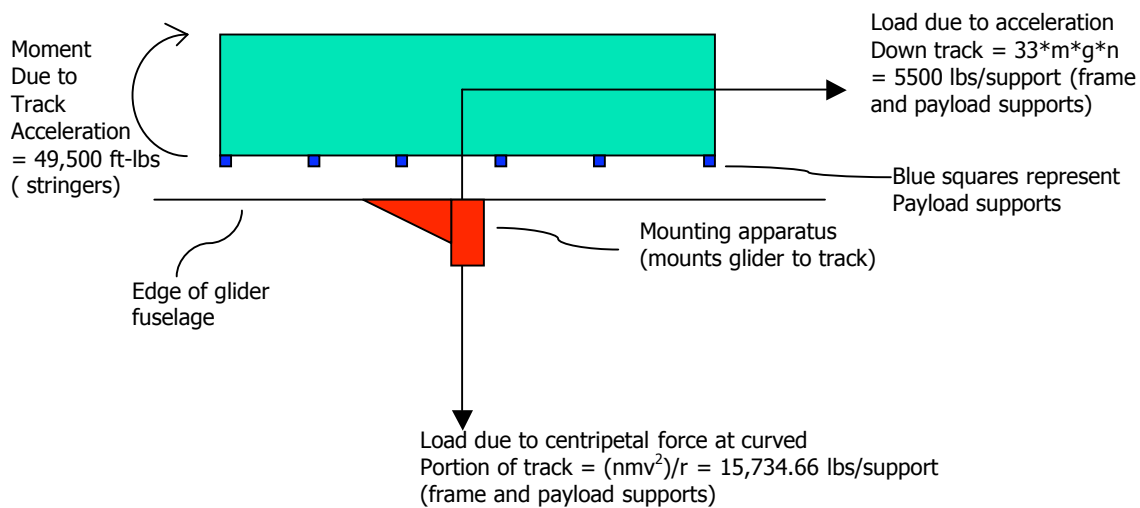


Figure 7.1 Diagram of Loading on Glider

Advanced Logistics Delivery System

Stringers and Skin:

The stringer's main function will be to carry the axial loads due to the bending moment produced by the payload. The stringers will be designed based on the maximum possible value of this bending moment, which will occur at launch. Since the majority of the stress on the stringers will occur at a location near the payload, and because the greatest stringer stress will occur where the fuselage is largest, design for the stringers will be based around the center fuselage (Megson, 1990). A figure of the cross section of this portion of the fuselage as well as the stringer distribution and stringer cross sections can be seen in figures 7.2 and 7.3.

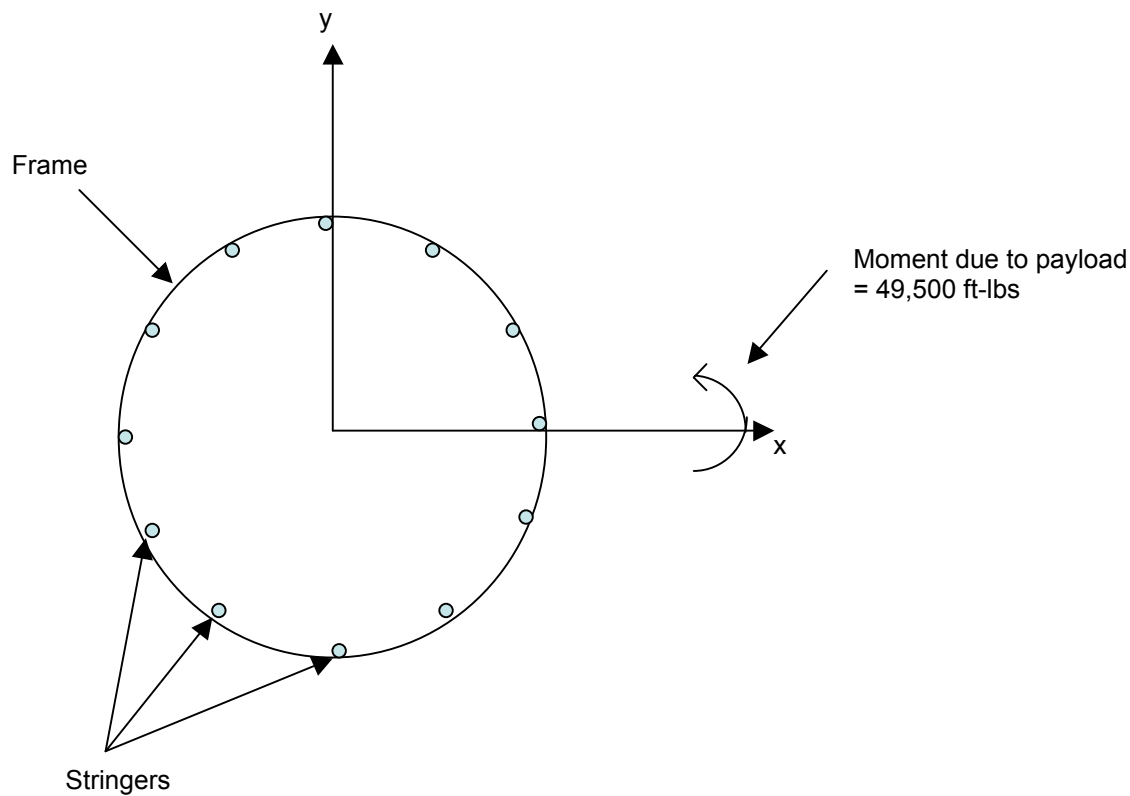


Figure 7.2: Stringer Displacement Along the Frame Edge

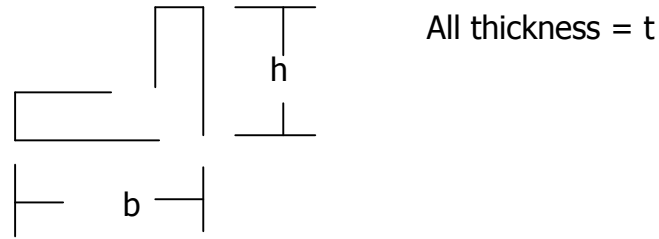


Figure 7.3 Stringer Cross Section

Stringer cross sections

Now that locations and cross sections of the stringers have been chosen, it is necessary to calculate what the cross sectional area of the stringers should be. These cross sections should be able to withstand the maximum possible moment applied to them during launch, while also having the minimum possible area. To do this, each stringer is idealized into a concentration of area, known as a boom. Each boom will carry a certain tensile stress, and the stringer cross section must be designed in order to be able to handle that tensile stress (Megson 1990). By setting the tensile stress in the stringers equal to the allowable tensile strength for the stringer material, and using the moment due to payload calculated, the minimum allowable cross section for the stringers can be computed. The results can be seen in the table 7.3, as well as a figure of the optimized stringer cross section, figure 7.4.

Table 7.3 Table of stringer stresses

Stringer	y (in)	B (in ²)	delta Ixx (in ⁴)	Normal Stress (psi)
1	15	0.227506	51.18875	24178.30072
2	13	0.227489	38.44560417	20954.52729
3	7.5	0.227506	12.7971875	12089.15036
4	0	0	0	0
5	-7.5	0.227506	12.7971875	-12089.15036
6	-13	0.227489	38.44560417	-20954.52729
7	-15	0.227506	51.18875	-24178.30072
8	-13	0.227489	38.44560417	-20954.52729
9	-7.5	0.227506	12.7971875	-12089.15036
10	0	0	0	0
11	7.5	0.227506	12.7971875	12089.15036
12	13	0.225979	38.19047917	20954.52729
			307.0935417	

Advanced Logistics Delivery System

T (in)	0.1			
a (in)	0.5			
b (in)	1			
Weight Per Stringer (lb)	2.5536			

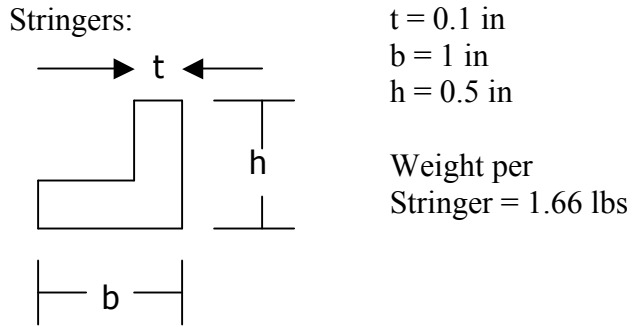


Figure 7.4 Optimized Stringer Cross Section

While the stringers will carry the normal stresses applied by the moment, the skin will have to carry the shear stresses. If the track mounting apparatus is placed directly below the center of gravity of the payload, the skin will not have to deal with the shear load due to the centripetal force. Thus, the skin thickness will only have to be calculated to handle the shear due to the aircraft weight in gliding phase in flight. Since we are assuming that lift is equal to weight in the gliding phase, the shear force during glide will therefore be equal to the weight of the glider, which is 1759 lbs.

To calculate the minimum possible thickness of the skin, a diagram of the shear flow in each skin panel (That is, the panel between each stringer) must be made. For these calculations, it can be assumed that the shear flow is constant along each panel (Megson 1990). The fuselage skin thickness is designed so that the maximum shear in the skin calculated is less than the shear strength of the skin material. For our fuselage design, the maximum shear will occur at the x-axis and can be calculated using the formula $\tau_{\max} = q_{\max}/t$. The resulting shear flow in each skin panel is calculated, and the skin thickness is minimized using excel solver. A table of the shear flow, and shear stress in each panel, as

Advanced Logistics Delivery System

well as the resulting minimum skin thickness can be seen in the table 7.4. A figure of the skin panel numbering convention can also be seen in the figure 7.5.

skin panel	q (lb/in)	Shear Stress (psi)
1 2	-25.00317154	-5000.634307
2 3	-46.67098923	-9334.197846
3 4	-59.172575	-11834.515
4 5	-59.172575	-11834.515
5 6	-46.67098923	-9334.197846
6 7	-25.00317154	-5000.634307
7 8	0	0
8 9	21.66781769	-4333.563538
9 10	34.16940346	-6833.880692
10 11	34.16940346	-6833.880692
11 12	21.66781769	-4333.563538
12 1	0.143787622	-28.75752434
	skin thickness (in)	0.005

Table 7.4 Table of Shear Stresses in Skin

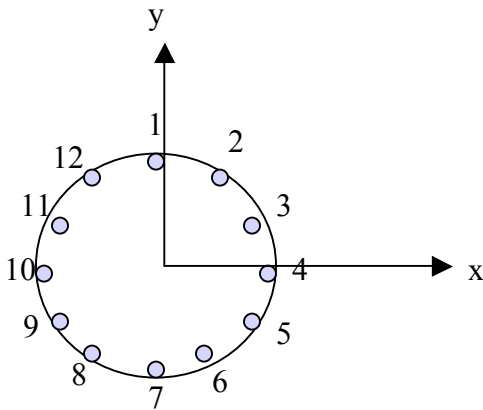


Figure 7.5 Stringer and Skin Panel Numbering Convention

From observing the calculated minimum skin thickness, it is obvious that a thickness of 0.005 inches is impossible to manufacture and retain the given material properties. Thus, the skin thickness we will use will be one that is a little more standard: 0.02 inches.

Advanced Logistics Delivery System

Frames

The major structural consideration when designing the frames is to make sure that the frame can support the payload under the large loads during launch. To support the payload, a bar acting as a floor beam will be used to connect the payload to the frames. There will be six of these frames and floor beams placed under the payload section to support it. It should be noted however, that only four of these frame sections shall be closed and circular. As a result of the manner in which our wings are being inflated, for the two frame sections that are adjacent to the wing, there needs to be a gap. The sodium azide and airbag systems, described in Chapter 9, will be placed in this gap. To account for this gap, we will assume that the sodium azide and airbag system are packed tight enough so that these two frame components can still remain rigid. Also, in these two frame components, the frame will extend out into four spars that will run along the top and bottom sections of the non-inflatable portions of the wing. A figure of the payload supports attached to the frame and their cross sections, as well as a figure of the gapped frames with their spars can be seen in figure 7.6.

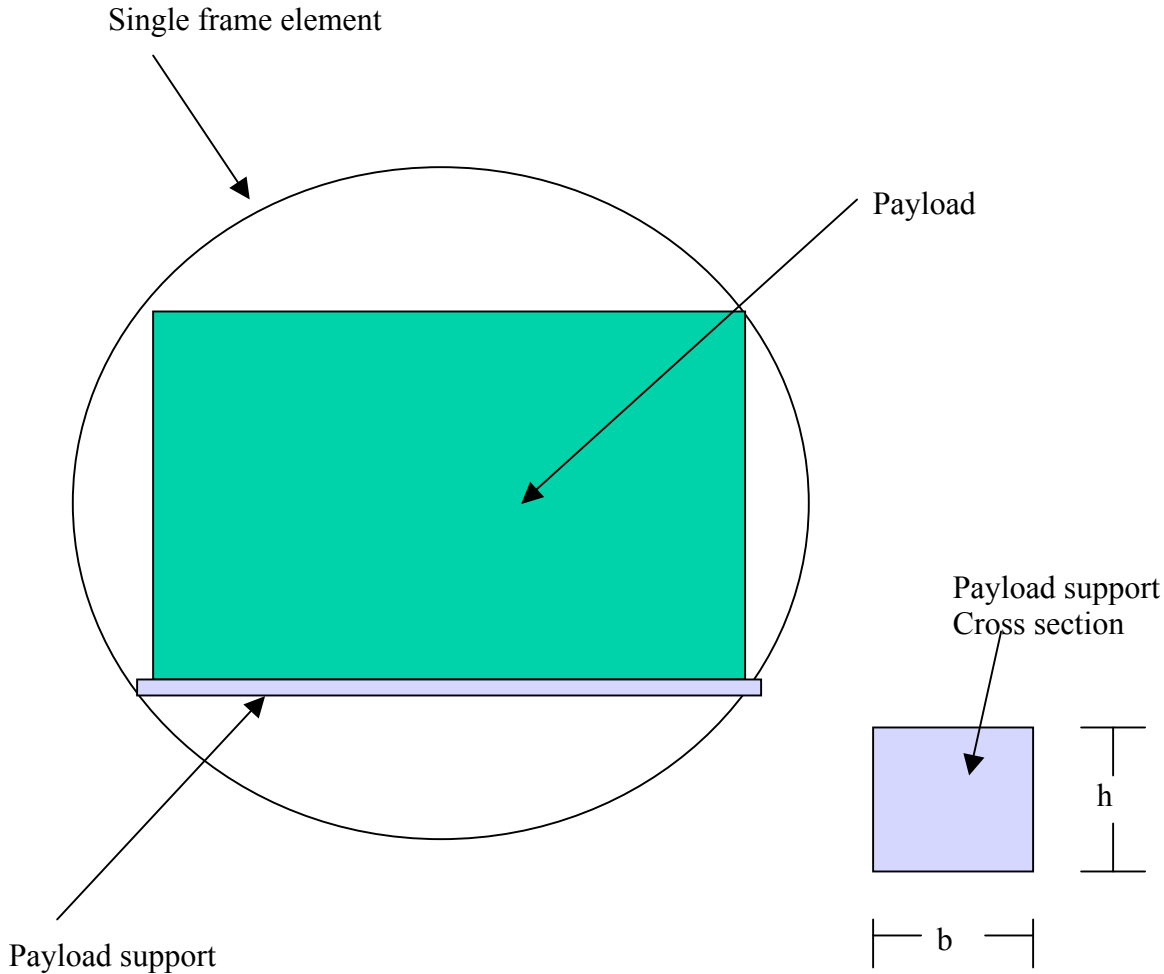
Advanced Logistics Delivery System

Figure 7.6 Diagram of Payload Supports

Next, the forces and moments in the payload supports need to be calculated. Since the payload supports will handle both the load due to launch acceleration and the centripetal load due to traveling over the curved portion of the track, the payload supports must be able to handle the maximum stresses caused by those two loads. To calculate these stresses, the values for maximum shear and moment must be calculated for a payload support. This can be achieved by using simple beam analysis. By treating the payload support as a beam attached to a rigid frame, the resulting moments and shear forces due to each load on the payload supports can be calculated using the figure 7.7 as a basis.

Advanced Logistics Delivery System

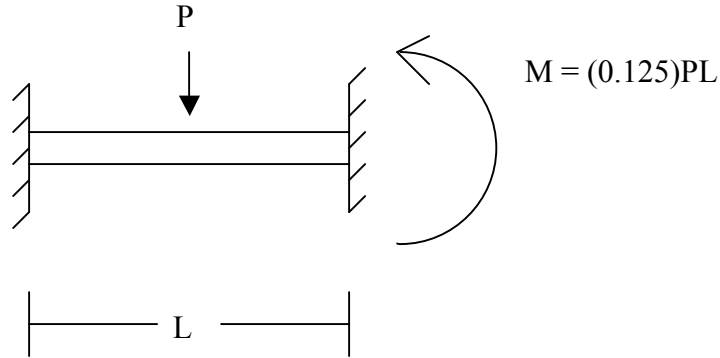


Figure 7.7 Major Loads on Payload Supports (Beer 2001)

In this figure, P represents the force acting on the payload support (which will either be the force due to acceleration or the centripetal force). To calculate the maximum stresses due to these forces, the following two equations are used.

$$\tau_{\max} = \sqrt{(P_1^2 + P_2^2)} / A$$

$$\sigma_{\max} = (Mh/2I_{xx}) + (Mb/2I_{yy})$$

With the methods for calculating these stresses known, the optimized minimum dimensions of the payload support cross section can be calculated. Since the supports can now hold the payload, it is necessary to design a frame that can hold the forces due to those supports. The cross section for the frame was chosen to be an I-Beam because of its high moment of inertia, making it able to withstand greater loads than other designs. The primary stresses that our frame must be able to withstand are the flexural stress caused by the moment due to the centripetal force, and the shear stress caused by the torque due to the load from acceleration. Using the equations for maximum axial stress due to bending moment, and maximum shear stress due to torque, given by:

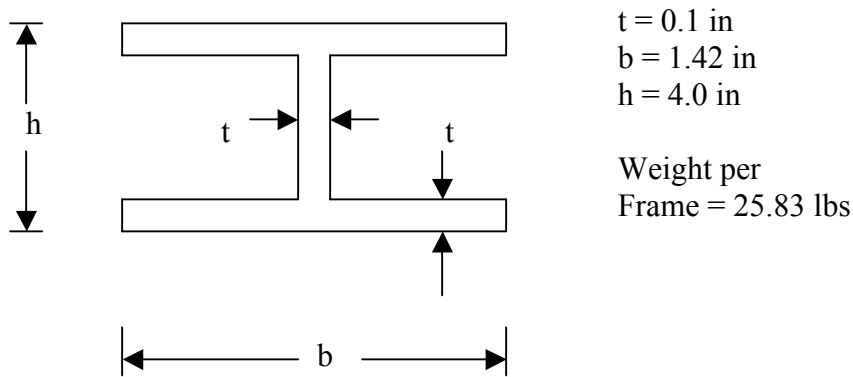
$$\sigma_{\max} = \frac{M(h/2)}{I_{xx}}$$

$$\tau_{\max} = Tc/J \quad (\text{Beer 2001})$$

Advanced Logistics Delivery System

The cross section dimensions will be optimized so that the cross sectional area is a minimum, while the maximum shear stress does not violate the allowable shear strength, and the maximum axial strength does not violate the flexural strength of the carbon fiber. The dimensioned optimized cross sections for the frame and payload support can be seen respectively in the figures 7.8.

Frame:



Payload supports:

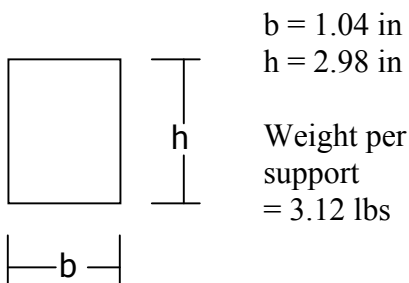


Figure 7.8 Frame and Payload Support Optimized Dimensions

7.4 Structural Analysis on Stub Wings

Spars:

As mentioned before, two of the frame sections will branch out into four spars that will support the wings once inflated, and insure that they do not separate from the fuselage during the gliding

Advanced Logistics Delivery System

portion of flight. To begin the spar design, it is necessary to know all the loads and moments that will be applied to the wing during launch and during flight. Since the wings are not yet inflated in launch, there will be little to no lift during the takeoff phase. Thus, the large load factor during takeoff will not be as important as the loads applied to the wing during glide.

While the aircraft is in flight, assuming that the load varies elliptically along the wingspan, the moments and shear on the wing can be estimated using simple beam theory. A diagram of the loads placed on the wings can be seen in the figure 7.9.

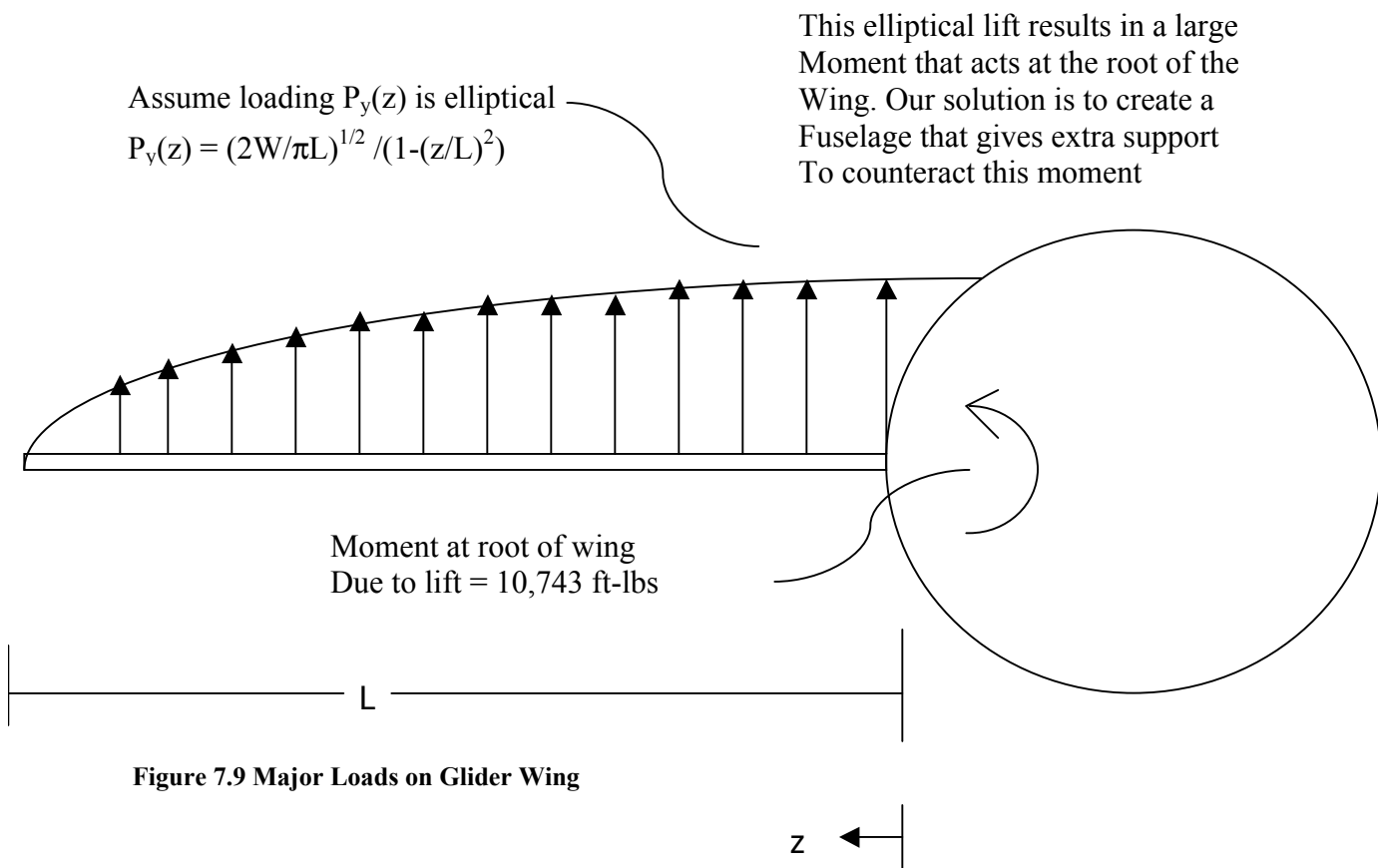


Figure 7.9 Major Loads on Glider Wing

As stated before, each stub wing will have four spars that extend out from the two gapped frames. This implies that each spar is responsible for withstanding a quarter of the moment that acts on the root of the wing. The resulting moment is actually less than the moment due to the centripetal

Advanced Logistics Delivery System

launch force for which the frames were originally designed. This means that there needs to be no cross sectional optimization done on the spars, because the current spar dimensions, equal to that of the frames, are already designed to handle a moment greater than that produced by the lift. Considering the fact that the moment produced by the payload at launch is greater than the moment produced by lift at glide, and that the frame was over designed and included a factor of safety of 1.5, it should be safe to assume that the frame can handle any additional load factors produced by gusts, sharp turns, etc.

Chapter 8: Inflatable Wing Structures

8.1 Criteria for an Acceptable Wing

The stability and load reaction of inflated structures is a variable that is not easily calculated to an exact measure. However, careful theoretical analysis can reduce the errors associated with illustrating the structural stability of, in this case, the glider's inflatable wing. The structure of this inflated wing has been altered numerous times in the duration of the design process as various criteria were introduced. It is important that the following criterion is satisfied in order for this wing to meet the flight requirements. The first and possibly the most important requirement is that the wing must not bend a significant amount, meaning no more than 4 feet for a 28 foot wing, when placed under the aerodynamic loads while in flight, increasing the tip deflection. The tip deflection can be minimized by insuring that the internal pressure from the gas that the wings will be filled with is large enough to prevent wrinkling on the top side of the wing. The term "wrinkling" refers to the condition that the tensile stress due to the internal pressure inside the wing is just equal to the compressive stress due to the bending. Once the theory behind the close approximations of this required pressure is discussed in a later section, numerical constraints can be established. Also, Chapter 9 will discuss the process of

Advanced Logistics Delivery System

the inflation of the wings as well as describe the properties of the gas that these wings will be filled with.

Another important attribute is the physical properties of the material chosen for the interior pressure bearing fabric and the outer wing skin. The inner material must have a high tensile strength and be able to hold the internal pressure without exploding. The inner material must also have a high modulus of elasticity, meaning the material is not easily stretched. This insures a low tip deflection once the wings are deployed, assuming the absence of wrinkling. The main concern for the outer material is that it must be smooth and durable enough to maximize the aerodynamic potential of the airfoil. The decision that there will be an inner material covered by an outer material was derived from the fact that any type of internal cross sectional pattern of an inflated fabric will result in numerous bumps along the surface, affecting the laminar airflow. So, a generously tightened outer wrap will help to smooth out the wing surface by filling in the bumps as best as possible. Both of these materials must also have a low density, because of the strict weight requirement. A low cost for each of these materials is also important, because of the high number of gliders that will be deployed each day.

Finding the torsion of an inflated structure using theory is imprecise, especially since this wing is such a large structure composed of fabric rather than the more traditional metal or composite. The method used in past applications such as the I-2000 was to simulate the loads on a scaled-down model and record the data²⁴. The required geometric twist that maximizes stability will be found from theory in a later section, but before that a requirement that will be considered to reduce the twist is an intricate internal structure. If there are a series of webbed connections inside the wing, this will keep the individual spars from fluttering independently, increasing the overall stiffness of the wing. Now that the general constraints of the wing are outlined, the steps taken to decide upon a final structural wing pattern and material can be described.

Advanced Logistics Delivery System

8.2 Original Concepts

The original idea for the internal structure of the inflated wings was a cross section involving 5 spars, where only the spars would be inflated. The remainder of the airfoil would be filled in using either a lower concentration of nitrogen or aluminum foam. There would also be a series of aluminum alloy ribs every few feet along the span of the wing, which hold the outer skin that is not attached to a spar in place, maintaining the airfoil shape. Figure 8.1 shows this original idea of the cross section.

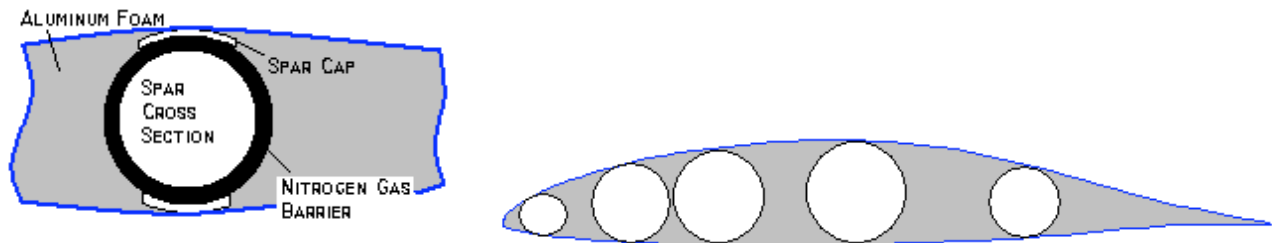


Figure 8.1: 5 Spar Cross Section Concept

Problems began to arise with that idea when it came to the insurance of a smooth airfoil surface. The top and bottom of the inflated spars must remain flush with the outer surface, which will not work because the rib placement interferes. This design has very little webbed connections inside it as well. As discussed earlier, this sparse internal design will lower the overall stiffness because each of these spars will act more independently of one another under their individual air loads.

After further research on the deployment method, it was concluded that it would be acceptable to inflate the entire wing. This was concluded based upon the increased weight of the gas being minimal compared to the increase in stability of the wings. Since the internal pressure is the only mechanism keeping the wings from failing in free flight, the increase of the inflated areas makes the wing to less likely to buckle under the loads. So, a new concept was developed which inflates the entire wing and eliminated the use of ribs and spar caps. Figure 8.2 shows this revised airfoil cross section.

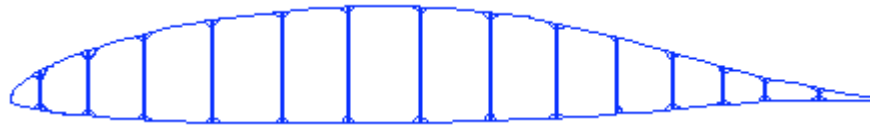


Figure 8.2: Original Fully Inflated Wing Concept

While this design satisfies the fully inflated decision, it does not appear to be very reliable once inflated; meaning it probably will not reduce the twist or the flutter of the wings under flight conditions. Because of the high pressure (close to 1000 psi) inside the wing, it became clear that this design would be inefficient for a couple of reasons. The first reason is that there will be large bumps in between each vertical “beam” along the airfoil surface, impairing the laminar flow as well as shortening the chord length. Another flawed attribute of this design is the absence of cylindrical spars. The circular spars are important because the shape of the airfoil is not changed when inflated. If individual rectangles are inflated, the edges will round off and skew the wing shape.

8.3 Final Concept

Late in the design process, the wing profile had to be modified once again. Figure 8.3 shows the new concept, which combines the original two airfoil designs into an entirely inflated overlapping spar design.

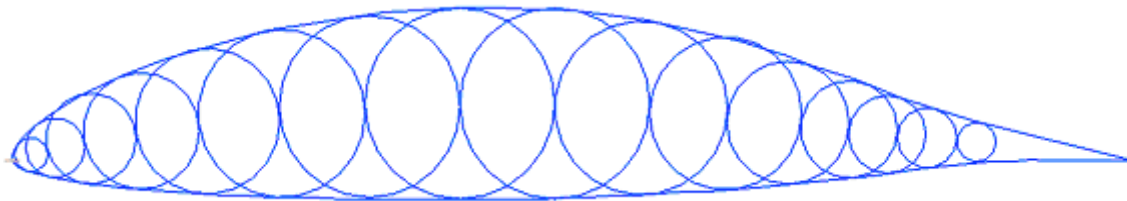


Figure 8.3: Combination of Original Concepts on Wortmann 170 Airfoil

This idea is derived from a wing design used in an inflatable winged glider called “Big Blue,” developed by University of Kentucky graduate students³⁰. Big Blue is shown in Figure 8.4, and is

Advanced Logistics Delivery System

slightly different than the wing of this glider in that it does not have the outer material cover to smooth out the surface.

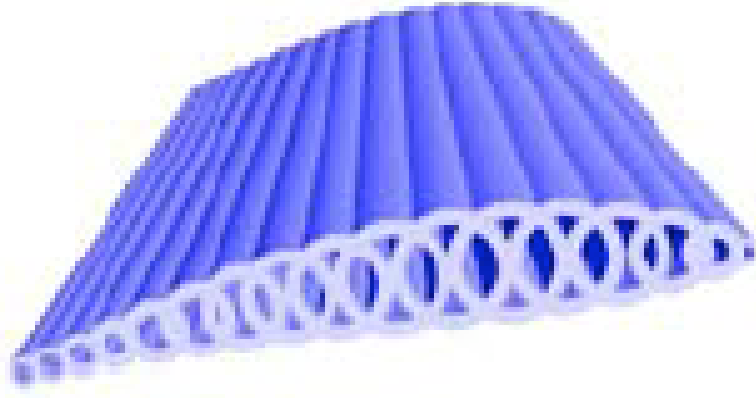


Figure 8.4. Cross Section of University of Kentucky's "Big Blue" Airfoil.

8.4 Force, Moment, and Pressure Calculations

Using the pressure coefficient profile obtained from aerodynamic theory, an estimated lifting profile could be obtained. This lifting profile was obtained using theory, where $C_l = \int (C_{p, \text{bottom}} - C_{p, \text{top}}) dx/c$. C_l is the lift coefficient, C_p is the pressure coefficient, and dx/c is the displacement along the airfoil normalized on the chord length. Figure 8.5a and 8.5b represent the pressure coefficient and normalized sectional lift along the chord, respectively.

Advanced Logistics Delivery System

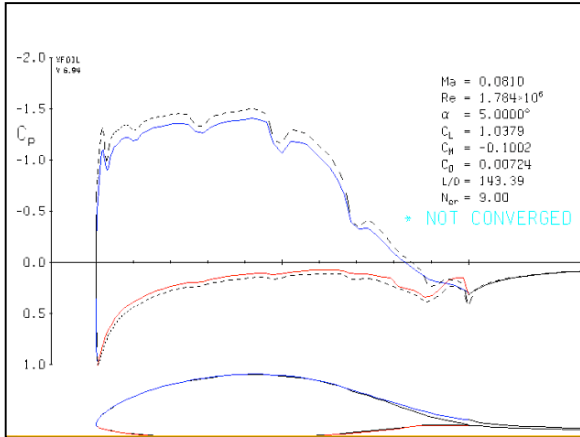


Figure 8.5a. Pressure Coefficient Along Chord

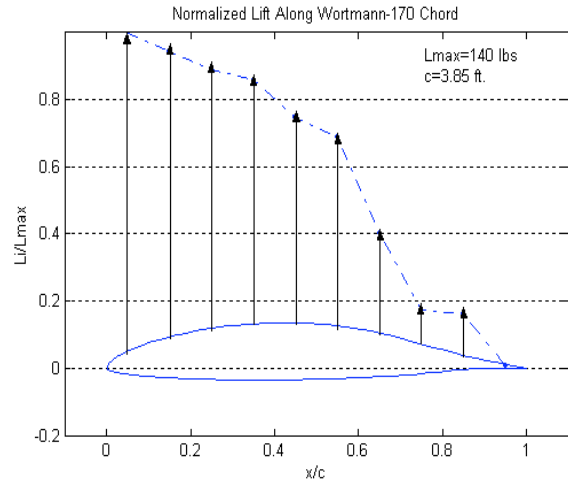


Figure 8.5b. Normalized Lift Along Chord

Using the estimated sectional lift of each portion along the chord, the moments can be estimated by relating the normalized lift to the normalized moment, where the maximum moment is about 9000 ft*lbs. The result of the estimated moments is shown along with the airfoil thickness in Figure 8.6.

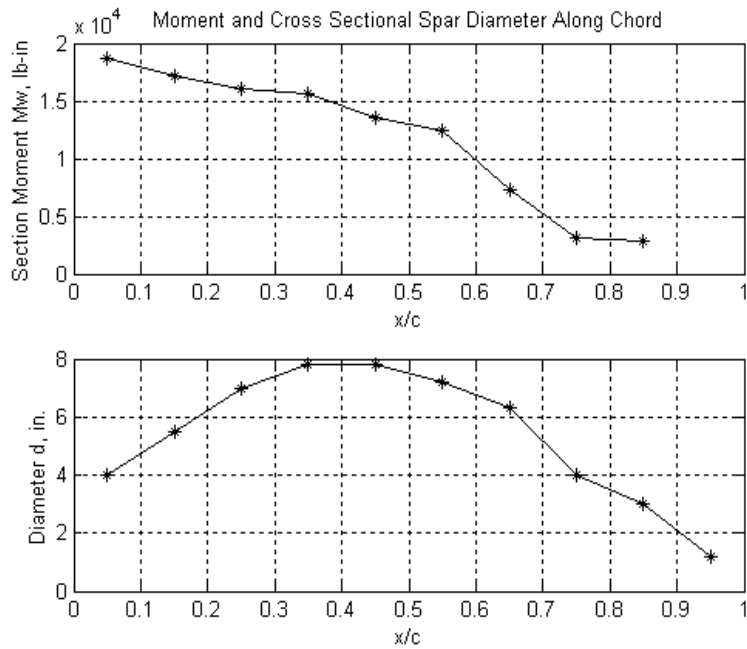


Figure 8.6. Section Moment and Spar Diameter along Chord

Advanced Logistics Delivery System

These moments are important because they determine the wrinkling pressure P_w in each of the airfoil sections. For cylindrical spars, theory states that $P_w = 2M_w/\pi r^3$, where r is the radius of the spar. The wrinkling pressure of each individual section was determined, and the results are shown in Figure 8.7.

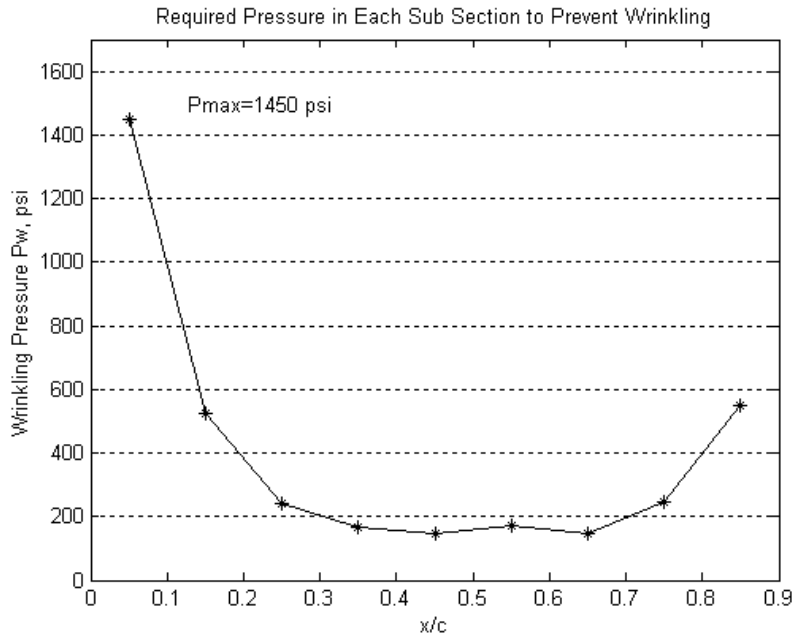


Figure 8.7. Individual Required Wrinkling Pressure along Chord

Besides the leading 10% of the airfoil, the wrinkling pressure is less than 600 psi. A compromise was made since all of the spars are connected to each other. If the internal pressure is setup to be about 1000 psi, then each of the middle and rear spars will not wrinkle, and will therefore hold the leading edge in place since it is a webbed structure.

8.5 Material Selection

Now that an internal pressure has been determined, it is now necessary to choose a suitable material that will hold the high pressure gas inside without bursting. To find the pressure at which a material will explode when inflated, theory says that $P_b = 2tS/D$ ¹⁸, where P_b is the burst pressure, t is the wall thickness, S is the tensile strength of the material, and D is the outside diameter of the spar. A

Advanced Logistics Delivery System

material that was used on the Mars Pathfinder to soften the landing called Vectran ($S=412,000$ psi, $t=0.1$ in.) was applied to this equation and as it turns out the burst pressure is about 10,500 psi (Celanese, 2005). So, this material will sustain the internal pressure without bursting. However, as weight calculations became important near the end of the design, a new material had to be chosen. Because of the high density of the Vectran, the weight of each wing turned out to be about 400 lbs, which is unacceptable. The glider will not fly if the wings are this heavy.

Another material, called Vela Carb 335U, is a unidirectional carbon fiber reinforced fabric that is normally used to strengthen masonry structures and concrete. According to the manufacturers, Edge Structural Composites, this material can be treated with a urethane epoxy to make it air-tight. Applying the physical properties of Vela Carb 335U ($S=150,000$ psi, $t=0.023$ in.) to the bursting pressure equation, $P_b=880$ psi (Edge Structural Composites, 2005). This is unacceptable because this is less than our chosen pressure of 1000 psi. However, if two layers of this material are used, the bursting pressure will be twice as high and within the acceptable range. The low density of this material ($\rho=0.068$ lb/ft²) leads to a satisfactory weight of only 79.4 lbs/wing, even with two layers of the fabric. Dacron, traditionally used in fire hoses, boat sails, and kites, is a suitable material to be used for the outer fabric covering the wing. The highly smooth fabric is more aerodynamic, and the overall weight is only about 7.4 lbs/ wing. This leads to an overall wing weight of 174 lbs. for both of the wings.

Chapter 9 Wing Deployment

9.1 Introduction

To complete the mission objectives, the unmanned glider requires the ability to deploy wings rapidly at the apogee of its flight path. The method chosen for wing deployment was to inflate the wings using nitrogen gas. Inflation was chosen to avoid complications with using a mechanical system. Nitrogen gas was chosen for the inflation process because it is a stable inert gas which can be created in chemical reactions or stored in tanks. This chapter is comprised of two sections. The first section describes the primary inflation system, which will provide the majority of the required nitrogen gas. The second section describes a backup system which will provide the wings with additional nitrogen gas when needed.

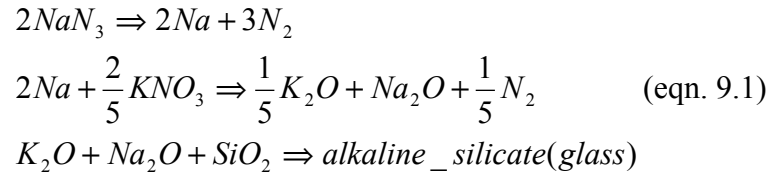
9.2 Primary Inflation

To create the required pressure in each wing, nitrogen gas was chosen to fill the inflatable structures. Nitrogen gas was chosen to fill the inflated structures because it can be created using chemical reactions. This is the same method of inflation used in a standard car airbag or in the Mars Pathfinder mission. An airbag inflates by igniting sodium azide (NaN_3) which decomposes into potassium (Na) and nitrogen gas (N_2). Using this method, it is possible to create massive amounts of nitrogen gas out of solid reactants stored inside the fuselage of the glider. It is important to note that sodium azide is a highly volatile substance which requires the utmost care during manufacturing. The maximum concentration of sodium azide allowed in the workspace is 0.2 mg/m^3 air. This provides positive and negative aspects to the inflation system. The negative aspects include high costs due to usage of such a harmful material; however, since the substance is so volatile it will only require a small electrical charge to begin the chemical reactions. The reaction will produce the majority of nitrogen

Advanced Logistics Delivery System

gas produced; however, it also creates sodium which could possibly react and destroy the wings.

Therefore the process will require three total chemical reactions, which are listed as follows.



The first reaction was described previously using the sodium azide. The second reaction uses potassium nitrate (KNO₃) to stabilize the potentially dangerous sodium byproduct. This reaction will produce additional nitrogen gas as well as additional harmful byproducts. These byproducts are neutralized in the third reaction using sodium dioxide (SiO₂). By comparing the chemical reactions above, the amount of nitrogen gas created can be compared to the total amount of reactants required. In summary, to safely create the nitrogen gas required for inflation, a mixture of sodium azide, potassium nitrate, and silicon dioxide is required. The amount of this mixture will determine the amount of nitrogen gas created during the inflation process.

Equation 9.1 is very helpful because it shows how the amounts of reactants in the mixture vary with the amount of nitrogen gas created. The next step is to determine exactly how much nitrogen gas is needed to inflate the wings at a predetermined pressure. To do this the ideal gas equation is used to relate the molar amount, pressure, and volume of the nitrogen gas. This relationship is described in the following equation.

$$\frac{P_{req}}{RT_{8,000.ft}} V_{req} = n \quad (\text{eqn. 9.2})$$

In equation 9.2 P_{req} represents the pressure required in each wing (The required pressure was determined in the previous chapter of this report to be 1,000 psi), V_{req} is the total volume of all inflated structures located in each wing, T is the temperature at an altitude of 8,000 feet (This is the altitude at

Advanced Logistics Delivery System

which the wings will be deployed), R is the universal gas constant, and n is the molar amount of nitrogen gas. By analyzing the chemical reactions described in equation 9.1 the molar amount of nitrogen gas created can be compared to the molar amount of the mixture used in the chemical reactions. By using the densities of all the reactants in the mixture, the mass of the reactants can be determined using the following equation.

$$MASS_{Mixture} = 2 \times (0.0224) \frac{3.2}{8.3144} [170.484 + X 60.09] \frac{P_{req} V_{req}}{T_{8,000ft}} \quad (\text{eqn. 9.3})$$

In this equation the variable $MASS_{Mixture}$ is the mass of the mixture required in kilograms to create a given amount of nitrogen gas. This value is converted into pounds to maintain unit consistency. The variable X will determine the amount of silicon dioxide required in the reaction to stabilize the system. X must be equal to one or greater to balance out all harmful byproducts. The amount of silicon dioxide can be more accurately determined by experimenting with the inflation system. Without testing, this value it is assumed to be at the minimal case of X equaling one. Once a value for X is determined, the amount of reactants required to fill each wing can be determined for various pressures and temperatures. The amount of reactants in pounds compared to the required wing pressure is summarized in Figure 9.1 for two different temperature values.

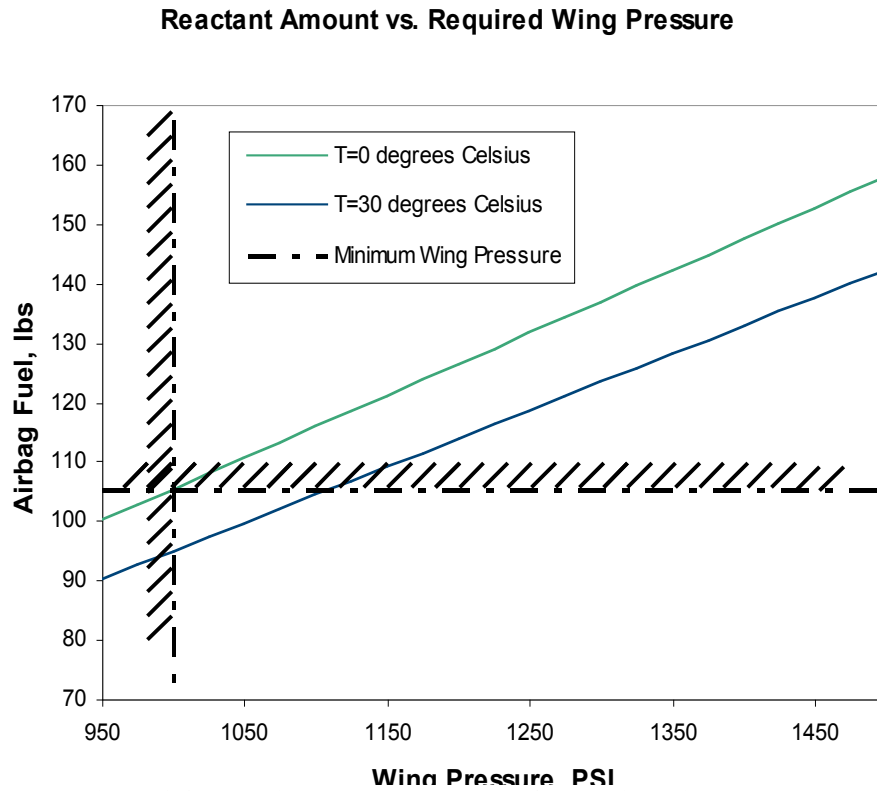


Figure 9.1: Required reactant amounts for varying wing pressure

Figure 9.1 shows how the temperature during the reaction will play a crucial role in the amount of pressure produced. It can be assumed that the temperature at 8,000 feet will not vary much during normal conditions; however it might be possible that the material which will house the reactants and the wings is insulated so that the reaction temperature will be higher than the temperature in the surrounding environment. This would cause an increase in created pressure as seen in Figure 9.1. To determine the safest execution of wing inflation the amount of reactants was chosen for a temperature of 0 degrees Celsius. This concludes that 105 pounds of the reactant mixture must be used to create the required amount of nitrogen gas. Therefore if the temperature increases, the nitrogen gas will inflate at a higher pressure. It is important to consider that this amount of reactants will produce the minimum allowable pressure. The maximum allowable pressure is larger than the range seen on

Advanced Logistics Delivery System

Figure 9.1. By increasing the temperature the minimum amount will only improve the inflatable structures.

The other advantage of using this inflation system is the fast deployment times it provides. The theoretical deployment time can be determined by comparing the span of the wing (distance the inflation process must travel), the cross section of the airfoil (the area which is inflated), the amount of pressure which the wings will inflate with, and the weight of the wings which will be inflated. These factors can be related using the following equations.

$$v_{final}^2 - v_{initial}^2 = 2ad \text{ (eqn. 9.4)}$$

$$Pressure = \frac{Force}{Area} \text{ (eqn. 9.5)}$$

Assuming the initial velocity zero the final velocity can be solved in terms of the acceleration and distance traveled. In this case the distance traveled is the span of the wing. Equation 9.5 can then be substituted into equation 9.4 using Newton's Law, $F=ma$. The final velocity is then used to determine the time at which it takes the wing to inflate. The results of this ideal situation are summarized in Figure 9.2. Figure 9.2 shows the times of inflation versus the weight of the wing. Also highlighted in Figure 9.2 is the determined wing weight of 87 pounds. This value was determined using the final selection of inflatable structure material in the previous chapter. This shows that at an ideal case, with the minimum amount of pressure, the wings will deploy in a total time of 0.0217 seconds.

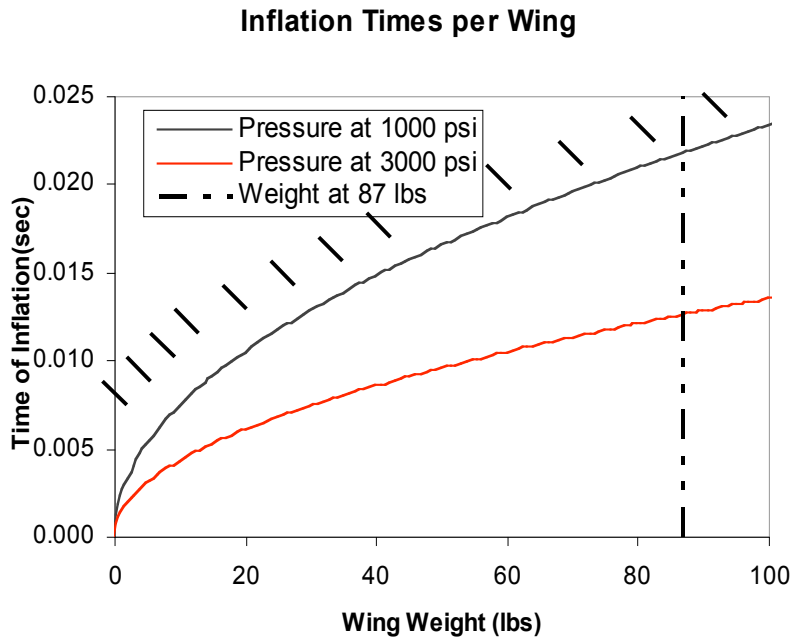


Figure 9.2: Inflation Time per Wing

With the time for inflation calculated and the materials used for inflation determined the primary inflation system must now be connected to the avionics package to begin the inflation process. As stated before, only a small electrical charge is required to begin the chemical reactions. This is done using an igniter which is a device similar to a car spark plug. The igniter is controlled by the avionics package, located behind the payload, using a wire connection. The time of ignition is determined by software attached with the avionics package. Since the chosen time of ignition is at the apogee of the flight path the avionics package must be able to record vertical position rates so that once the glider reaches its peak it will deploy the wings. It is possible that there will be more than one optimum point of inflation for different conditions. These conditions could be based weather, payload weight, range requirements, etc. These points should be determined by testing the glider under various circumstances.

Advanced Logistics Delivery System

9.3 Reserve Inflation

There is one drawback to using an airbag similar system as the primary source of inflation. Once the chemical reaction is complete it is impossible to create more nitrogen gas. If a situation occurs in which the inflatable structure loses pressure, the airbag system could not inflate the wings a second time. It would be possible to design a secondary airbag system; however that will not solve the problem of pressure loss if the problem occurs multiple times during the glide phase of the mission. To solve this problem a direct inflation method is used. The direct inflation method requires that a storage tank be supplied in the fuselage to directly fill the wings with nitrogen gas. This method is useful for supplying small amounts of nitrogen gas; however, it could not be used as a primary inflation method because of the large amounts of nitrogen gas required. As a reserve inflation device, the tank will weigh 20 pounds and fit above the payload inside the midsection of the fuselage. The tank size is approximately the same size as used in commercial scuba gear. Once the primary inflation process is completed valves from the reserve tank will be released to the inflated structures through a control system. The control system is a small device placed inside the fuselage attached to the inflated section on either side of the payload. Both wings will share one reserve tank to reduce the total weight of the glider.

The reserve system controller is an analog device using a spring to control the pressure amount inside the inflated structures. Figure 9.3 details the method of the reserve controller. In the diagram _X represents the movements of the control spring during operation.

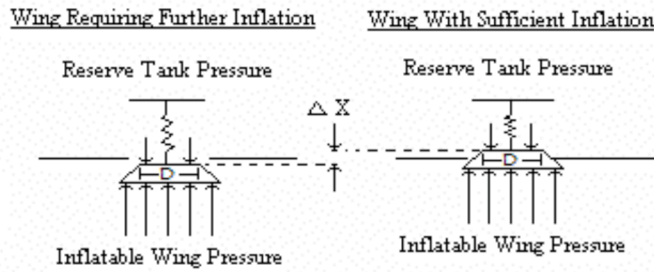


Figure 9.3: Reserve inflation controller diagram

By studying the system described in Figure 9.3 a relationship can be determined between the spring constant and the amount of pressure lost inside the inflatable structures. The relationship below is determined by comparing the spring force with sufficient pressure in the inflated structures and the spring force with a pressure loss.

$$1 - \frac{P_U}{P_S} = \frac{k\Delta x}{P_s \pi (D/2)^2} \text{ (eqn. 9.6)}$$

In equation 9.6 the value $1 - \frac{P_U}{P_S}$ represents the percentage amount of pressure loss in the wing. The value $P_s \pi (D/2)^2$ represents the force exerted on the control surface by the pressure inside the inflated structure. The value $k\Delta x$ represents the spring force at a given spring deflection. The amount of movement in the actuator for different pressure losses is than summarized in Figure 9.4.

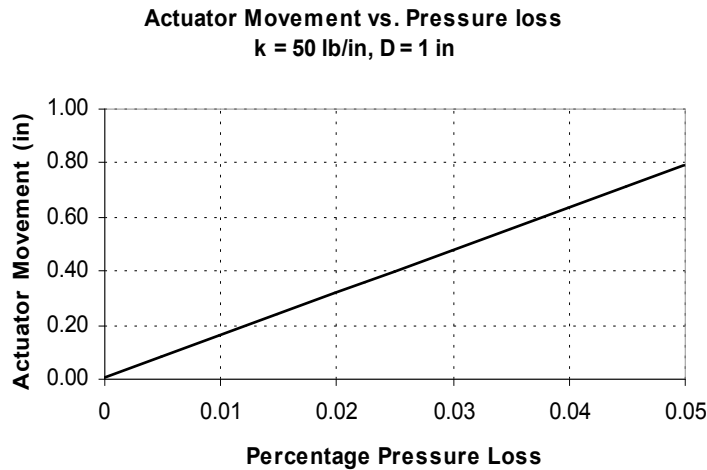


Figure 9.4: Reserve pressure controller activity compared with pressure loss

Figure 9.4 shows the reserve inflation controller activity during different pressure losses. It can be seen from this figure that a small pressure loss on the order of 1% will cause the controller to open up and release the reserve nitrogen gas into the inflated structures. With the reserve inflation system functional the pressure inside the inflatable wing structure will not decrease thus allowing the wings to remain inflated throughout the glide phase.

9.4 Future Thoughts

This section discussed the inflation systems allowing for expandable wings. An airbag system will be used as the primary inflation to create the large amounts of nitrogen gas required. To maintain pressure a reserve inflation system is designed using storage tanks of nitrogen gas with a controller monitoring the amount of pressure inside the wing. This system requires physical testing before use to determine the optimum amounts of silicon dioxide needed and optimum sizing for the reserve storage tanks. It is also important to consider the deflation process once the glider has landed. Because cargo must be taken out of the glider by people, human safety becomes a factor. It is potentially dangerous to have an inflated structure at 1,000 psi near humans. To safely deflate the wings it is possible to install a valve which can be operated remotely or by hand. The location of the valve is immaterial;

Advanced Logistics Delivery System

however, it must be able to control the rate of deflation so that a safe unloading environment can be created.

Chapter 10: Weights and Center of Gravity Location

Weights and center of gravity locations are two critical aspects in the design process of any aircraft. They will determine how well the aircraft will perform during flight. The target weight, as was stated in the RFP is roughly 1,500 lbs, including a 1,000 lbs payload and an empty weight of 500 lbs. The rest of this section will discuss in more detail the breakdown of each glider weight component, the final total weight calculation and the center of gravity location.

10.1 Weights

To begin the weight calculations the glider was divided into 3 different weight groups, structures, equipment and load. These are summarized in table 10.1.

Table 10.1 Weights Grouping

<u>STRUCTURES GROUP</u>		
*Wings (Including Stub)	*Tail: <i>Horizontal</i> <i>Vertical</i>	*Body: <i>Main Fuselage</i> <i>Nose</i> <i>Rear Fuselage</i>
<u>EQUIPMENT GROUP</u>		
*Avionics package	*Servo Motors	
*Wing Deployment Ignition		
<u>LOAD GROUP</u>		
*Cargo	*Sodium Azide Tank	
*Airbag fuel	*Nitrogen Tank	

In the structure group are the primary load-bearing components of the glider, these include the tail, wings (including the stub section) and the body. The equipment group is comprised of the systems that will operate the glider during flight. These include the avionics package and the wing deployment

Advanced Logistics Delivery System

ignition system and the motors that will operate the horizontal and vertical stabilizers. Finally the load group consists of cargo, fuel for the wing deployment, the sodium azide tank and the nitrogen tank.

The next task was to then sub-divide each group into their respective components and then analyze the parts that made up each component. For example the main fuselage was made up of 12 lateral stringers and 6 support frames, plus the skin. To accomplish this task the CAD tool AutoDesk Inventor 9 was used. In AutoDesk one could highlight a section to analyze and then use a properties tool to estimate the weight and CG. For example figure 10.1 shows the final glider drawing with the fuselage stringers highlighted for examining.

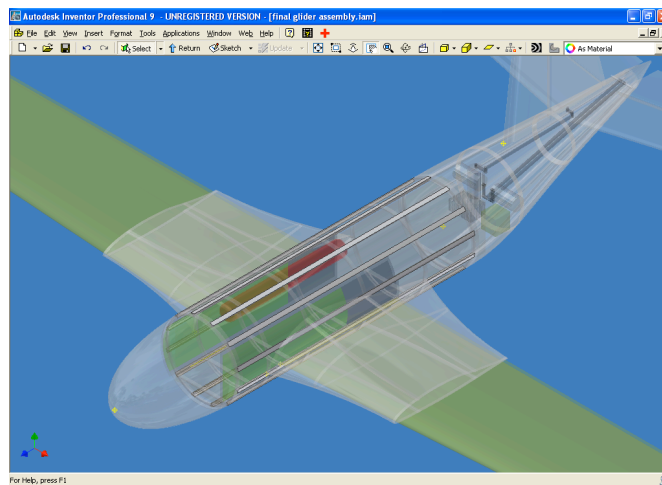


Figure 10.1 – Fuselage stringers highlighted for examining

Now in the properties menu under the physical tab, the material type could be entered and the corresponding density would be displayed. For our case the material used for stringers, frames and other such material was carbon fiber reinforced carbon with a density of 0.05238 lb/in^3 . The skin material was a composite of density 0.14 lb/in^3 , assuming a thickness of 0.005 in . These materials however were not listed and as such the material with the closest density was used as a replacement. For the stringers and frames the material was PVC-Piping with a density of 0.051 lb/in^3 , for the skin, titanium was the closest material with a density of 0.163 lb/in^3 .

Advanced Logistics Delivery System

Table 10.2 summarizes the weight breakdown of each component and the total weight both with and without the payload and fuel. Note that the combined masses were each round up or down to the nearest tenth.

Table 10.2 - WEIGHT BREAKDOWN

Component (Count)	Individual		Combined	
	lbs	kg	lbs	kg
Main Fuselage				
Stingers (12)	1.66	0.75	20	9
Frame Support (6)	26.83	12.16	155	70
Skin Material	3.68	1.67	4	2
Rear Fuselage				
Stringers (12)	2.41	1.09	29	13
Frame Support (2)	1.28	0.58	3	1
Skin Material	---	---	4	2
Tail Section				
Vertical	26	11.79	26	12
Horizontal (2)	22.19	10.06	88	40
Wing Stub				
Stub Frame support (6)	2	1	4	2
Stub Lateral Support (8)	4.95	2.24	10	5
Stub Skin Material	3.81	1.72	8	4
Wing (2)	87	39	174	79
Nose Cone	---	---	2	0.907
Sodium Azide Tank	---	---	50	23
Nitrogen Tank	---	---	20	29
Servo Motors (3)	19	9	57	26
Avionics & Battery Pack	---	---	0.467	0.211
Payload	---	---	1000	454
Sodium Azide Fuel	---	---	105	48

TOTAL WEIGHT (with payload & fuel):	1,759 lbs	798 kg
TOTAL WEIGHT (without payload & fuel):	654 lbs	297 kg

Our final weight was roughly 259 lbs over the target weight of 1,500 lbs. In figure 10.2 and 10.3 we see a clearer distribution of the weight in terms of percentages.

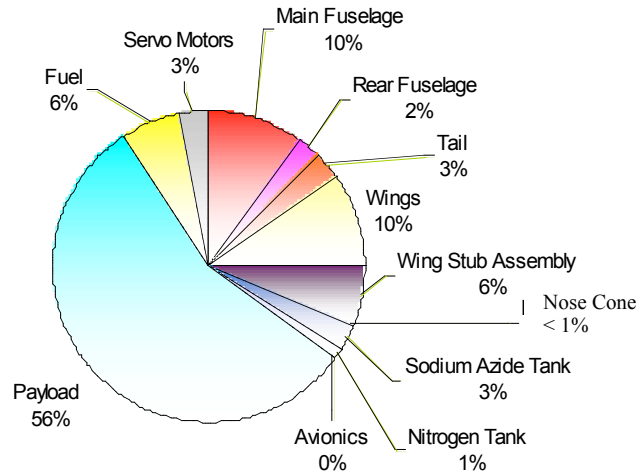


Figure 10.2 Glider Weight Distribution

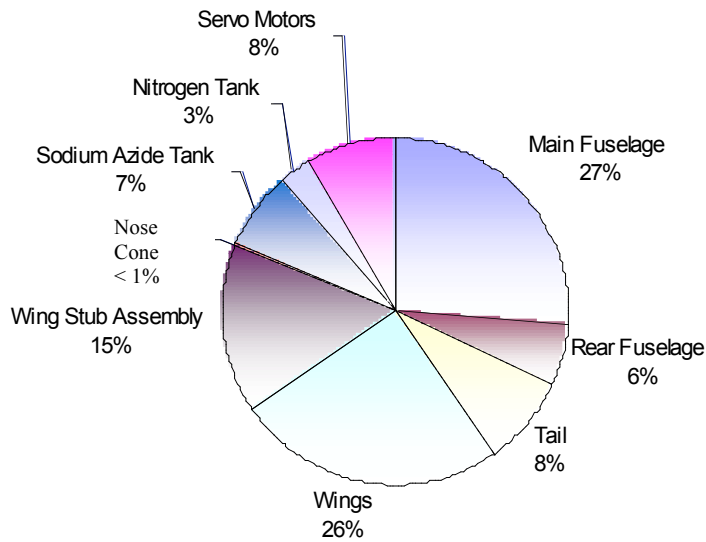


Figure 10.3 Glider Weight Distribution without Payload and Fuel

Advanced Logistics Delivery System

It is clear from figure 10.2 that the payload accounts for most of the weight of the glider followed by the wing assembly. From figure 10.3 however we see now that without the payload and fuel the wing assembly takes a combined 41% of the total weight.

10.2 Center of Gravity

The last task was to calculate the center of gravity of the glider with the wings deployed and with the payload and fuel added and removed. To do so a reference point was established at the nose of the glider. From this point distances were estimated to each weight component, i.e. the fuselage, the wing, the tail, sodium azide tank, the nitrogen tank, and finally the payload. Table 10.3 summarizes the distances to each weight component and the resulting moment.

Weight Component	Distance from the nose (in)	Moment about the nose (lb*in)
Horizontal tail	201.55	17,736.9
Vertical tail	201.556	5,240.46
Wing	76.99	8,392.56
Nitrogen tank	70.137	1,402.74
Sodium azide tank & fuel	67.279	10,428.2
Payload	81.013	81,013
Motor 1	147.085	2,794.62
Motor 2	151.716	2,882.6
Main fuselage	86.806	15,538.8
Rear fuselage	177	6,372

Table 10.3 – Distance and moments

The total of the moments were then divided by the total weight to find the center of gravity locations.

The results were as follows:

- With Payload and sodium azide fuel:
 - CG \approx 0.40 C-bar (86 in from nose)
- Without Payload and sodium azide fuel:
 - CG \approx 0.45 C-bar (97 in from nose)

Chapter 11 Analysis of Glider Stability and Control

11.1 Introduction

The following section describes the constraints, processes, and finally the overall aerodynamic configuration needed to obtain a glider that is both stable and controllable.

11.2 Constraints

The nature of the launch created a list of usually unseen constraints when it comes to glider design. The narrow tunnel the glider must be launched through limits the glider span and height. The span constraint limited the solid span of the wings and the overall span of the tail to 10 feet. Due to the wings being filled completely with inflatable structure, there would not be enough structure in the wings to allow control surfaces on them. The span constraint on the tail limited the overall tail area and effectiveness, and will be discussed later in the report. Another constraint due to the launch process was the overall length of the glider. The overall length was constrained to 18.5 feet for storage reasons. This would affect the magnitude of the moments the tail would be able to create, as well as influence the overall sizing of the tail.

11.3 Requirements

There were a few basic requirements that needed to be fulfilled in order to deliver optimum performance from glider. First, all the constraints listed above needed to be met. Second, the glider and most importantly the tail boom and tail surfaces must be able to withstand the severe loads encountered during launch. Next, the glider will be stable and controllable during wing deployment. The glider must be navigated without the use of an on-board pilot. Finally, the glider must be stable and controllable during the descent.

Advanced Logistics Delivery System

11.4 Launch Loads

The severe loads encountered during launch were mentioned earlier in the structural section of the report. The tail will undergo loads of 3783.1 pounds backwards and 7244.3 pounds downward. These loads are large enough to cause concern, but not so large to create major problems.

11.5 Wing deployment

There were two main concerns associated with wing deployment, center of gravity location and stability during deployment.

Center of gravity

The first issue to be addressed was the location of the center of gravity. This property is a major concern in the overall design process of this aircraft. The craft will act much like a rocket before the wings are deployed. For a rocket to be stable, it is necessary for the center of gravity to be located forward of the neutral point, this can be seen below in Figure 11.1.

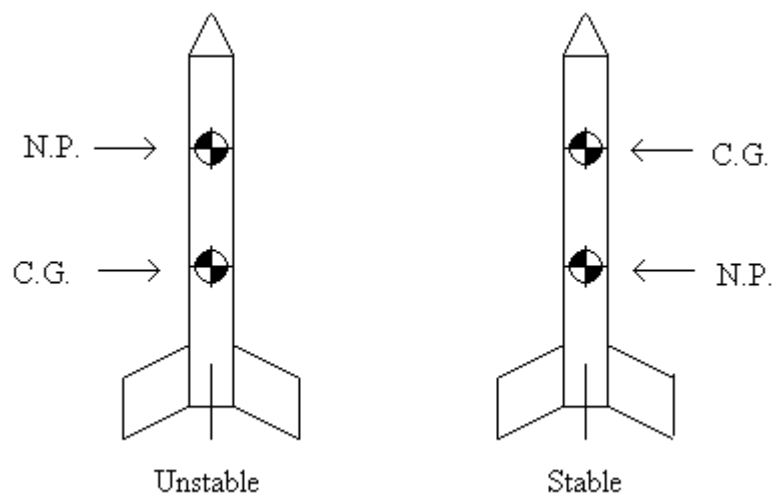


Figure 11.1. Locations of center of gravity and center of pressure for stability of rocket or missile.

For the deployed glider to be stable the center of gravity will need to be located forward of the neutral point. The neutral point however will shift forward, as seen in Figure 11.2 below, on its own

Advanced Logistics Delivery System

during wing deployment to solve this problem. The location of neutral point for the launch stage and glider stage can be adjusted through tail sizing and tail boom length.

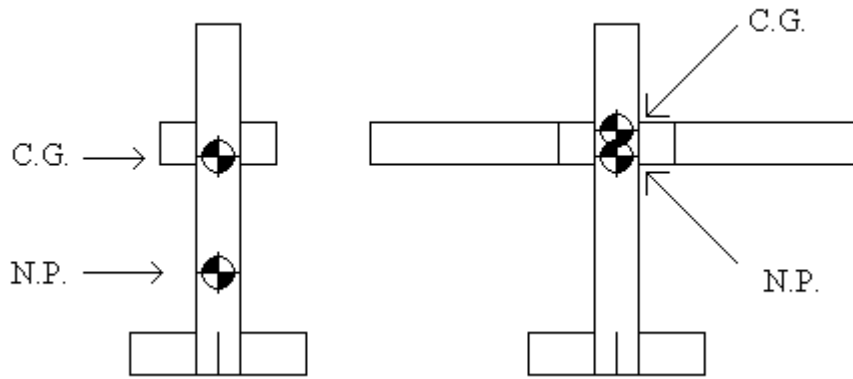


Figure 11.2. The shift of center of pressure before and after wing deployment.

There are several stability factors that are avoided since the aircraft is a mostly disposable glider. These factors reduce the usable center-of-gravity range and include but are not limited to engine-on thrust effects and ground effects (including landing gear, and flaps).

Stability during deployment

There are two keys to insure stability during deployment. The first is to have a quick and even deployment. This is accomplished through two symmetric tanks and the quick reaction in inflation process. The second is to be at a straight and level position during wing deployment. This can be accomplished through our advanced avionics system, described later in report.

11.6 Control system

The glider will be controlled and navigated using an advanced avionics package. This control system is described in section 11.15 of the report.

Advanced Logistics Delivery System

11.7 Tail Configuration

The selection of type of tail to be used in this aircraft was a vital decision due to the limited chances for control surfaces on the wings. The five types of tails considered can be seen in Figure 11.3, they are the conventional tail, T-tail, Y-tail, V-tail, and inverted V-tail.

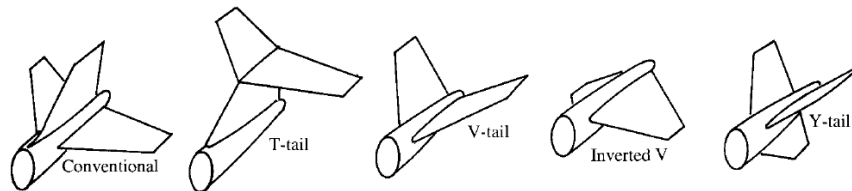


Figure 11.3. Tails being considered for glider.

Conventional

The main advantage of a conventional tail is reliability. The conventional tail is used on approximately 70% of all aircraft. Most basic stability and control calculations and theory is based on the conventional tail. The conventional tail provides adequate stability and control at the lightest weight.

T-tail

The T-tail has several defining characteristics. The T-tail is heavier than a conventional tail due to the added structural support needed. The main advantages of the T-tail are that it is a smaller vertical tail and has the ability to avoid wing wake. The ability to avoid wing wake may be useful if the wings contain very small control surfaces that are close to fuselage and have high angles of deflection.

V-tail

The V-tail is another interesting tail configuration. The use of V-tails is being seen more and more, especially in unmanned air vehicles. The V-tail is intended to reduce the wetted tail area. The use of a V-tail also creates a larger vertical distance from the wings and therefore reduces the effects of

Advanced Logistics Delivery System

wash created by the wings. The main advantage however is the reduction of interference drag. Due to the surfaces not being perpendicular or parallel with fuselage, the V-tail does not operate with standard elevators and rudders, rather combined fins called rudder-vators. The operation of these rudder-vators requires control inputs to be mixed and therefore requires a more complex control system. The main disadvantage of the V-tail is “adverse roll-yaw coupling”, this occurs due to the rudder-vators creating a moment in the opposite direction to desired turn.

Inverted V-tail

The inverted V-tail is has very similar characteristics of the normal V-tail with two exceptions. First, the tail is inverted. Second, the inverted V-tail produces “pro-verse roll-yaw coupling” as opposed to “adverse roll-yaw coupling”. This condition, where the roll and yaw with as opposed to against each other, is much more desirable.

Y-tail

The Y-tail may be considered the best tail for the glider. The Y-tail reduces interference drag just like the V-tail does, but without the use of complex rudder-vators. Like the V-tail, the Y-tail also creates a larger vertical distance from the wings and therefore reduces the effects of wash created by the wings. The Y-tail also has a rudder and closely resembles the fins of a rocket. This resemblance may be useful in the control of aircraft during launch and flight. The Y-tail can also be inverted in the same manner as the V-tail.

Tail Type decision

The choice of tail was done through a conventional elimination process. After researching a large number of glider configurations, it was concluded that gliders consist mostly of conventional, V- and T-tails. The use of a T-tail was eliminated on the basis of the large loads and launch, as well as the added weight to support these loads. The conventional tail was chosen over the V-tail for several

Advanced Logistics Delivery System

reasons. The conventional tail allowed for more wetted surface area in compliance with the launch tunnel constraints. The conventional tail also provides more rudder control, which will be needed in the absence of ailerons. Finally, the conventional tail is considered more reliable and structurally sound.

Tail configuration

The final tail configuration, seen below in Figure 11.4, was based primarily on other gliders with similar properties and adjusted to maximize stability and control.

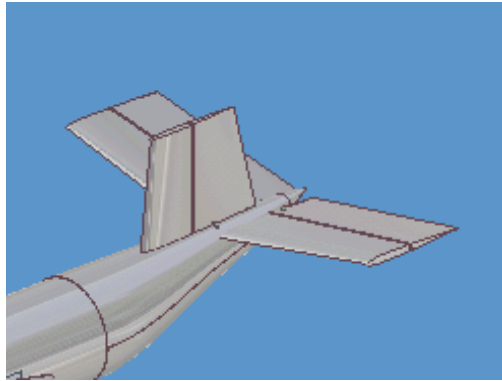


Figure 11.4 Final Tail Configuration.

A Wortmann FX 67-k-170/17 airfoil was chosen for the horizontal vertical tail. This airfoil is commonly used in gliders and has similar qualities to airfoil used for the wings. The horizontal and vertical tails are staggered to allow large control surfaces and deflections without the possibility of collision. The horizontal tail benefits the most from an increasing lever arm and is thus positioned aft of the vertical tail. The final properties of both tails can be seen below in Figure 11.5.

TAILS	Horizontal	Vertical
Airfoil	FX 67-K-170/17	FX 67-K-170/17
Span	10 ft	3.5 ft
Root Chord	3.00 ft	3.50 ft
Tip Chord	2.75 ft	2.50 ft
Sweep Angle	2.86 degrees	4.09 degrees

Figure 11.5. This table explains the configuration and geometry of the vertical and horizontal tail.

Advanced Logistics Delivery System

11.8 Conventional Design Process

The conventional design process was used to find early estimates of fuselage length and surface area for the horizontal and vertical tail. The typical length of an un-powered sailplane versus weight was calculated from equations found in Raymer (27), and can be seen below.

$$\text{Fuselage Length} = aW_o^C$$

a = fineness ratio C = provided constant

Typical values these values for an un-powered sailplane are $a = 0.86$ and $C = .48$.

Fuselage length versus overall weight of glider can be seen below in Figure 11.6. The figure also includes a red constraint line that represents the 18.5 foot maximum fuselage length constraint from the launch system. From these results, it can be concluded that our glider will not have a fuselage length to overall weight ratio that is found in typical gliders.

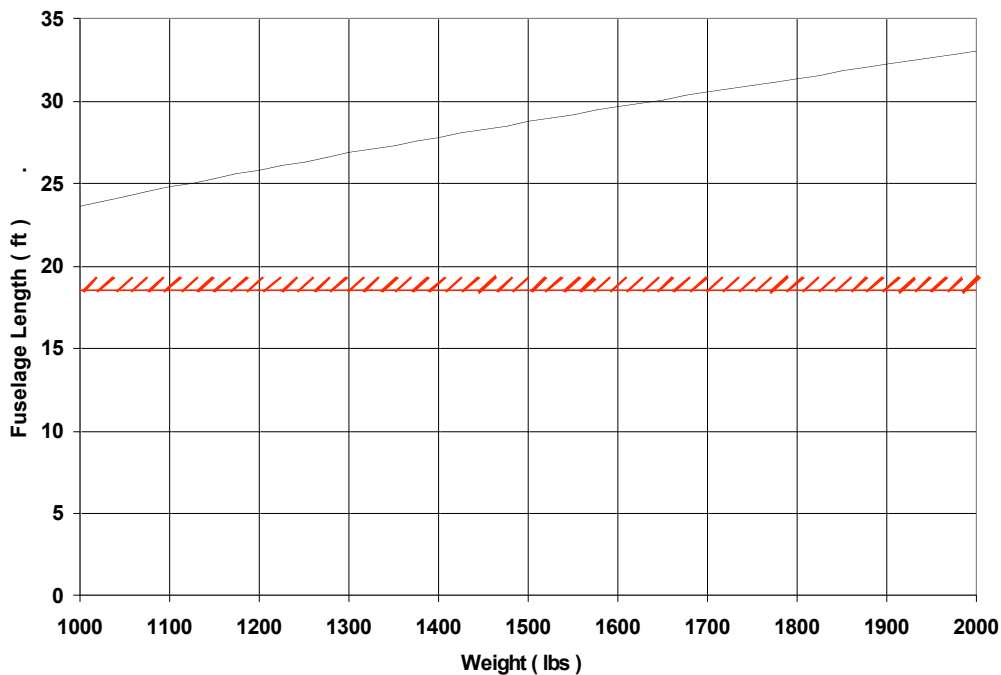


Figure 11.6 Typical fuselage lengths versus overall weight. (The red constraint line represents the maximum fuselage length constraint.)

Advanced Logistics Delivery System

Conventional sizing was also used for preliminary estimates of horizontal and vertical tail surface areas. These calculations were also done using equations found in Raymer(27), and can be seen below:

$$S_{VT} = c_{VT} b_w S_w / L_{VT} \qquad S_{HT} = c_{HT} C_w S_w / L_{HT}$$

$$S_w = \text{wing area} \qquad b_w = \text{wing span} \qquad C_w = \text{mean wing chord}$$

$$L_{VT} = \text{Moment arm to vertical tail} \qquad L_{HT} = \text{Moment arm to horizontal tail}$$

$$c_{VT} = \text{Vertical tail volume coefficient} \qquad c_{HT} = \text{Horizontal tail volume coefficient}$$

Typical values these values for a sailplane are $c_{HT} = 0.50$ and $c_{VT} = 0.02$.

Tail area versus moment arm length of glider can be seen below in Figure 11.7. The figure also includes a red constraint line that represents the 18.5 feet maximum fuselage length constraint from the launch system. From these results, it can be concluded that our control surfaces will have similar areas and that these areas can be reduced as moment arm length is increased.

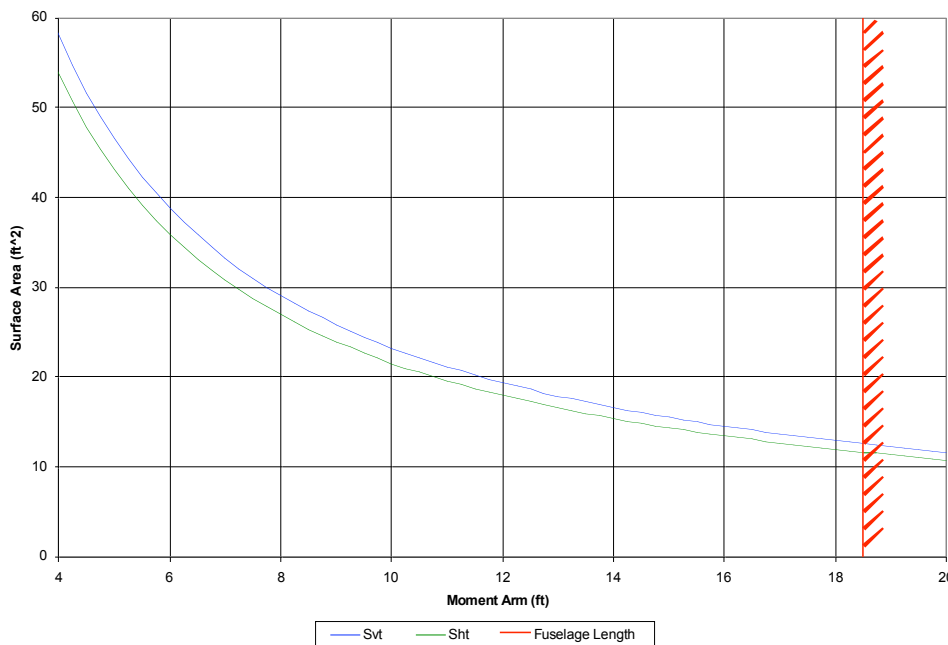


Figure 11.7 Surface area versus Moment arm length for glider.

Advanced Logistics Delivery System

11.9 Computer Aided Design

Due to the large number of simultaneous equations that are used in stability and control calculations, various programs were used to aid in the design process. The three programs used were Excel Solver, VLMpc (Vortex Lattice Method for personal computer), and AVL (Athena Vortex Lattice). The various properties of each program can be seen Figure 11.8 below. Eventually all calculations were done using AVL. The code provides more inputs and outputs than the other two methods.

	Inputs										Outputs			
	Planform View	Center of Gravity	Dihedral, Twist, and Camber	Mach Number	Desired Coefficient of Lift	Angle of Attack	Angle of sideslip	Control surfaces and deflections	Neutral Point	Static Margin	Calculated Coefficient of Lift	Stability Derivatives	2-D View	3-D View
Excel Solver	X	X							X	X				
VLM pc	X	X	X	X	X				X	X				
AVL	X	X	X	X		X	X	X	X	X	X	X	X	X

Figure 11.8 Input and output properties of each program used during design process.

11.10 Stability Derivatives

Stability derivatives are used to describe the moments and forces created by the plane during equilibrium and maneuver flight conditions. The sign and magnitude of these derivatives can quickly describe the equilibrium flight conditions, while the change in these values can describe how the glider will act under perturbations and maneuvers. In Figure 11.9, a table describes the primary stability derivatives and the interpretation of the associated values. All values found using AVL program.

Advanced Logistics Delivery System

Stability derivatives coefficients	Title	Value	Interpretation
$C_{L\alpha}$	Lift curve slope	6.475990	Should be positive and close to a value of $2\pi=6.2831$.
$C_{m\alpha}$	Pitch stiffness	-2.58497	Negative value creates pitch stiffness.
$C_{l\beta}$	Roll Stiffness	-0.051206	Negative value creates pitch stability.
$C_{n\beta}$	Yaw Stiffness (Weathercock Stability)	0.008806	Positive value creates yaw stability.
$C_{n\delta r}$	Rudder power	-0.0133499	Always Negative.

Figure 11.9 Summary of primary stability derivatives, values, and interpretations.

11.11 Longitudinal Stability

Longitudinal stability of the glider assures that the glider will return to an equilibrium position if it experiences a small typical disturbance in pitch. To obtain this condition the glider had to be trimmed to meet the following conditions:

1. The slope of C_m / C_L should be negative.
2. The glider should obtain equilibrium flight at desired coefficients of lift. (Pitching moment (C_m) can be trimmed to zero at desired range of C_L values.)
3. The C_{m0} (Coefficient of pitch moment at zero lift) should be a reasonable value.

These following constraints were all met and the results can be seen below in Figure 11.9. Adjusting the size of the control surfaces and adjusting the location of the CG met the first requirement. The second requirement was met by adjusting the angle at which the wings and horizontal stabilizer were mounted to the fuselage and tail boom. The wing was mounted at 6.90 degrees and the horizontal tail was mounted at -3.75 degrees. While these angles seem extreme, they were needed in order to trim the aircraft properly. The third requirement was obtained by comparison with other similar gliders. The straight line on graph represents the C_m / C_L slope found for desired lift. The plotted points represent more accurate values, which were computed using AVL.

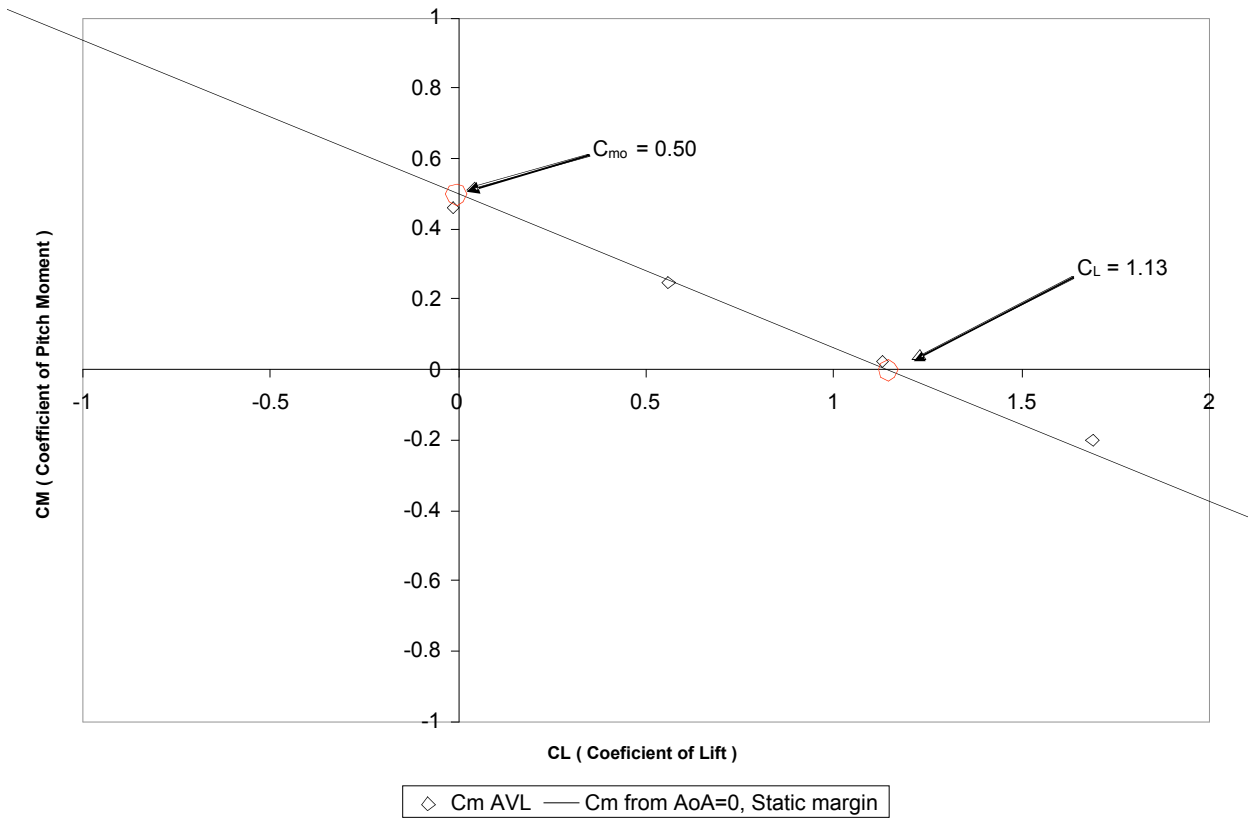


Figure 11.10 Coefficient of Pitch Moment versus Lift Coefficient for desired CG location, using static margin and AVL output.

The CG, calculated later in report, and neutral point were located at 0.8 and 1.84 feet from leading edge of root chord. The static margin for this desired condition calculated as 36% of the mean aerodynamic chord of the wing.

In Figure 11.11, seen below, the values for The C_L , L/D, and static margin for the maximum forward and aft positions of the center of gravity were calculated. These locations were determined by adjusting the CG location forward and aft so that the trimmed L/D didn't drop below 33.2. The results yielded a maximum forward and aft CG location of 0.23 and 0.35 of mean chord back from the leading edge of the wing root chord.

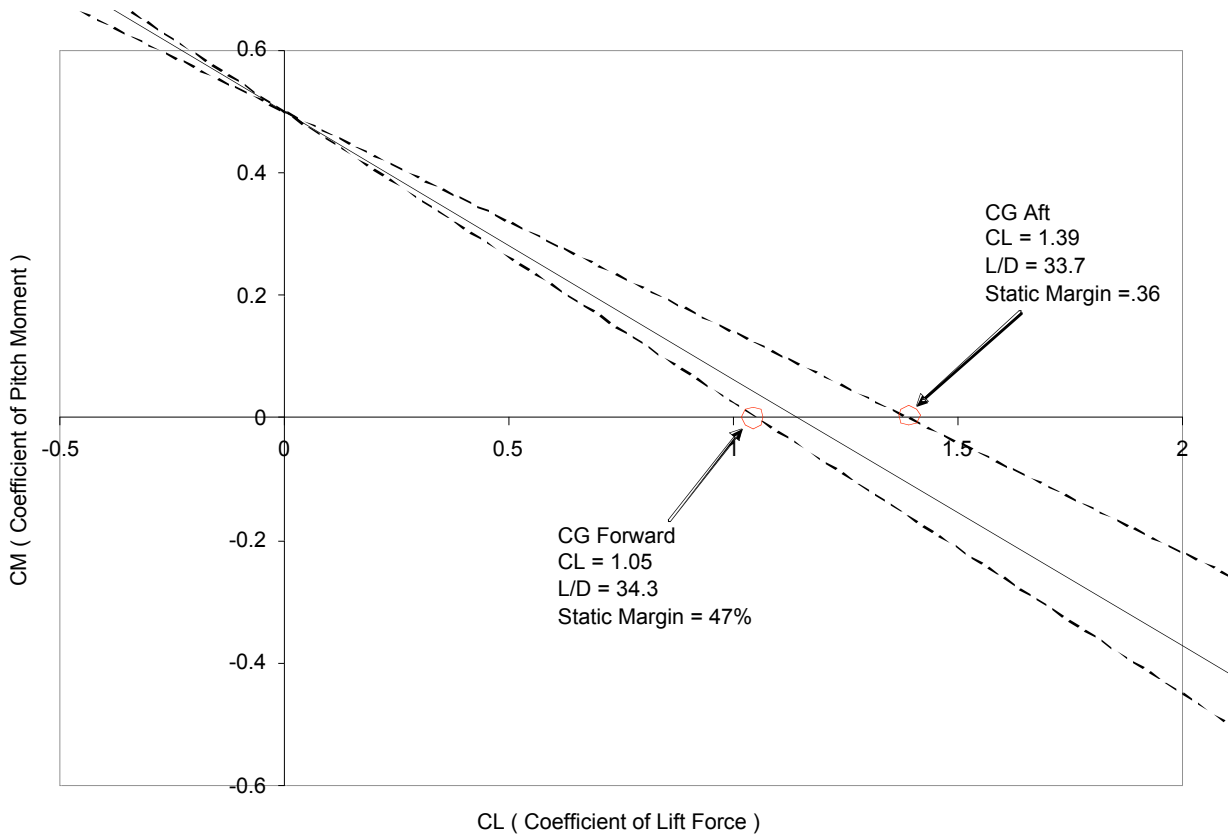


Figure 11.11 Coefficient of pitch moment versus coefficient of lift for optimum CG location, and maximum forward and aft CG location.

11.12 Pitch Control and Elevator Performance

Once longitudinal stability has been achieved, pitch control, and effectiveness were determined. It was important that as the glider performed well even at various CG locations, angles of attack, and elevator deflections. The desired angle of attack range was set from -5 to 5 degrees. Maximum elevator deflections were set at ± 20 degrees, this value was determined later in the report. The maximum and minimum trimmed C_L values were set so that corresponding value of L/D would not drop below 33.2 . The forward and aft positions also required a minimum elevator deflection of ± 2 degrees to create trim. The different slopes of locations of CG means different elevator deflections are needed to create trim. In Figure 11.12 below, the trimmed conditions for the glider at the most desirable CG location can be seen.

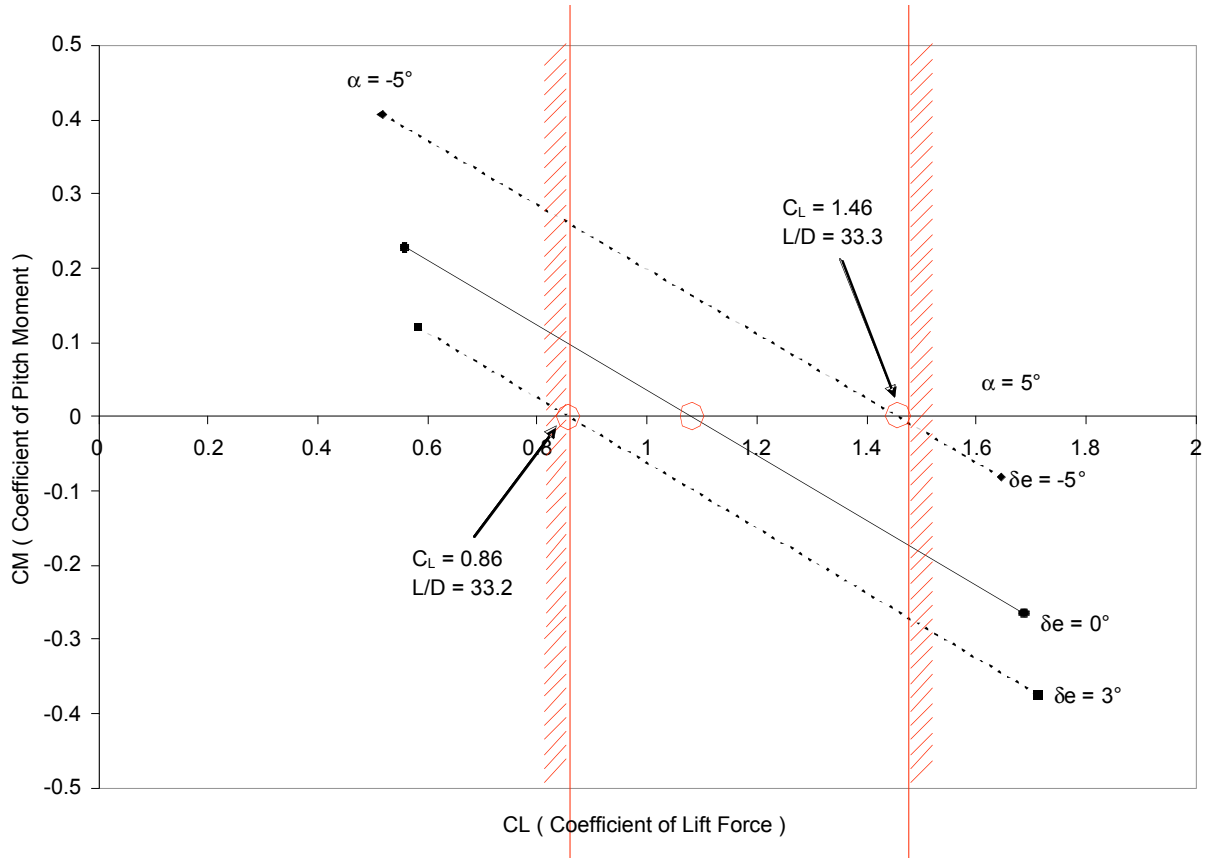


Figure 11.12 C_m / C_L slopes for various elevator deflections at location of desired CG location. The aircraft is considered trimmed when dC_m is equal to zero. (The red lines represent the minimum and maximum coefficients of lift necessary to maintain an L/D of at least 22.5.)

With the desired CG location the glider requires elevator deflection range of approximately -5 to 3 degrees. In Figures 11.13 and 11.14, the results for trimmed flight at maximum forward and aft CG locations can be seen.

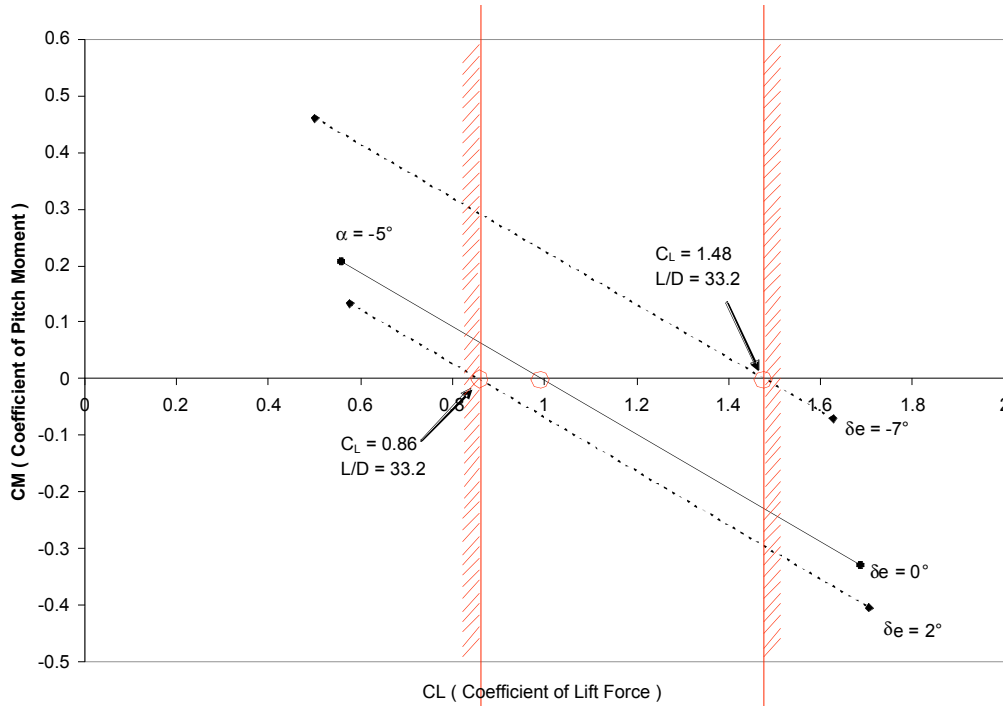


Figure 11.13 C_m / C_L slopes for various elevator deflections at location of forward most CG location. The aircraft is considered trimmed when dC_m is equal to zero. (The red lines represent the minimum and maximum coefficients of lift necessary to maintain an L/D of at least 22.5.)

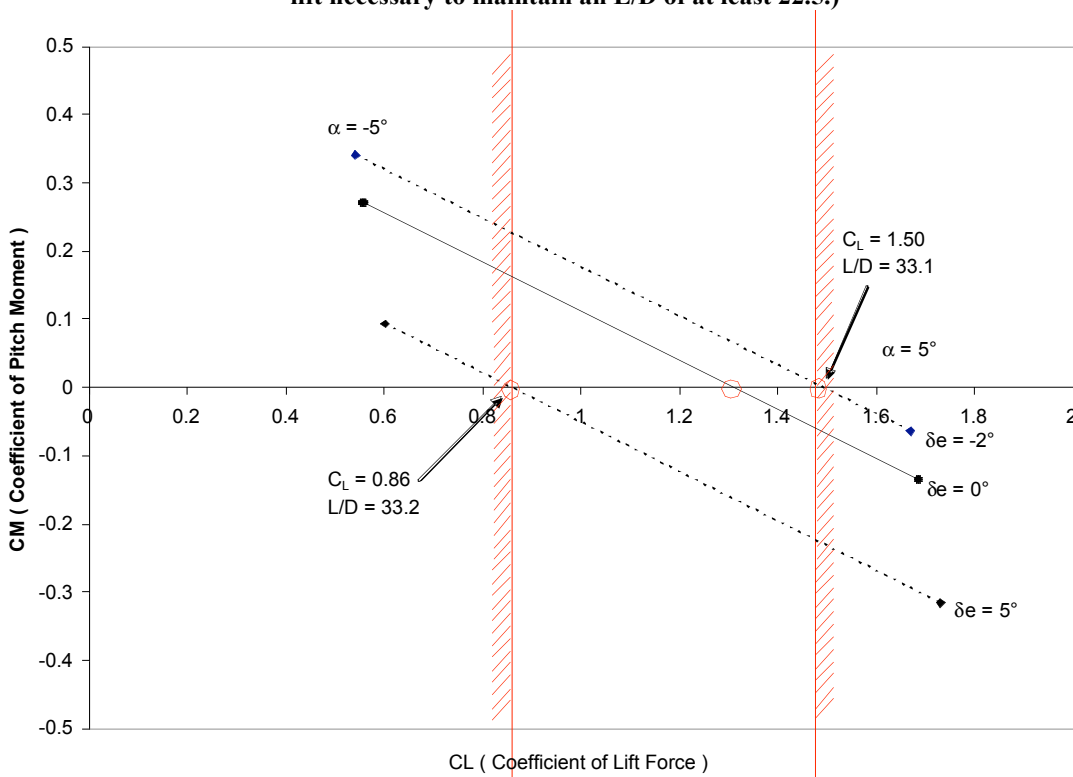


Figure 11.14 C_m / C_L slopes for various elevator deflections at location of aft most CG location. The aircraft is considered trimmed when dC_m is equal to zero. (The red lines represent the minimum and maximum coefficients of lift necessary to maintain an L/D of at least 22.5.)

Advanced Logistics Delivery System

The forward most CG location requires elevator deflections range of approximately -7 to 2 degrees, while the aft most CG location requires elevator deflection range of approximately -2 to 5 degrees.

11.13 Yaw Stability and Rudder Performance

Yaw control and performance were also obtained through procedures similar to pitch control. The magnitudes of yaw moments are limited due to the vertical height constraints on the vertical tail and moment arm constraints. The vertical tail size and deflections were maximized to obtain stability without creating any structural concerns. The hinge of rudder was set the same manner as the elevator, by comparing to other similar gilders and to maximize the effectiveness. The maximum rudder deflections were set at the same value, ± 20 degrees, as the elevator. Following set of equations were used to determine the yaw angle and moment created by rudder deflection:

$$C_{nB} B + C_{n\delta r} \delta r = 0$$

This equation can be transformed to find yaw angle as a function of rudder deflection:

$$B = -(C_{n\delta r} \delta r) / C_{nB} \quad (\text{Yaw angle})$$

The results from these calculations can be seen below in Figures 11.15 and 11.16.

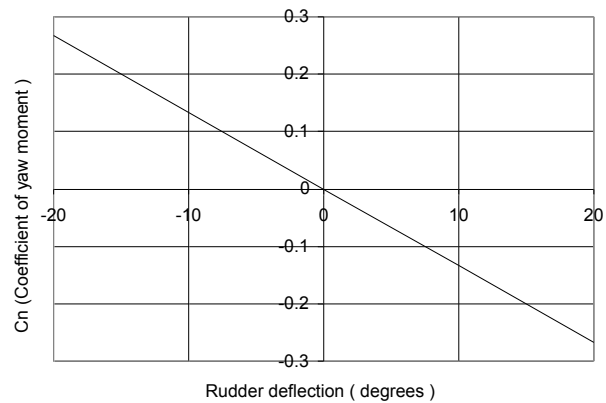
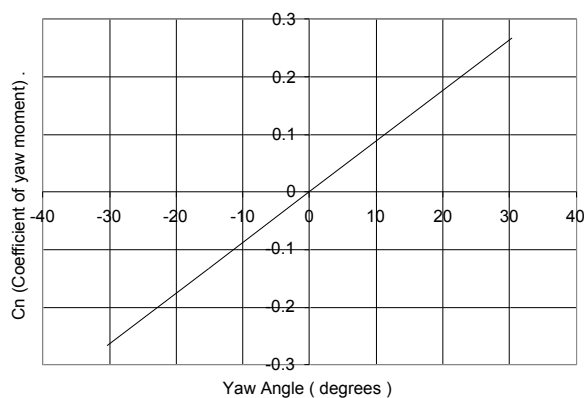


Figure 11.15 Coefficient of yaw moment versus yaw angle (left)

Figure 11.16 Coefficient of yaw moment versus rudder deflection (right)

Advanced Logistics Delivery System

It can be seen from these graphs that at maximum rudder deflection, a yaw angle of approximately ± 30 degrees can be created. This value is only approximate due to the code used to generate the value. Thus value of yaw angle may be a bit different, probably less, in real flight. The maximum value of crosswind the glider at desired flight speed is calculated as follows:

$$V_{\text{MaxCrosswind}} = V_{\text{Desired}} \sin(B_{\text{Max}})$$

The value for maximum crosswind the glider can handle is 30 ft/sec.

11.14 Roll Stability and Control

Roll stability was achieved through tail sizing and increased by adding 1.65 degrees of dihedral angle to the wings. Roll control was extremely limited due to the absence of ailerons and control surfaces on the wings. The following set equations were used to find the roll rate for the glider at various rudder deflections:

$$p = (-2 V C_{l\beta} B) / (C_{lp} b) \quad (\text{Roll Rate})$$

The value of sideslip was set using:

$$B = -(C_{n\delta r} \delta r) / C_{n\beta} \quad (\text{Yaw angle})$$

The results from these calculations can be seen below in Figure 11.17.

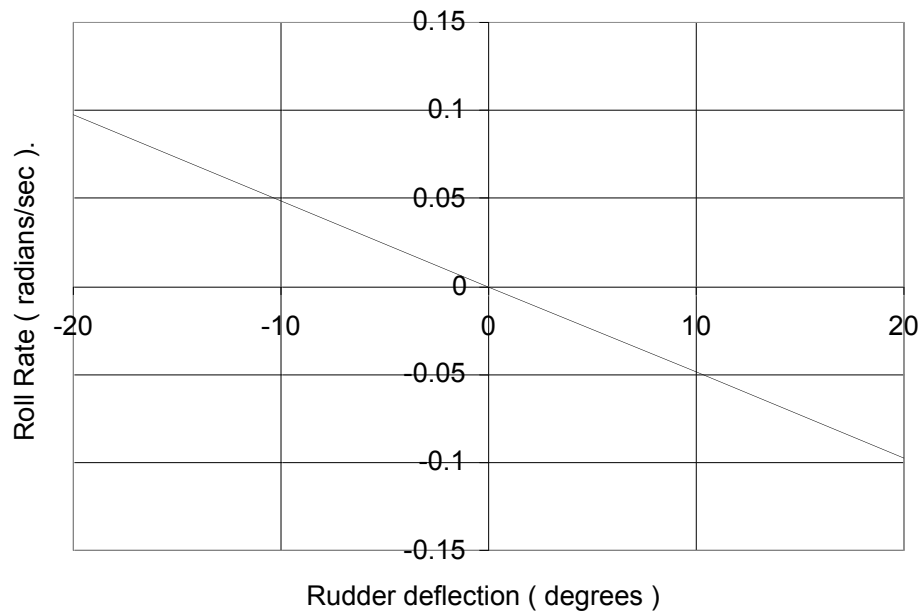


Figure 11.17 Roll rate versus rudder deflection.

From this graph we can note the glider is capable of a roll rate of 0.1 radians/sec, or 5.85 degrees/sec, at maximum rudder deflections. This value equates to completing a 45 degree turn in 7.7 seconds. Since the glider can only create minimal rolling and yawing moments, it will be very important for the ship to aim the glider at target pre-launch.

11.15 Servo Motors

To move the control surfaces on the tail three servo motors will be installed in the tail section of the fuselage. Each servo will move one control surface. The control surfaces are as follows: one rudder with a 4 ft span and a 2 ft chord and 2 elevators each with a 5 ft span and 2 ft chord. The servos are located behind the avionics package inside the tail section of the fuselage for configuration purposes. The locations of each motor can be seen in figures 4.11 and 4.12 of Chapter 4 of this report. The avionics package has the capability to control the servo movements so there will be no need for additional hardware. In order to determine the servos required for this mission, it must be realized that there are two phases, launch and glide. During launch phase the control surfaces must act similar to

Advanced Logistics Delivery System

control surfaces on a ballistic. During the glide phase the control surfaces must act as those on a normal sailplane. The servo motors were designed with the glide phase in consideration. This is because the glide phase will require more control surface movement to change flight paths mid flight. The launch phase does require some consideration; however, their only criterion is that it maintains stability up to the point of wing deployment. To compensate for the changing phases the software accompanying the avionics package must have the ability to vary the gain factors in the avionics so that the servos will be controlled in two different aspects depending on the phase of the flight.

To decide on a servo motor the required torque on each control surface is determined. This is done by factoring in the control surface size, the glider velocity and the configuration of the servo to the control surface. To expedite this process the design software Linkage Design Version 1.01 developed by Envision Designs was used (Blaine, 2005). This software allows the user to configure the servo-control surface connection. These connections can be seen in Figure 11.18 in which the maximum deflections of the control surface are shown in dashed lines.

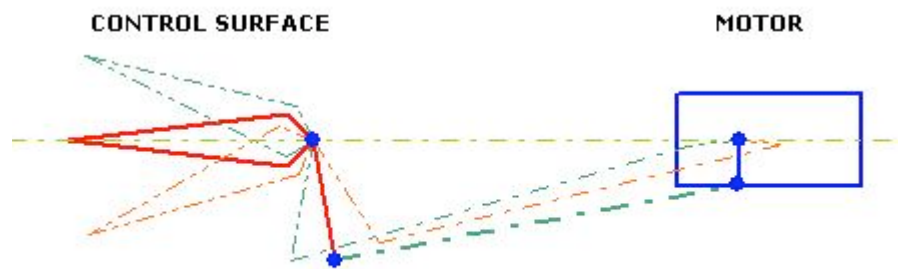


Figure 11.18n Design Layout for Motor Control Surface Connection (drawing is not to scale)

The Linkage Design program also takes in the control surface properties and the speed at which the glider is traveling. Two speeds were analyzed. The first speed analyzed was the glider cruise speed of approximately 70 mph. The second speed analyzed was the launch speed estimated at

Advanced Logistics Delivery System

500 mph. The results for the estimated torque values for each servo at the glide speed are summarized in Figure 11.19. The results for the launch phase are summarized in Figure 11.20.

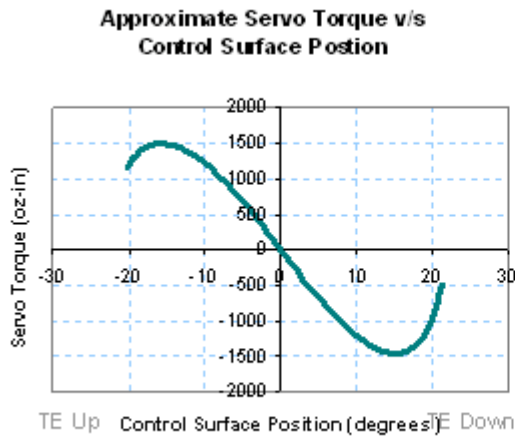


Figure 11.19 Approximate Torque Req.

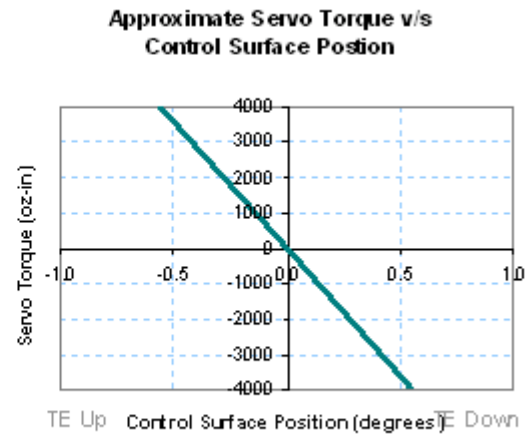


Figure 11.20 Approximate Torque Req.

For the glide phase the servos must be capable of handling about 1500 oz-in of torque. It is important to note that in Figure 11.19 there is a non-linear relationship between the torque required and the deflection angles. This is explained through the design configuration shown in Figure 11.18. Each connection point in Figure 11.18 is connected by a pin, except for the connection at the control surface. This means that as the motor rotates, there will be a point where the motor will not need to apply as much torque since the angles it must rotate through will be shortened. Figure 11.19 shows how the torque requirements for the launch phase for the same size control surfaces. As expected with the large speed difference, a much larger torque is required. This means that the tail will not be able to deflect as much during the glide phase. Since the larger control surfaces are designed for the glide phase the launch phase performance there are two options to solve this problem. The first solution is two use the tail control surfaces to maintain stability. The second solution is to use smaller control surfaces attached behind the stub wings. Keeping both solutions in mind a suitable servo motor was chosen.

Advanced Logistics Delivery System

The servo for this aircraft was chosen to optimize performance during glide phase and keep the total weight of the combined motors at a minimum. The size must also be considered because there is little space allowed in the tail section of the fuselage. With these aspects in mind the Parker Hannifin Corporation's Servo Motor 1053K was chosen. The motor weighs 19 pounds adding a total of 60 pounds to the glider weight. The motor has a peak torque of 3513 oz-in (Parker, 2005). This provides more than enough power to move the control surfaces during the glide phase and sufficient amount of power for the launch phase for small angle deflections or for additional control surfaces controlled by the same type of motors.

Chapter 12 AVIONICS PACKAGE

The project at hand involves deploying a military glider from a naval ship about 50 miles from the arrival destination. The primary objective will be to deliver prepackaged military artillery and other items to military personal on shore. To ensure a quick and safe arrival to its destination, the glider will use an advanced avionics package.

12.1 Piccolo Plus: An Introduction

The avionics package that will be used is the Piccolo Plus autopilot system made by Cloud Cap Technology in Hood River, Oregon. This package is depicted in figure 12.1 below.

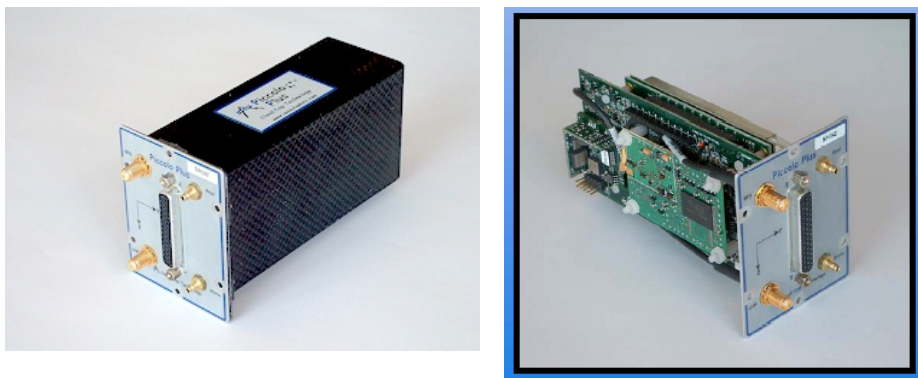


Figure 12.1: Piccolo Plus avionics package (taken from www.coudcaptech.com)

Advanced Logistics Delivery System

The Piccolo Plus is a second generation of the original Piccolo package and has advanced capabilities that most other avionics systems do not have. Figure 12.2 is the block diagram of the Piccolo Plus. The block diagram shows how all of the sensors, the GPS system and gyros feed back into the central processor.

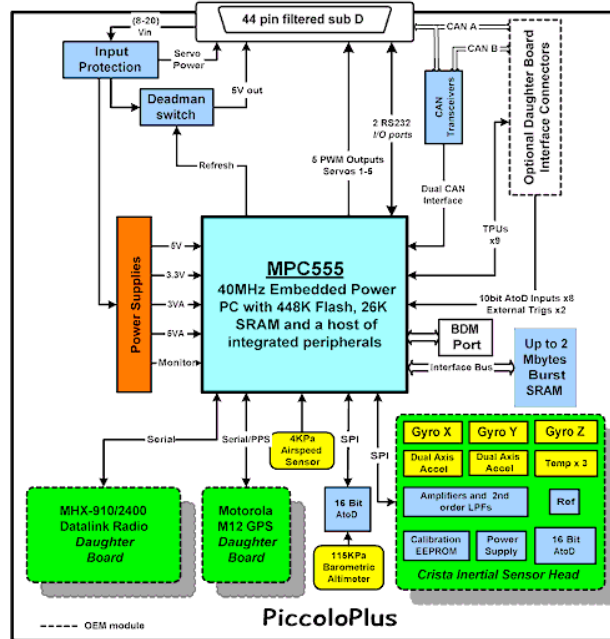


Figure 12.2: Piccolo Plus block diagram (taken from www.coudcaptech.com)

It is a complete package that includes avionics hardware and software, ground station hardware and software, and a development simulation environment. These will be discussed in further detail later.

Some key characteristics of the Piccolo are listed in table 11.1 below:

Table 12.1 Key Characteristics

Size	4.8" x 2.4" x 1.5" (121.92mm x 60.96mm x 38.1mm)
Weight	212 grams (7.5 oz)
Power	8 to 20 V DC, 3.6 Watts at 12 Volts nominal
Temperature Range	-40 to 185°F (-40 – 85°C)

Other key features that are important to the operation of the glider are:

- It's highly integrated with sensors, GPS, enclosure and communications link.
- Autonomous flight operation (with catapult launch and autoland)

Advanced Logistics Delivery System

- End-user programmability
- It supports up to 10 aircraft with a single operator interface and Ground station (especially important because of reduced costs)
- Integration with FalconView – an advanced mapping and flight planning system based on military planning

12.2 Components of the Piccolo Plus

The Piccolo Plus is comprised of several different components each with its own function within the system. Here are several components that make up the Piccolo:

1. **CPU** – First there is the brain of the system, the Central Processing Unit, a MPC555 microcontroller. Based on the PowerPC architecture, this unit joins a wide range of interfaces with a powerful RISC engine that delivers 40 MHz PowerPC operations.
2. **Sensors**- Inertial sensors and air data sensors are the two primary sensors offered in this package. The inertial sensors are composed of 3 Tokin CG-16D rate gyros and 3 ADXL202 accelerometers which when combined, allows the Piccolo to operate a variety of aircraft and installation in any attitude. The air data sensors are comprised of a dual ported mpxv50045 4kPa dynamic pressure sensor, an absolute ported barometric pressure sensor and an air temperature sensor. These give the Piccolo the ability to measure true air speed and altitude.
3. **Navigation**-The navigation system used in the Piccolo follows circled paths as defined by waypoints stored in a typical flight plan. The flight plan can also be changed during flight if necessary. To obtain position and ground speed for each flight plan, the Piccolo uses a GPS the Piccolo uses a Motorola M12 GPS. It is capable of making corrections via the data link. To measure winds the Piccolo fits the true airspeed with the groundspeed.

Advanced Logistics Delivery System

4. **Datalink-** The datalink is used primarily for command and control, autopilot telemetry differential GPS corrections, and pilot in the loop modes. This datalink also allows multiple aircraft to be controlled from one ground station.

12.3 Ground station

As previously stated the Piccolo Plus ground station gives the operator the ability to control the aircraft from a base on the ground. It has the ability to control up to 10 aircraft at once and also manage the communication link to each of the avionics systems in the aircraft. It uses the same hardware used for the avionics package, and provides an interface to the pilot in the loop console, a source that oversees the operation of the ailerons, elevator, rudder, autopilot, flaps, brakes and other components not applicable to our aircraft. It also provides a command and control stream to the operator interface PC. Powered will be supplied by a supply unit included with the package. There is also a battery backup available in case of a power failure.

12.4 Components of Avionics System (Some Operator Interfaces):

Piccolo Autopilot

The autopilot will be used to direct the glider to its destination. The autopilot commands page will display the status of the commands and allows for updating commands. With various inputs and parameters entered into the commands page, the glider will be capable of flying unmanned. Figure 12.3 is an example of the autopilot command page.

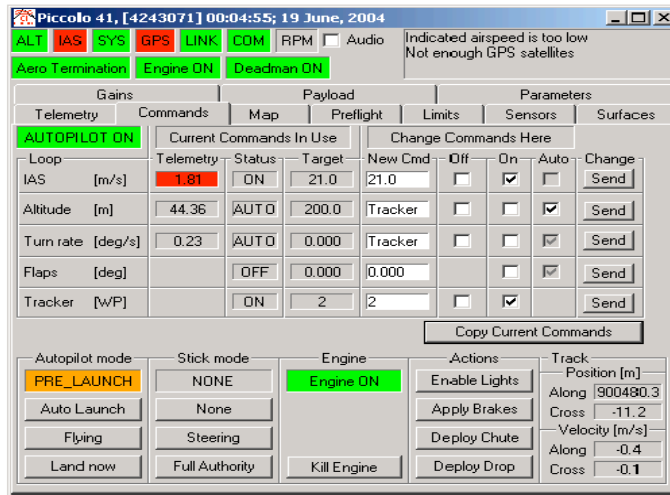


Figure 12.3: Autopilot commands page

Flight plans

Flight plans can be created and stored in the map display page in the user interface. This page will also be capable of displaying the current location of the vehicle, in our case the glider. Figure 12.4 is an example of the map page and the flight plan, in our case the map will be of the target area on the shore.

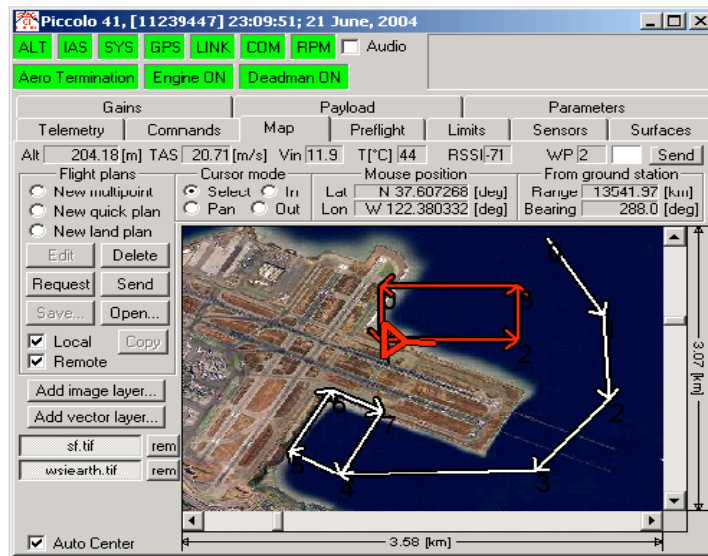


Figure 12.4: Map page

The vector arrows indicate two types of flight plans, local and remote flight plans. The remote flight plans shown in red, are stored in the avionics unit, the local flight plans, shown in white are usually

Advanced Logistics Delivery System

stored on the user interface and have not been sent to the avionics unit. Each flight plan will be made using linked waypoints. Each waypoint will include latitude, longitude, altitude and the index of the next waypoint to be used. The Piccolo has 100 waypoints stored. To prevent the system from veering off the segment that follows the way point a feature called a pre-turn can be enabled. To perform a landing a mark would be made on the map where touch down will occur with a waypoint, in the landing plan screen we would enter the starting index of the landing plan and a touchdown altitude. With this information a landing plan will be generated and sent to the aircraft which will then use such settings as approach length and glide angle to make the landing. The landing plan generation is created by simply checking the “land” box next to the last index number in the flight plan view.

12.5 Avionics Integration to Glider Aircraft

The Piccolo Plus will be installed in the rear portion of the glider fuselage in a horizontal or vertical mounting system. The Piccolo will be bolted down to the frame of the glider to ensure its safety during the flight. Two antennas will also be installed along with the Piccolo. These are the COMM antenna and the GPS antenna. The COMM antenna is used for line of sight communication between the Piccolo and the ground station, the GPS antenna is used for position and velocity determination. To maximize performance and data collection the antennas will likely be stuck out the back end of the tail, free from any obstruction. The Piccolo comes with pressure port inputs to measure total and static pressure. The pitot-static tube for these ports will be placed on nose of the glider and linked to the avionics package. The Piccolo Plus will also be linked to the control surface motors so that the auto-pilot and flight planning options can be used to control and stabilize the glider.

Advanced Logistics Delivery System

12.6 Piccolo Pricing

Table 11.2 lists the prices of the avionics package as well as various accessories.

Item or Accessory	Cost
Piccolo Plus Avionics Package (including integrated data link, GPS, operating environment and autopilot software)	\$6,000.00
Battery Pack, 12V 2700ma 10-Acell NIMH Piccolo	\$112.00
Generic Mounting Kit (optional)	\$85.00
Total (per glider)	\$6,197.00
Ground Station (includes desktop power supply, AC power chord, adaptor, antenna mag mount, GS antenna, serial cable, pilot console cable)	\$7,500.00
Ground Station Power Supply	\$66.00
Total (one time costs)	\$7,566.00

Table 12.2 Piccolo Pricing

Chapter 13: Sizing and Relationship to Ship Configuration

13.1 Introduction

The ship that the gliders are going to be launch off of is an extremely limiting factor in the sizing design of the glider and contributes the sizing requirement to the RFP. The ship dictates that the glider must be able fit into the 10 foot diameter launch tunnel. The other major issue that the ship provides the glider design team with is the need to be able to store 233 gliders per day on it.

13.2 Glider Storage

It is anticipated that 233 gliders can be assembled and launched off the ship in one day. For the following analysis the ship is assumed to be a four-day ship. Each ship will have four rooms, each room containing a days worth of gliders, coming to a total of 932 gliders per ship. The rooms are 2000 square foot in surface are and are eight feet high, allowing the planes to be stacked in any arrangement possible. Each room is to be completely filled, from floor to ceiling, with gliders. Unfortunately as the

Advanced Logistics Delivery System

following numbers will show it is impossible to fit 233 gliders into such a small room. Just by sheer volume (ignoring the fact that the gliders can only stack certain ways without interference), a total of 203 gliders can be stored in the given space. Due to the way the parts have been assembled and how they can physically stack within the required space, only 130 gliders will fit per room.

13.2.1 Volume Calculations

The total volume of an individual plane was determined by calculating the volume of different pieces of the plane and adding them all together. The glider was divided into four sections. The first section was the nosecone. The volume of the nosecone was found using inventor. Each of these pieces will occupy 16,190 cubic inches. The second section was the cylindrical fuselage, with radius of 30.125 inches and a length of 96 inches. The volume was determined using the equation for the volume of a cylinder, which is $\pi * r^2 * L$ where r is the radius and L is the length. Each fuselage will require 68,430 cubic inches of space. The third section was a combination of two identical pieces, the stub wings. The combined volume of the two wings came out to be 4,928 cubic inches. The fourth and final part of the plane to be included in the volume calculations was the tail. The tail was divided into two sub-parts; the main fuselage portion of the tail, and the vertical piece. The volume of the vertical piece was 522 cubic inches, taken off of inventor. The volume of the fuselage portion of the tail was estimated by taking two thirds of the volume of the cylindrical fuselage, which was approximately 45,620 cubic inches. All of the sections were added up and the total volume of a single glider is estimated to be 135,691 cubic inches. This total volume yields the result that 203 gliders can be fit in each room based on sheer volume alone.

13.2.2 Glider Arrangement

The configuration that allows the most planes to be stacked in the room divides the room into three main sections. All the nosecones will be stacked in two rows against one side of the room. Six

Advanced Logistics Delivery System

of these pieces can be stacked on top of each other before they reach the maximum height. In one row, there are 17 stacks, and in the second row there are 5 stacks. The fuselage is the second part of the configuration. Each fuselage has the stub wings already attached. There are four layers of this part of the plane. The first layer sits on the floor, with the gliders touching end to end. Five planes will fit in this fashion to form the first row. The planes also line up wing to wing forming a grid. The wings will overlap so the gap between it and the neighboring fuselage is 32 inches. This will allow for another fuselage to be stacked on top of the wings, in between each of the two lower ones. When this is done, there is room for seven planes to sit side by side in the bottom layer. The whole bottom layer will contain 35 fuselages with stub wings attached. The second layer will sit on top of the first. Each fuselage of the gliders in this layer will rest on top of the wings from the row below. Instead of seven rows of planes, there will only be six. This means that the second layer will consist of 30 planes. The first and the third layers will have the same number, and the second and the fourth layers will have the same, totaling to 130 gliders. The third section of the room consists of all the remaining empty space. The tail section of the glider will be stored in this space. This configuration assumes that the gliders can be stored on top of one another without sustaining any damage.

13.3 Glider Storage Conclusions

The 2,000 square foot storage room cannot hold all of the 233 gliders. The room dedicated to storing the gliders consists of 27,648,000 cubic inches. By volume only, the room can hold 203 gliders. That is 30 short of the estimated amount per room. However, this figure does not take into account the way the gliders are placed in the room. Each plane must stack on top of another plane in a specific way. Several configurations were considered, but the final design for placing the planes in the room (described above) allows for a maximum of 130 gliders. 64% of the volume in the room will be taken up by the plane in its current configuration.

Advanced Logistics Delivery System

The 130 gliders that can be staked in the intended storage rooms falls 103 short of the anticipated number of 233. This discrepancy was discussed with the ocean engineers working on the ALDS project and as a result the remaining gliders are going to be stored on decks lower in the boat and brought up to the assembly room by an elevator for production.

Chapter 14: Cost Analysis

14.1 Individual Glider Costs

The price of each glider is based on the materials that they are composed of and the unit prices of the materials. This is a good estimate for the cost of the glider without the labor included, which would be primarily done on the ships. The price may also turn out to be less than the prices quoted here because the military may be able to negotiate a bulk discount on the materials if they plan on launching 233 of these gliders a day. Table 14.1 summarizes the cost estimates for each glider and for the ground station technology if it is determined to be necessary.

Table 14.1 Cost Summary per Glider

Structures: Fuselage (110 lbs. Al Alloy and Carbon Fiber)	\$2,500
Avionics Package	\$6,197
Airbag System	\$5,500
Inflatable Wings: Material	\$8,383
Control Motors	\$6,042
Total (per glider)	\$28,622
One time cost (Avionics Ground Station)	\$7,566

14.2 Cost per Pound Payload Deliverable

The cost of each individual glider however does reveal how financially viable the glider delivery system is. A way to compare the ALDS to other currently used methods for delivery of

Advanced Logistics Delivery System

supplies to troops in hostile territories is by calculating how much each method cost to deliver a pound of payload to troops. The cost per pound deliverable calculation takes into account all costs that go into delivering supplies including operational cost and the costs of the ships that the gliders launch from. The cost per pound payload deliverable for the glider will be compared to the cost per pound payload deliverable for the C-130 Hercules and the Chinook Heavy-Lift Helicopter two current aircraft used to deliver supplies to troops. The equation used to calculate the cost per pound payload deliverable for the glider is:

$$\frac{Cost}{lb} = \frac{GliderCost + \frac{ShipCost / years}{\# Launches / Ship / year} + \frac{OperationalCosts}{\# Launches / Ship / year}}{1000lbs.}$$

In the above equation the GliderCost is the cost for each glider that was calculated in the previous section, the ShipCost is \$110.03 million (from the Ocean Design Group), the number of years that the ship is expected to be in operation for is 20 years. The operational cost for the ship is \$59.98 million per year (from the Ocean Design Group) and since the ship is assumed to be a four day mission ship that goes out 5 times a year and make 233 launches a day the #Launches/Ship/year is 4660. When all of those values are plugged in the equation becomes:

$$\frac{Cost}{lb} = 28.62 + 1.18 + 12.87 = \$42.67$$

Therefore it cost \$42.67 for each pound of payload delivered to the troops.

The C-130 Hercules is the lowest priced aircraft designed to deliver large amounts of payload that is currently on the market. The unit cost for a C-130 Hercules is \$44.1 million. Operational costs for the C-130 Hercules in 2002 for the 148 active C-130 Hercules planes in the airforce was \$1,198.9 million. The Hercules can carry a maximum payload of 42000 lbs. per trip and can make around 33

Advanced Logistics Delivery System

trips per year for a total of 20 years(GAO report, 2003). This information and the following equation yields the cost per pound payload deliverable for the C-130 Hercules:

$$\frac{Cost}{lb} = \frac{\frac{UnitCost}{TotalDrops} + OperationalCost / trip}{MaxPayload} = 1.59 + 5.84 = \$7.43$$

Therefore the cost per pound payload deliverable for the C-130 Hercules is \$7.43.

The Chinook Heavy-Lift helicopter is also designed to carry large amounts of supplies to troops. The unit cost of the Chinook is \$26.1 million. The maximum payload it can carry is 3038 lbs. The GAO reported that the operational costs for the Chinook from 1989 to 1999 were \$3.6 billion for an average of 115 helicopters. For the calculations for cost per pound payload for the Chinook the same equation is used as for the Hercules and the Chinooks is assumed to be able to make 30 trips per year. The cost per pound payload delivered is as follows:

$$\frac{Cost}{lb} = \frac{\frac{UnitCost}{TotalDrops} + OperationalCost / trip}{MaxPayload} = 14.32 + 34.35 = \$48.67$$

Therefore the Chinook Helicopter is the most expensive method of payload delivery based on the assumption that it will make 30 deliveries per year.

14.3 Cost Conclusions

The following table compares the cost of the three payload delivery methods.

Delivery Method	Unit Cost	Cost per Pound Payload
Glider	\$16,697	\$42.67
Hercules	\$44.1 million	\$7.43
Chinook	\$26.1 million	\$48.67

Table 14.2 Cost Comparison between Delivery Methods

Therefore the glider delivery method is not to expensive and is a financially feasible option because even though the Hercules is approximately \$35 per pound payload cheaper the pilots life is in danger in an airdrop but with the glider no ones life will be in definite danger. The avionics system and the

Advanced Logistics Delivery System

motors in the glider are also reusable and could be used either in another glider if recovered or by the ground troops, which would make the gliders even more cost effective. All of these calculations were done using assumptions on the usage of each method, the more often any of these methods are used the more the price per pound payload will decrease.

Chapter 15 Conclusions and Future Work

In this report a glider design was presented that will be capable of sustaining extreme launch forces and gliding for 50 miles to deliver supplies to troops in hostile territories. The glider design currently satisfies all of the RFP criteria. It will be capable of obtaining a range of 50 miles, it can structurally withstand the launch acceleration of 30g's and launch speed of 500 knots, it is within the launch size specifications, it has room for the 1000 lb payload and the structural integrity to hold it, the ability to cruise at 60 knots and although it does weight above 500 lbs it is not so much heavier that it will be a problem. The \$28,622 per glider price tag is a slightly higher cost than would be required for the glider to be disposable a more realistic number would be approximately \$15,000 per glider but with future analysis we are confident that number can be reduced.

References:

- 1.) Beer, Ferdinand P. Mechanics of Materials. Third Edition, McGraw-Hill. New York, NY. ©2001.
- 2.) Bertin, John J. Aerodynamics for Engineers. 4th Edition. New Jersey: Prentice Hall. © 2002.
- 3.) Blaine K. Beron-Rawdon. Linkage Design. Version 1.01. Envision Design, 1536 W. St. PMD 104, San Pedro CA. Accessed 2005. Available at:
members.cox.net/evdesign/pages/about_envision_design.html
- 4.) Carbon Fiber Reinforced Carbon. <http://www.sglcarbon.com>. © 2004.
- 5.) Casidy, Rachel and Regina Frey. “Gas Laws Save Lives: The Chemistry Behind Airbags.” Accessed 2005. Avail. www.chemistry.wustl.edu/~edudev/LabTutorials/Airbags/airbags.html
- 6.) Celanese. “Vectran Fiber a Unique Combination of Properties for The Most Demanding Applications” Accessed 2005. Avail. <http://www.vectranfiber.com/index1.html>
- 7.) Cloud Cap Technology Website. Accessed 2005. www.cloudcaptech.com.
- 8.) Crimi, Peter. “Divergence of an Inflated Wing,” *Journal of Aircraft*, vol. 37, no. 1, January-February 2000, pp. 184-186.
- 9.) Drela, Mark. XFOIL Subsonic Development System. Version 6.9. Massachusetts Institute of Technology. Accessed 2005. <http://raphael.mit.edu/xfoil/>
- 10.) Drela, Mark. XFOIL 6.9 User’s Guide. Massachusetts Institute of Technology. Accessed 2005. http://raphael.mit.edu/xfoil/xfoil_doc.txt
- 11.) E-A-R Specialty Composites. Accessed 2005. <http://www.earsc.com>. © 2002.
- 12.) Edge Structural Composites. “Fiberbond Technical Data” Accessed 2005. avail. <http://www.edgest.com/edgedatacarb335.html>
- 13.) Edwards. “Tech Space – Inflatable Wings Given A Flutter.” July 9, 2001 avail. <http://www.spacer.com/news/plane-inflatable-wing-01a.html>
- 14.) Government Accountability Office Report. Information on the Air force’s C-130 Aircraft. Accessed 2005. Avail: <http://www.gao.gov/archive/1998/ns98108.pdf>
- 15.) Government Accountability Office Report. Helicopters Cost is Understated. Accessed 2005. Avail: <http://161.203.16.4/t2pbat4/150587.pdf>
- 16.) Goodyear Aircraft. ”Engineering Report on the Development of a One-Place Inflatoplane,” April 1957. Report Number GER 8146.

Advanced Logistics Delivery System

- 17.) Hoerner, S.F. “Fluid Dynamic Drag”, Published by the author, Vancouver, WA. ©1958.
- 18.) Hong, Soongu. “A Study on the Modeling Technique of Airbag Cushion Fabric” Accessed 2005. avail.
http://www.automotive.tno.nl/Madymo/Publications/UMWorld2002/P07_Airbag_cushion_MOBIS.pdf#search='young%20s%20modulus%20for%20airbag
- 19.) MandevTubes. “Formulas and Specifications” Accessed 2005. avail.
<http://www.mandevtubes.com/specs2.html>
- 20.) Marchman, James F. Introductory Aircraft Performance. 2nd Edition. Blacksburg, Virginia: A-1 Copies. © 2001
- 21.) Mars Pathfinder Web Page. Accessed 2005. Avail.
<http://mpfwww.jpl.nasa.gov/MPF/mpf/mpfairbags.html>
- 22.) Mason, W. H. Simple Lifting Line Theory. Aerospace Engineering Dept. Virginia Polytechnic Institute and State University. Accessed 2005.
http://www.aoe.vt.edu/~mason/Mason_f/MRsoft.html
- 23.) Mason, W. H. Skin Friction/ Form Factor. Aerospace Engineering Dept. Virginia Polytechnic Institute and State University. Accessed 2005.
http://www.aoe.vt.edu/~mason/Mason_f/MRsoft.html
- 24.) Megson, T.H.G. Aircraft Structures for Engineering Students Second Edition, Halsted Press, New York, NY, © 1990.
- 25.) Murray, James E., “Ground and Flight Evaluation of a Small-Scale Inflatable-Winged Aircraft,” Nasa Dryden Flight Research Center, January 2002.
- 26.) Nihon University Student Group. Airfoil Database. Accessed 2005. <http://www.nasg.com/index-e.html>
- 27.) Parker Hannifin Corporation Servo Motor Online Catalog Accessed 2005. avail.
http://www.parker.com/compumotor/cat/english/M_Series.pdf
- 28.) Raymer, Daniel P. “Aircraft Design: A conceptual Approach, Third Addition”. AIAA Education Series. New York, NY. © 1999.
- 29.) Schetz, Joseph A. Boundary Layer Analysis. New Jersey: Prentice Hall. © 1993.
- 30.) Tsai, Stephen W. Theory of Composites Design, Think Composites, Dayton, OH, ©1992
- 31.) University of Kentucky, College of Engineering. “Big Blue 3” Accessed 2005. Avail.
<http://www.engr.uky.edu/~bigblue/>

Advanced Logistics Delivery System

- 32.) U.S. Centennial of Flight Commission. Accessed 2005.
http://www.centennialofflight.gov/essay/Theories_of_Flight/Stability/TH26.htm
- 33.) Wallace, Martin M. and Bert, Charles W. “Experimental Determination of Dynamic Young’s Modulus and Damping of an Aramid-Fabric/Polyester Composite Material” Accessed 2005. avail.
http://digital.library.okstate.edu/oas/oas_pdf/v59/p98_101.pdf#search='young%20s%20modulus%20for%20fabric%20material'
- 34.) Webber, J.P.H.,”Deflections of Inflated Cylindrical Cantilever Beams Subject to Bending and Torsion.” *The Aeronautical Journal*, vol. 86, no. 858, October 1982, Paper 1020, pp.306-312

Appendix A: Equations for Calculations

Name	Equation	Name	Equation
Aspect Ratio	$AR := \frac{b}{c}$	Mach Number	$Mach := \frac{V}{a}$
Wing Area	$S := b \cdot \bar{c}$	Drag Coefficient	$C_D := C_{D0} + C_{Di}$
Mean Chord	$\bar{c} := \frac{(c_t + c_r)}{2}$	Induced Drag Coefficient	$C_{Di} := \frac{C_L^2}{\pi \cdot AR \cdot e}$
Taper Ratio	$\lambda := \frac{c_t}{c_r}$	Glide Angle	$\theta := \tan^{-1} \left[\frac{1}{\left(\frac{L}{D} \right)} \right]$
Zero Lift Drag Coefficient	$C_{D0} := \left[\frac{1}{2 \left(\frac{L}{D} \right)} \right]^2 \cdot \pi \cdot AR \cdot e$	Minimum Sink	$Sink := V_{max} \sin(\theta)$
Maximum Lift Coefficient	$C_{Lmax} := \sqrt{C_{D0} (\pi \cdot AR \cdot e)}$	Reynolds Number	$Reynolds := \frac{(\rho \cdot V_{max} c)}{\mu}$
Maximum Velocity	$V_{max} := \sqrt{\frac{(2 \cdot W)}{\rho \cdot S} \cdot \left[\frac{1}{C_{D0} (\pi \cdot AR \cdot e)} \right]}$		
b = span (67 ft) c = mean chord (2.6 ft) c_t = tip chord (3.852 ft) c_r = root chord (1.348 ft) e = efficiency factor (0.96)		W = Weight ρ = Density (0.001884 slugs/ft ³) a = Speed of Sound (1086 ft/s) c = chord length (ft) μ = viscosity (3.583*10 ⁻⁷ lb*sec/ft ²)	

Table A1 Aerodynamics Equations Table

Appendix B: Boundary Layer Analysis Output

Wortmann 170 Rigid				Wortmann 170 One Percent Deflation			
Upper Surface		Lower Surface		Upper Surface		Lower Surface	
1	0	0.001028	-0.00211	1	0	0.001027	-0.00211
0.9864	0.003389	0.002597	-0.00383	0.985799	0.003387	0.002591	-0.00382
0.965576	0.008079	0.004595	-0.00536	0.963224	0.008059	0.00457	-0.00533
0.944449	0.012945	0.006795	-0.00674	0.939275	0.012874	0.006729	-0.00668
0.923203	0.018056	0.009185	-0.00796	0.914218	0.01788	0.009096	-0.00789
0.901927	0.023419	0.011793	-0.00899	0.89315	0.023191	0.011728	-0.00894
0.880719	0.02907	0.014609	-0.00988	0.875894	0.028911	0.014573	-0.00986
0.859617	0.035081	0.017601	-0.01073	0.857523	0.034996	0.01759	-0.01072
0.838601	0.041507	0.020743	-0.01162	0.83809	0.041482	0.020743	-0.01162
0.817637	0.048346	0.024053	-0.01255	0.817637	0.048346	0.024053	-0.01255
0.796683	0.055557	0.027564	-0.01347	0.796683	0.055557	0.027547	-0.01346
0.775695	0.063045	0.03131	-0.01437	0.775222	0.063007	0.031234	-0.01433
0.754677	0.070641	0.035314	-0.01524	0.752839	0.070469	0.035121	-0.01516
0.73369	0.078173	0.039599	-0.01611	0.729671	0.077745	0.039214	-0.01595
0.712774	0.085479	0.044193	-0.01698	0.705837	0.084647	0.043763	-0.01681
0.691915	0.092443	0.049133	-0.01786	0.685181	0.091543	0.048864	-0.01776
0.671093	0.098991	0.054466	-0.01875	0.667417	0.098449	0.054333	-0.0187
0.650281	0.105062	0.060244	-0.01965	0.648697	0.104806	0.060207	-0.01963
0.629449	0.11062	0.066529	-0.02056	0.629066	0.110553	0.066529	-0.02056
0.608579	0.115648	0.073393	-0.02148	0.608579	0.115648	0.073393	-0.02148
0.58766	0.120126	0.080915	-0.02242	0.58766	0.120126	0.080866	-0.02241
0.566682	0.124045	0.089188	-0.02339	0.566337	0.123969	0.088971	-0.02333
0.545641	0.127405	0.098311	-0.02438	0.544312	0.127095	0.097772	-0.02425
0.524543	0.130205	0.10839	-0.0254	0.521669	0.129492	0.107335	-0.02515
0.503395	0.132436	0.119533	-0.02643	0.498496	0.131147	0.11837	-0.02617
0.482197	0.134087	0.131833	-0.02746	0.477504	0.132782	0.131111	-0.02731
0.460946	0.135161	0.145353	-0.02848	0.458421	0.134421	0.144999	-0.02841
0.439646	0.135671	0.160112	-0.02948	0.438575	0.135341	0.160014	-0.02946
0.418301	0.135631	0.176072	-0.03044	0.418046	0.135548	0.176072	-0.03044
0.396919	0.135065	0.193139	-0.03134	0.396919	0.135065	0.193139	-0.03134
0.375515	0.134009	0.211168	-0.03216	0.375515	0.134009	0.211039	-0.03214
0.354121	0.132496	0.229992	-0.0329	0.353905	0.132415	0.229432	-0.03282
0.33278	0.130553	0.249446	-0.03352	0.331969	0.130235	0.24808	-0.03334
0.311547	0.128186	0.269381	-0.03404	0.30984	0.127484	0.266759	-0.03371
0.290481	0.12539	0.28967	-0.03446	0.287654	0.12417	0.286851	-0.03412
0.269643	0.122167	0.310212	-0.03476	0.267019	0.120978	0.308513	-0.03457
0.249108	0.118532	0.330936	-0.03495	0.247743	0.117883	0.33013	-0.03486
0.22898	0.11451	0.351792	-0.03503	0.228422	0.114231	0.351578	-0.035
0.209381	0.110131	0.372737	-0.035	0.209253	0.110064	0.372737	-0.035
0.190459	0.105447	0.393743	-0.03488	0.190459	0.105447	0.393743	-0.03488
0.172376	0.100528	0.414788	-0.03466	0.172376	0.100528	0.414535	-0.03464
0.155303	0.095446	0.435856	-0.03433	0.155208	0.095388	0.434794	-0.03425
0.139386	0.090287	0.456943	-0.0339	0.139046	0.090067	0.45444	-0.03371
0.124721	0.085134	0.47804	-0.03337	0.124038	0.084668	0.473388	-0.03304
0.111353	0.080076	0.499138	-0.03275	0.110269	0.079297	0.49428	-0.03243
0.099272	0.075167	0.520225	-0.03203	0.098306	0.074435	0.517375	-0.03185
0.088415	0.070446	0.541297	-0.0312	0.087931	0.07006	0.539978	-0.03112
0.078685	0.065939	0.562353	-0.03026	0.078493	0.065778	0.56201	-0.03024
0.069977	0.061646	0.583392	-0.02921	0.069934	0.061608	0.583392	-0.02921
0.062177	0.057559	0.604409	-0.02805	0.062177	0.057559	0.604409	-0.02805
0.055173	0.053672	0.625381	-0.0268	0.055173	0.053672	0.625	-0.02678
0.048864	0.049978	0.646298	-0.02541	0.048834	0.049948	0.644724	-0.02535
0.043172	0.046457	0.667152	-0.02388	0.043067	0.046344	0.663497	-0.02375
0.038034	0.043073	0.687936	-0.02217	0.037826	0.042837	0.681241	-0.02196
0.033379	0.039815	0.708661	-0.02024	0.033054	0.039428	0.701764	-0.02004
0.029102	0.03673	0.729361	-0.01807	0.028819	0.036373	0.725365	-0.01797
0.025122	0.033857	0.750057	-0.01571	0.024984	0.033672	0.74823	-0.01567
0.021427	0.031154	0.770751	-0.01322	0.021375	0.031078	0.770281	-0.01321
0.01806	0.028512	0.791395	-0.0107	0.018049	0.028495	0.791395	-0.0107
0.015044	0.025852	0.811899	-0.00825	0.015044	0.025852	0.811899	-0.00825
0.012351	0.023174	0.83221	-0.00598	0.012351	0.023174	0.831703	-0.00598
0.009943	0.020509	0.852308	-0.00398	0.009937	0.020497	0.850232	-0.00397
0.007785	0.01788	0.87215	-0.00226	0.007766	0.017836	0.867372	-0.00225
0.005858	0.015282	0.891665	-0.00096	0.005826	0.015198	0.882987	-0.00095
0.004147	0.012708	0.910812	-0.00037	0.004107	0.012584	0.901948	-0.00037
0.002659	0.010151	0.929731	-0.00068	0.002633	0.010052	0.924638	-0.00068
0.001468	0.007604	0.94867	-0.00124	0.00146	0.007562	0.946359	-0.00124
0.000635	0.005064	0.967785	-0.00119	0.000633	0.005052	0.967195	-0.00118
0.000158	0.002529	0.987077	-0.00058	0.000158	0.002527	0.987077	-0.00058
0.000042	0.001275	1	0	0.000042	0.001275	1	0
0	0			0	0		

Figure B1 Wortmann FX 67-K-170 Contours

Wortmann 150 Rigid				Wortmann 150 One Percent Deflation			
Upper Surface		Lower Surface		Upper Surface		Lower Surface	
1	0	0.001429	-0.00181	1	0	0.001428	-0.001806
0.986543	0.003209	0.003291	-0.00318	0.985942	0.003207	0.003283	-0.003176
0.965916	0.007573	0.005466	-0.00436	0.963563	0.007555	0.005436	-0.004339
0.94495	0.012056	0.0078	-0.0054	0.939773	0.011990	0.007724	-0.005348
0.923835	0.016722	0.010301	-0.0063	0.914844	0.016559	0.010201	-0.006236
0.902665	0.021585	0.012977	-0.00707	0.893880	0.021375	0.012906	-0.007027
0.881534	0.026684	0.015822	-0.00776	0.876705	0.026538	0.015783	-0.007740
0.860481	0.032084	0.018822	-0.00845	0.858385	0.032006	0.018811	-0.008444
0.839496	0.037829	0.021977	-0.00917	0.838985	0.037806	0.021977	-0.009166
0.818562	0.043938	0.025307	-0.00989	0.818562	0.043938	0.025307	-0.009894
0.797635	0.050376	0.02884	-0.01061	0.797635	0.050376	0.028822	-0.010607
0.776685	0.057056	0.032599	-0.01131	0.776212	0.057021	0.032520	-0.011286
0.755716	0.06385	0.036609	-0.012	0.753875	0.063694	0.036408	-0.011937
0.734761	0.070595	0.040894	-0.01269	0.730736	0.070208	0.040496	-0.012565
0.713858	0.077165	0.045486	-0.01338	0.706911	0.076414	0.045043	-0.013245
0.693018	0.083458	0.050423	-0.01407	0.686274	0.082646	0.050147	-0.013990
0.67222	0.089386	0.05575	-0.01477	0.668538	0.088896	0.055614	-0.014731
0.651436	0.0949	0.061519	-0.01548	0.649849	0.094669	0.061482	-0.015469
0.63065	0.099963	0.067792	-0.0162	0.630266	0.099902	0.067792	-0.016199
0.609839	0.104546	0.074639	-0.01693	0.609839	0.104546	0.074639	-0.016930
0.588989	0.108642	0.082142	-0.01768	0.588989	0.108642	0.082092	-0.017666
0.5681	0.112241	0.09039	-0.01845	0.567754	0.112173	0.090170	-0.018401
0.547163	0.115327	0.099484	-0.01924	0.545830	0.115046	0.098939	-0.019131
0.526174	0.117909	0.10953	-0.02003	0.523292	0.117263	0.108464	-0.019839
0.505145	0.119983	0.120634	-0.02084	0.500229	0.118815	0.119460	-0.020632
0.484074	0.121529	0.132886	-0.02165	0.479363	0.120346	0.132158	-0.021527
0.46295	0.122562	0.146345	-0.02245	0.460414	0.121891	0.145989	-0.022399
0.441785	0.123107	0.161025	-0.02323	0.440709	0.122807	0.160927	-0.023219
0.420591	0.123167	0.176891	-0.02398	0.420335	0.123092	0.176891	-0.023976
0.399374	0.122764	0.19384	-0.02467	0.399374	0.122764	0.193840	-0.024673
0.378158	0.121923	0.211729	-0.0253	0.378158	0.121923	0.211600	-0.025285
0.356971	0.120659	0.230395	-0.02585	0.356754	0.120585	0.229834	-0.025785
0.335846	0.118978	0.249674	-0.02631	0.335028	0.118688	0.248306	-0.026169
0.314825	0.116886	0.269415	-0.02669	0.313100	0.116246	0.266793	-0.026432
0.293952	0.114378	0.289496	-0.02698	0.291091	0.113265	0.286679	-0.026719
0.273276	0.111476	0.309821	-0.02718	0.270616	0.110391	0.308124	-0.027030
0.252885	0.108207	0.330322	-0.02728	0.251500	0.107614	0.329517	-0.027216
0.23288	0.104575	0.350947	-0.0273	0.232313	0.104320	0.350733	-0.027283
0.213376	0.100615	0.371655	-0.02723	0.213246	0.100554	0.371655	-0.027234
0.194527	0.096372	0.392423	-0.02708	0.194527	0.096372	0.392423	-0.027082
0.176492	0.091895	0.413233	-0.02685	0.176492	0.091895	0.412981	-0.026835
0.159432	0.087275	0.434066	-0.02654	0.159335	0.087222	0.433009	-0.026476
0.143508	0.082582	0.454916	-0.02615	0.143158	0.082381	0.452424	-0.026006
0.128816	0.077882	0.475777	-0.02568	0.128110	0.077455	0.471147	-0.025431
0.115401	0.073272	0.496638	-0.02514	0.114278	0.072559	0.491805	-0.024891
0.103263	0.068798	0.517493	-0.02451	0.102258	0.068128	0.514658	-0.024371
0.092341	0.064478	0.538346	-0.02379	0.091835	0.064125	0.537035	-0.023730
0.082535	0.060353	0.559193	-0.02299	0.082334	0.060206	0.558852	-0.022974
0.073736	0.056439	0.580027	-0.02211	0.073691	0.056405	0.580027	-0.022107
0.065842	0.052714	0.600844	-0.02114	0.065842	0.052714	0.600844	-0.021141
0.058743	0.049162	0.621638	-0.02009	0.058743	0.049162	0.621259	-0.020075
0.052336	0.045781	0.642401	-0.01894	0.052304	0.045753	0.640836	-0.018897
0.046535	0.042566	0.663122	-0.01769	0.046422	0.042462	0.659489	-0.017591
0.041273	0.039491	0.683805	-0.0163	0.041047	0.039275	0.677150	-0.016136
0.03649	0.036528	0.704459	-0.01475	0.036135	0.036173	0.697603	-0.014608
0.03212	0.03368	0.725094	-0.01305	0.031807	0.033352	0.721122	-0.012980
0.028088	0.030975	0.745725	-0.0112	0.027934	0.030805	0.743908	-0.011172
0.024339	0.028429	0.766361	-0.00924	0.024280	0.028360	0.765894	-0.009231
0.020868	0.025997	0.786982	-0.00724	0.020855	0.025981	0.786982	-0.007241
0.017686	0.023611	0.807532	-0.0053	0.017686	0.023611	0.807532	-0.005298
0.014792	0.021227	0.827978	-0.00348	0.014792	0.021227	0.827474	-0.003481
0.012173	0.018842	0.84831	-0.00186	0.012166	0.018831	0.846244	-0.001855
0.009806	0.016467	0.868528	-0.00049	0.009782	0.016427	0.863770	-0.000488
0.007672	0.014112	0.888638	0.00059	0.007630	0.014035	0.879990	0.000584
0.005736	0.011779	0.90864	0.001368	0.005680	0.011664	0.899797	0.001355
0.003967	0.009468	0.928517	0.001829	0.003928	0.009376	0.923430	0.001819
0.002396	0.007168	0.94824	0.001931	0.002383	0.007129	0.945930	0.001926
0.001163	0.004839	0.967787	0.001608	0.001160	0.004827	0.967197	0.001607
0.00037	0.00245	0.987165	0.000783	0.000370	0.002449	0.987165	0.000783
0.000137	0.001243	1	0	0.000137	0.001243	1	0
0	0			0	0		

Figure B2 Wortmann FX 67-K-150 Contours

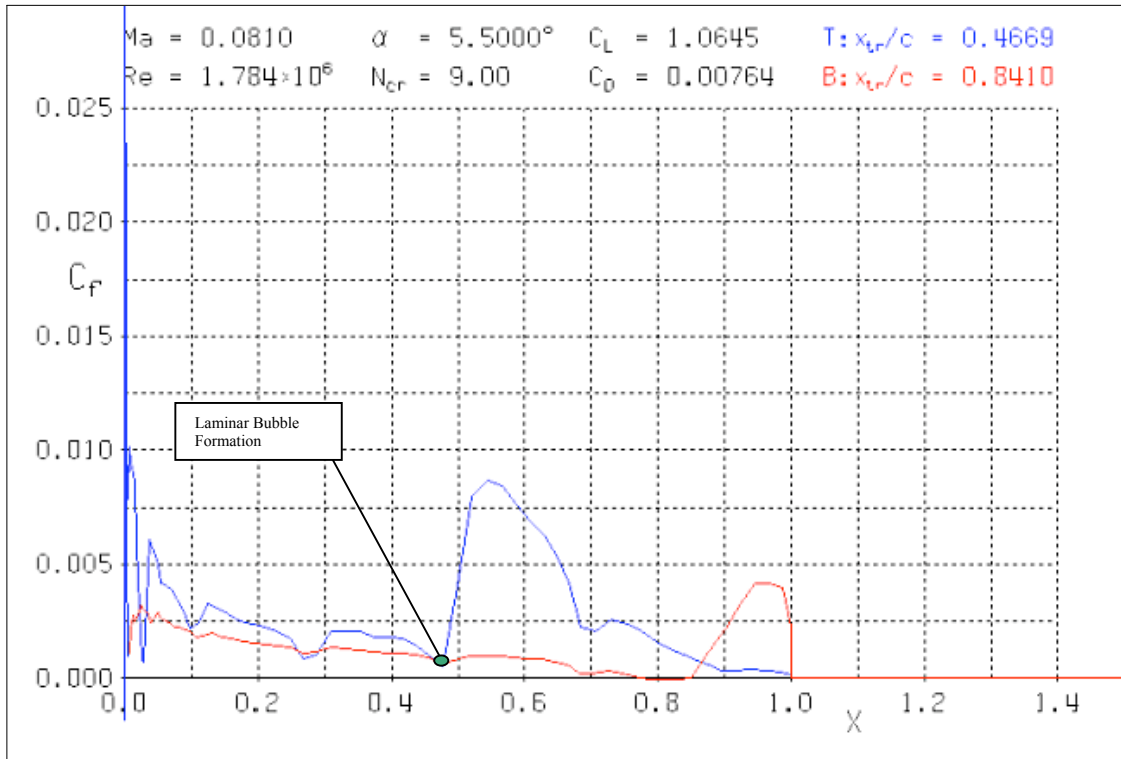


Figure B3 Skin Friction-Wortmann FX 67-K-170 Root Airfoil at One Percent Deflation

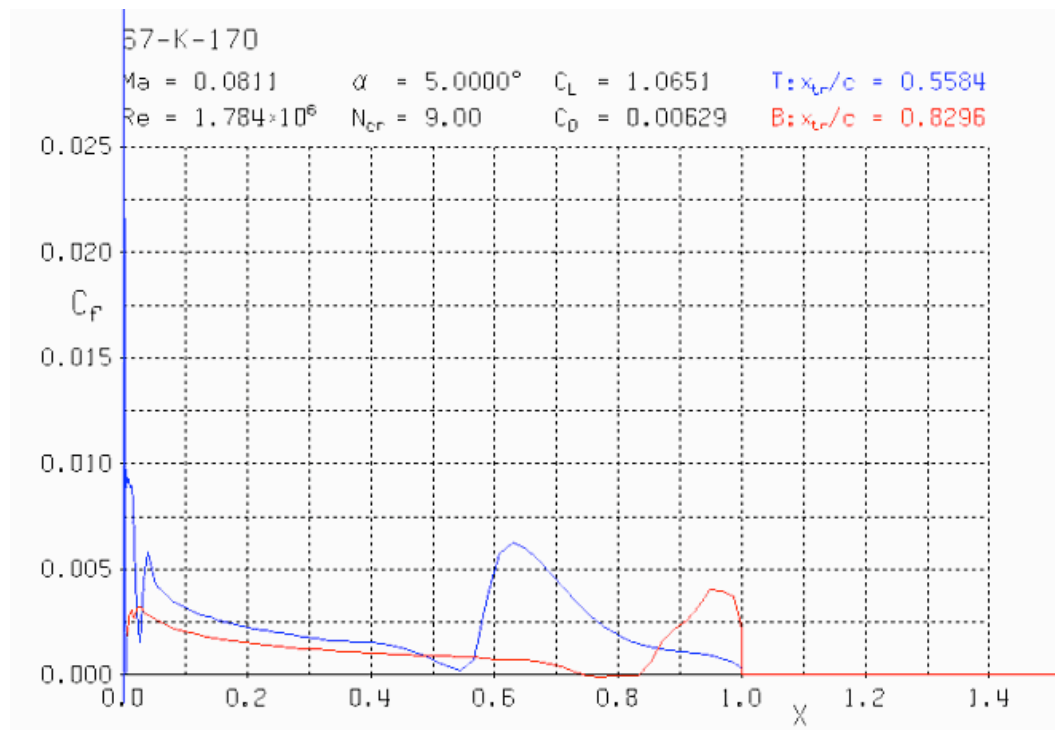


Figure B4 Skin Friction Graph - Wortmann FX 67-K-170 Rigid Root Foil

alpha	CL	CD	CDp	CM	Top_Xtr	Bot_Xtr	L/D
0	0.5147	0.00523	0.00152	-0.1004	0.6343	0.7577	98.41
0.5	0.5715	0.00537	0.00161	-0.1011	0.6291	0.7746	106.4
1	0.6289	0.00543	0.00171	-0.1018	0.6272	0.7885	115.8
1.5	0.6863	0.00548	0.00177	-0.1027	0.6245	0.7966	125.2
2	0.7433	0.00555	0.00186	-0.1035	0.6208	0.8033	133.9
2.5	0.799	0.00565	0.00193	-0.104	0.6146	0.8083	141.4
3	0.8545	0.00582	0.00206	-0.1046	0.6083	0.8118	146.8
3.5	0.9109	0.0058	0.00211	-0.1054	0.6033	0.818	157.1
4	0.965	0.0059	0.00221	-0.1057	0.5948	0.8221	163.6
4.5	1.0179	0.00604	0.00235	-0.1058	0.5848	0.8259	168.5
5	1.0651	0.00629	0.00253	-0.1048	0.5584	0.8296	169.3
5.5	1.1015	0.00679	0.00288	-0.1016	0.5231	0.8336	162.2
6	1.104	0.0076	0.00349	-0.0916	0.4678	0.841	145.3
6.5	1.0593	0.00941	0.0051	-0.0735	0.415	0.8495	112.6
7	1.01	0.01259	0.00805	-0.0576	0.3516	0.8602	80.22
7.5	0.9629	0.01625	0.01137	-0.0434	0.2728	0.8704	59.26
8	0.9245	0.02023	0.01495	-0.032	0.1823	0.8837	45.7
8.5	0.8968	0.02472	0.01895	-0.0238	0.074	0.9002	36.28
9	0.9377	0.02774	0.02178	-0.0271	0.0253	0.9121	33.8
10	1.0801	0.03292	0.02694	-0.0443	0.0005	0.9243	32.81

Figure B5 Wortmann FX-67-K-170 Rigid Airfoil Output

alpha	CL	CD	CDp	CM	Top_Xtr	Bot_Xtr	L/D
0	0.5081	0.00511	0.00125	-0.098	0.6154	0.7199	99.43
0.5	0.5638	0.00516	0.00131	-0.0984	0.6052	0.7502	109.3
1	0.6184	0.00532	0.00141	-0.0986	0.5875	0.7703	116.2
1.5	0.6707	0.00556	0.00158	-0.0985	0.5614	0.7847	120.6
2	0.72	0.00597	0.00183	-0.0978	0.5317	0.7922	120.6
2.5	0.7721	0.00619	0.00204	-0.0977	0.5206	0.802	124.7
3	0.8245	0.00642	0.00223	-0.0977	0.5151	0.8089	128.4
3.5	0.8752	0.00666	0.00246	-0.0974	0.5095	0.8157	131.4
4	0.9239	0.00692	0.00272	-0.0966	0.503	0.824	133.5
4.5	0.9735	0.00714	0.00295	-0.0961	0.4984	0.8297	136.3
5	1.0162	0.00748	0.00331	-0.0943	0.4826	0.8355	135.9
5.5	1.0635	0.00765	0.00352	-0.0934	0.4681	0.8412	139
7	0.9337	0.01545	0.0106	-0.0458	0.2804	0.8723	60.43
8	0.8998	0.0219	0.01645	-0.0291	0.1432	0.8912	41.09
8.5	0.8775	0.02605	0.02008	-0.0215	0.0329	0.9009	33.69
9	0.9214	0.02784	0.02189	-0.0233	0.0261	0.9125	33.1
9.5	1.0044	0.03036	0.02431	-0.0343	0.009	0.9112	33.08
10	1.0652	0.03278	0.02676	-0.0405	0.0006	0.9166	32.5

Figure B6 Wortmann FX-67-K-170 One Percent Deflated Airfoil Output

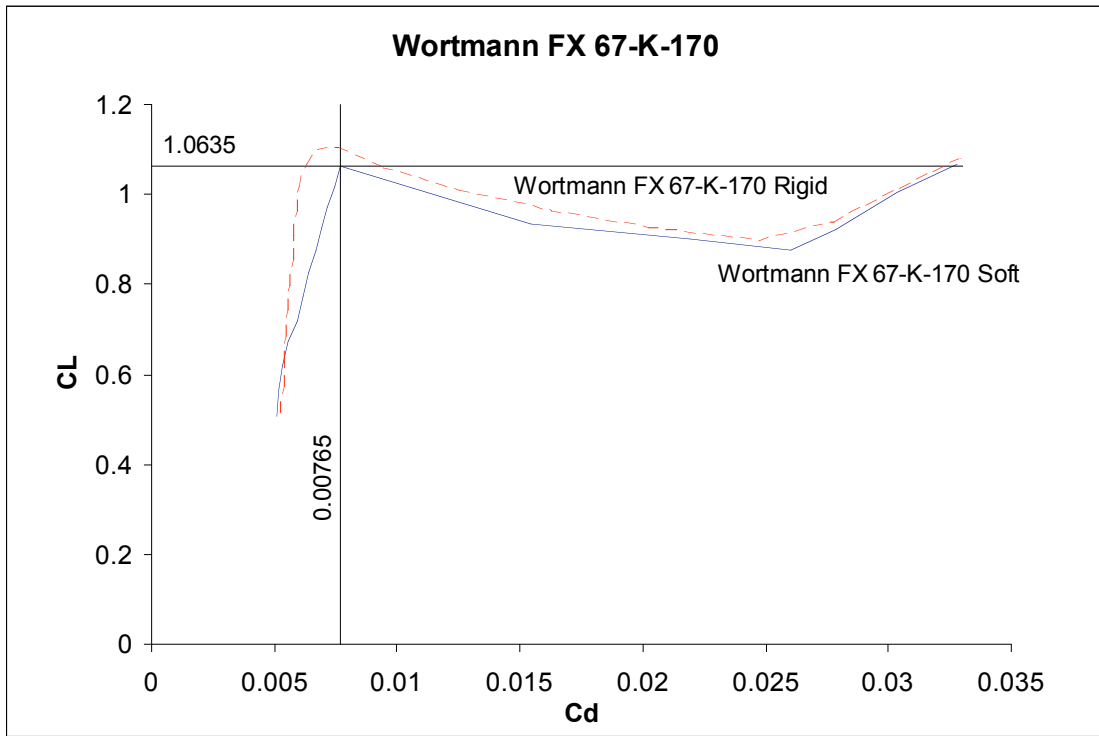


Figure B7 Section Lift to Drag Comparison for Root Airfoil

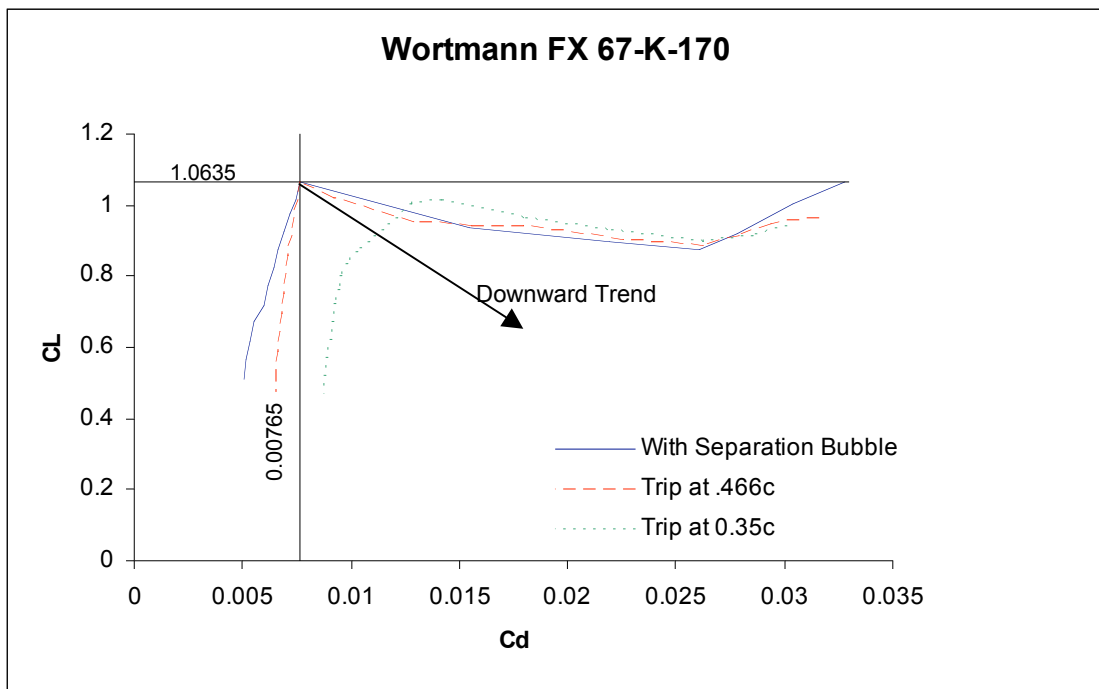


Figure B8 Tripped Flow Comparison Graph For Deflated Root Airfoil

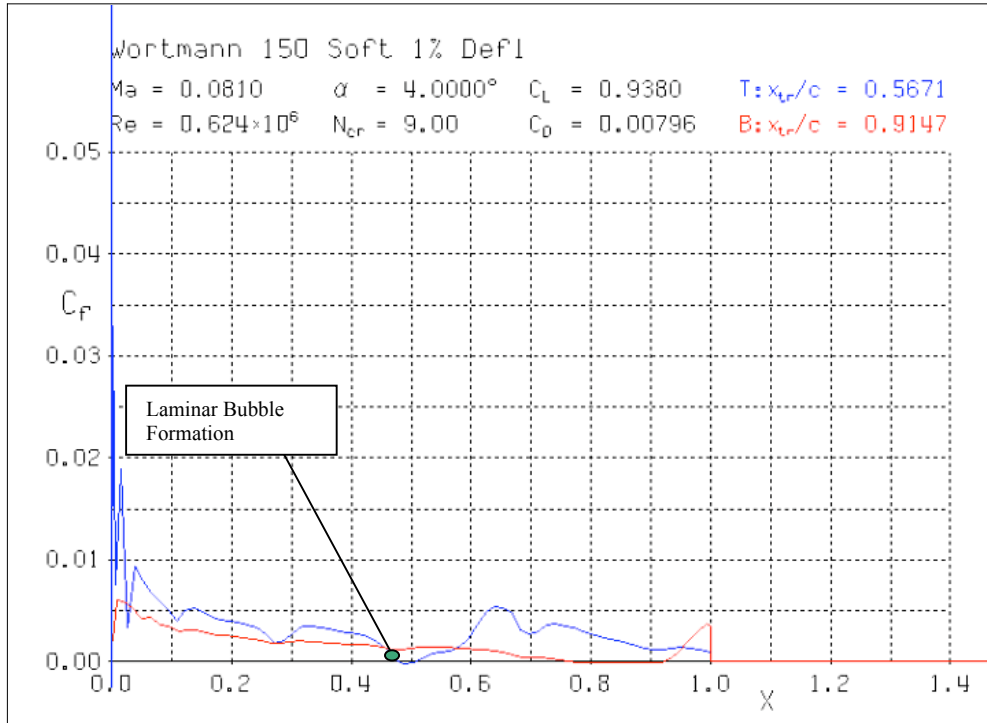


Figure B9 Wortmann FX 67-K-150 Tip Airfoil at One Percent Deflation

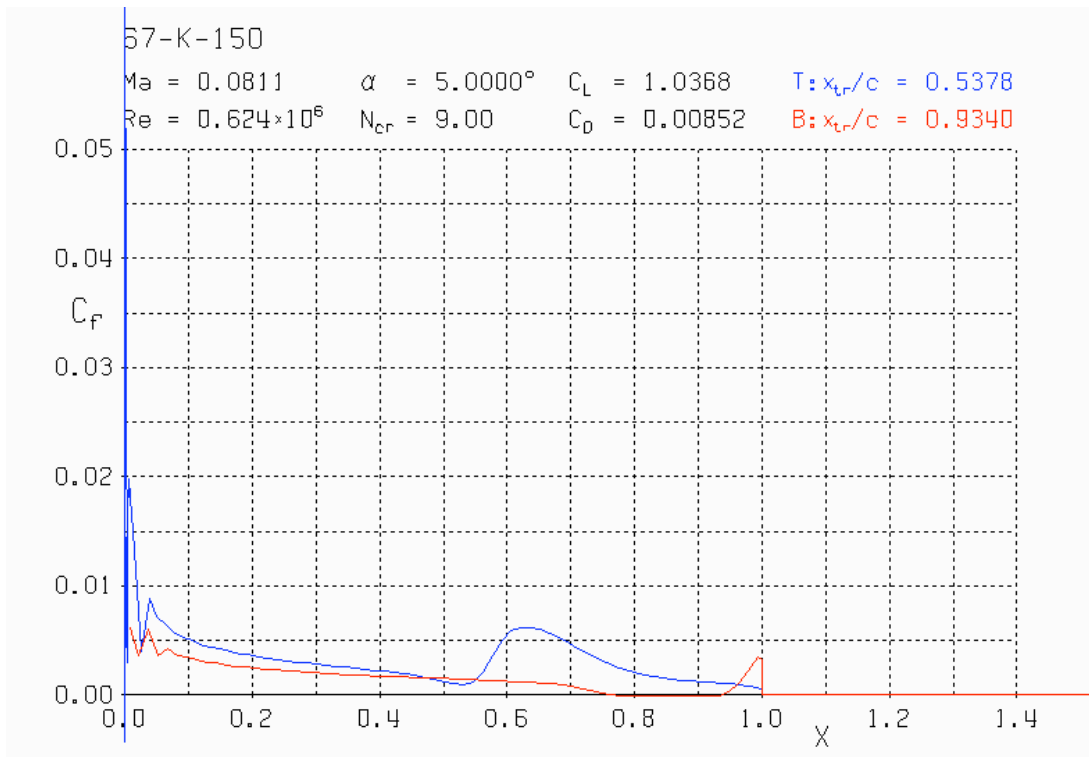


Figure B10 Skin Friction Graph - Wortmann FX 67-K-150 Tip Foil

alpha	CL	CD	CDp	CM	Top_Xtr	Bot_Xtr	L/D
0	0.5107	0.00848	0.00383	-0.103	0.6778	0.8428	60.2
0.5	0.5668	0.00854	0.00384	-0.1036	0.6738	0.8527	66.4
1	0.6227	0.00857	0.00382	-0.1039	0.6701	0.8635	72.7
1.5	0.6798	0.0087	0.00389	-0.1048	0.6666	0.8725	78.1
2	0.7336	0.00874	0.004	-0.1049	0.6623	0.8809	83.9
2.5	0.7897	0.00873	0.00399	-0.1056	0.6571	0.8885	90.5
3	0.8447	0.00858	0.00385	-0.1058	0.6485	0.8961	98.4
3.5	0.8963	0.00812	0.00332	-0.1052	0.6247	0.9041	110
4	0.9421	0.00808	0.00316	-0.1037	0.5822	0.9133	117
4.5	0.9905	0.00826	0.00337	-0.1029	0.5623	0.9226	120
5	1.0367	0.00852	0.00365	-0.1017	0.5376	0.934	122
6.5	0.9419	0.02026	0.01312	-0.0683	0.0859	1	46.5
7	0.9437	0.02341	0.01594	-0.0632	0.0046	1	40.3
7.5	0.9746	0.02493	0.0175	-0.0613	0.0034	1	39.1
8	1.0042	0.02658	0.01926	-0.0594	0.0032	1	37.8
8.5	1.0311	0.02846	0.02135	-0.0572	0.0032	1	36.2
9	1.0534	0.03081	0.02386	-0.0547	0.0035	1	34.2
9.5	1.0699	0.03374	0.027	-0.0518	0.0038	1	31.7
10	1.079	0.03744	0.03095	-0.0485	0.0042	1	28.8

Figure B11 Wortmann FX 67-K-150 Rigid Tip Foil Output

alpha	CL	CD	CDp	CM	Top_Xtr	Bot_Xtr	L/D
0	0.4989	0.0095	0.00489	-0.1003	0.6767	0.8314	52.5
0.5	0.5554	0.00945	0.00478	-0.1008	0.6727	0.8446	58.8
1	0.6125	0.00938	0.00465	-0.1013	0.6697	0.8573	65.3
1.5	0.668	0.00935	0.00466	-0.1017	0.6659	0.8687	71.4
2	0.7237	0.00917	0.00451	-0.1021	0.6604	0.8774	78.9
2.5	0.7826	0.00861	0.00389	-0.103	0.6539	0.8865	90.9
3	0.8367	0.00831	0.00371	-0.1031	0.6433	0.8954	101
3.5	0.8921	0.00816	0.00359	-0.1035	0.6356	0.9045	109
4	0.9373	0.00798	0.00308	-0.1018	0.5645	0.9148	117
4.5	0.9698	0.0088	0.00363	-0.0981	0.5112	0.9281	110
5	1.0048	0.00942	0.00418	-0.095	0.4845	0.9461	107
5.5	1.0488	0.01024	0.00487	-0.0943	0.4143	0.9774	102
6	1.0161	0.01368	0.0077	-0.0825	0.2964	1	74.3
7	0.9571	0.02301	0.01564	-0.0647	0.0292	1	41.6
7.5	0.9802	0.02507	0.01765	-0.0621	0.0045	1	39.1
8	1.0097	0.02675	0.0194	-0.0603	0.0034	1	37.7
8.5	1.0373	0.02859	0.02144	-0.0583	0.0032	1	36.3
9	1.0625	0.03069	0.0237	-0.0561	0.0032	1	34.6
9.5	1.0825	0.03326	0.02643	-0.0536	0.0033	1	32.5
10	1.0975	0.03638	0.02975	-0.0507	0.0035	1	30.2

Figure B12 Wortmann FX-67-K-150 One Percent Deflated Airfoil Output

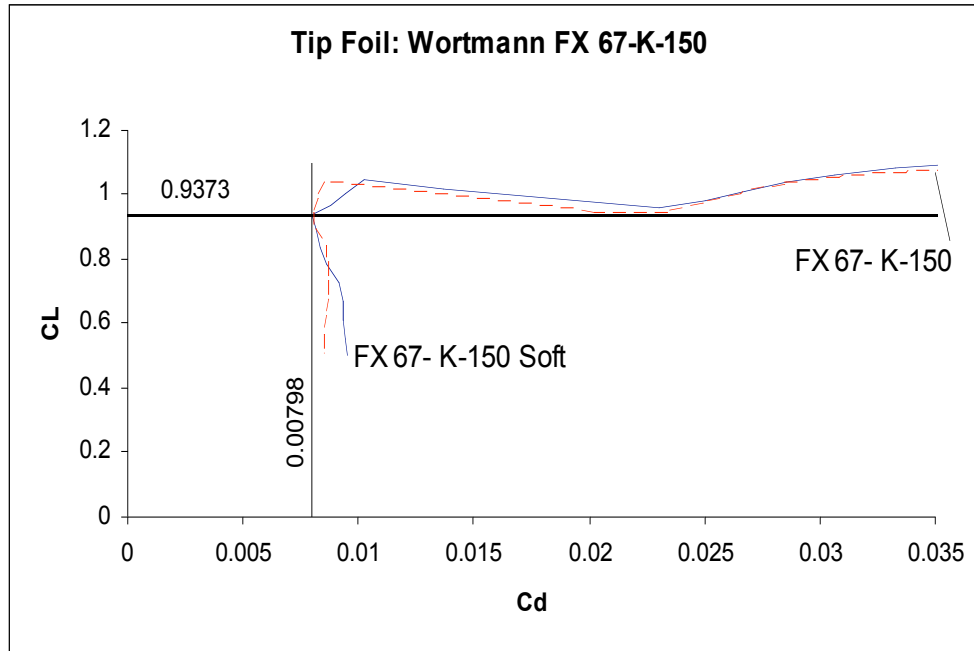


Figure B13 Section Lift to Drag Comparison for Tip Airfoil

Input							
COMPONENT TITLE	SWET(FT2)	REFL(FT)	TC	ICODE	FRM FCTR	FTRANS	
FUSELAGE	117.01	18.5	0.135		1	1.0918	0
HORIZ. TAIL	57.5	2.875	0.11		0	1.2053	0
VERT. TAIL	25.5	2.75	0.11		0	1.2053	0
TOTAL SWET	=	200.01					
REYNOLDS NO./FT	463000	Altitude	=	7750	XME	=	0.081
Output							
COMPONENT	RN	CF	CF*SWET	CF*SWET*FF	CDCOMP		
FUSELAGE	8.56E+06	0.00301	3.52E-01	0.38439	0.00221		
HORIZ. TAIL	1.33E+06	0.00418	2.40E-01	0.28935	0.00166		
VERT. TAIL	1.27E+06	0.00421	1.07E-01	0.1294	0.00074		
SUM =	0.69949	0.80314	0.00461				
FRICITION DRAG: CDF	=	0.00402	FORM DRAG: CDFORM	=	0.0006		

Figure B14 Output of Friction Analysis